Investigation and Prediction of Yaw Bearing Fatigue in Floating Offshore Wind Turbines

Jianwen Xu

A thesis submitted for the degree of

Doctor of Philosophy (PhD)

in Marine Technology

School of Engineering

Newcastle University, United Kingdom

December 2021

Abstract

Onshore and offshore wind turbines are increasingly important renewable energy generation devices. With increasing energy demand and limited land and nearshore coastline resource, installation of wind turbines is moving to deeper waters. Floating offshore wind turbines (FOWTs) are sensitive to the complex environment loads they are subjected to, which are more extreme than for onshore fixed and offshore fixed wind turbines.

This thesis assesses a floating offshore wind turbine's yaw bearing asset integrity during its operational lifetime. The yaw bearing is a connection component which is located at the top of the wind turbine tower. It is a critical component that connects the wind turbine nacelle to the tower. Although the yaw bearing fails less frequently when compared to other components in a wind turbine, its location on the tower top increases the difficulties of maintenance and replacement, resulting in a higher cost of maintenance and replacement than the other components in the nacelle.

The fatigue life and crack propagation of yaw bearings are complex as they are exposed to varying working conditions. Current industrial standards and guidelines for wind turbine yaw bearings are limited and focus on yaw bearings which are used in traditional fixed wind turbines. Some parameters used to assess them are from accumulated experience which is limited for FOWTs.

This thesis develops a systematic assessment method for assessing the integrity of yaw bearings in wind turbines. For FOWTs, the influence of complex dynamic loads is considered. Fatigue life assessments of yaw bearings and crack propagation results in yaw bearings are compared in 5 MW wind turbines with six different support foundations: onshore, monopile, ITI barge, Tension Leg Platform (TLP), spar and semi-submersible. A time-domain method is applied to predict the wind and hydrodynamic loads on the yaw bearings using three wind velocities. A Gumbel distribution, rain flow counting algorithm, linear cumulative damage law and S–N curve theory are used to generate the life-time damage equivalent loads. The fatigue life of the yaw bearing is then calculated using a finite element method (FEM) and a code-based approach. The crack propagation analysis of critical locations points

in yaw bearings is conducted using a submodel technique with extended finite element method (XFEM). Finally, the corresponding fatigue lives and fatigue crack propagation in yaw bearing are analyzed and compared.

Fatigue life, crack propagation and stress intensity factor (SIF) results show that yaw bearing's life is significantly affected by both the environment conditions and support foundations. Thus, it is necessary to assess the integrity of yaw bearings in wind turbines especially the ones installed in novel FOWTs. Compared with traditional analytical methods, which are designed only for yaw bearings in fixed onshore and offshore wind turbines, the results show that the fatigue lives of yaw bearings calculated using code-based methods are non-conservative. The proposed method is more practical to assess yaw bearing service life under actual operational conditions and can be used as part of asset integrity management of FOWTs.

Acknowledgements

My first greatest thanks to my parents, Mrs Zhuanying Gao and Mr Jiayou Xu. You gave me everything you have. During the past twenty-seven years in my life, I was taught by many excellent and connotative teachers. However, you are the only two mentors who were always supporting me. It's my greatest luck to be your son. No matter where and no matter when I met difficulties, you gave me sufficient confidence that I can overcome them. You sometimes felt confused about the insufficient education you experienced, thus you provided me with the best education environment and gave me the chance to chase my dream without intervene. You gave me a life and a pair of wings that can fly in the blue sky. You have taught me what it means to have deep love and selfless dedication. I wish you good health and good mood. It is my turn to share the pressure you bear for me. The second greatest thanks to my beloved lady, Xiaoteng Zhang. We have known each other for seven years and got married for two years. You tried your best to support my study and our decisions in life. I understand the difficulties that you met before, but I believe that we can overcome all of them together.

I believe that life will find a way and some people are the beacons on the way. During the beginning of my Ph.D. project, I met an unforeseen event. It was the darkest moment for the research project. Suddenly, the sun shone in my research career. My supervisors, Dr. Simon and Dr. Ben Wetenhall gave me the courage to move on. Simon and Ben took good care of my study and left me with a free learning atmosphere. During the past four years, you think what I think about and worry what I worry about. The COVID-19 pandemic prevented my returning to Newcastle University and our offline meeting in the Armstrong building. However, we overcame the China-UK time issue and inconvenience of online guidance. Your excellent academic teaching and persuasive life guidance will benefit me throughout my life. Please accept my sincere gratitude.

I am hoping to be a competent father for you, my beloved twin boys：Lexuan Xu and Leyuan Xu. The middle words in your names are quoted from ‘Xuanyuan’ who a well-known leader for his outstanding contributions to people in ancient Chinese history was. You were born in a special year, that is, the epidemic that is

seen in a hundred years is raging around the world. People all over the world are in suffering, so are our families. Your birth brings so much happiness to our family, especially during my thesis writing-up period. I wish you can bring happiness to the world as well as you grow up. That is the meaning of the word ‘Le’ in your names, happiness. May you have a happy future, my sons.

It’s my honor to meet Prof. Nianzhong Chen, who is my former supervisor. You led me to the academic path and gave me research direction. It’s lucky to meet my friends: Yibo Li, Yichi Zhang, Hongbo Hou, Haidan Li, Dr. Chang Li, Mincui Liang, Dr. Eleni Bougioukou, Dr. Ankang Cheng, all my colleagues of the Office 2.66, all the members of the Huishan branch of WRSA. You gave me a lot of suggestions for my research and life. Wish you all the best!

Finally, I would be much grateful to my closest relatives, Mrs Chunya Gao and Mr Jiachun Xu. You treat me like or more than your own children since I was born. As my extended family members, you care so much about me and my little family. I wish you all the best! The last blessing to my cousins: Ruijun, Ruiqi, Yu, Jianyu, Jie, Suqin, Jing, Jianhao, Jianjie, Xiang, Zhicheng. May you have a bright future.

Table of Contents

List of Figures

List of Tables

List of Publications

Journal Papers

Jianwen Xu, Simon Benson, Ben Wetenhall. Comparative Analysis of Fatigue Life of A Wind Turbine Yaw Bearing with Different Support Foundations. Ocean Engineering, Volume 235, 1 September 2021, 109293

Conference Papers

Jianwen Xu, Simon Benson, Ben Wetenhall. Fatigue Analysis on Yaw Bearing of Wind Turbine to Turbulent Wind. Proceedings of the 4th International Conference on Offshore Renewable Energy (CORE). Glasgow; 2019. ISBN 978-1-9996144-7-8

Jianwen Xu. Dynamic Load Response Analysis on Yaw Bearing of Wind Turbine to Turbulent Wind. Proceedings of the 2nd International Offshore Wind Technical Conference (IOWTC). Malta; 2019. ISBN: 978-0-7918-5935-3

Jianwen Xu, Simon Benson, Ben Wetenhall. Crack propagation in yaw bearings in offshore wind turbines: an XFEM comparative study. Proceedings of the 5th International Conference on Offshore Renewable Energy (CORE). Online; 2021

Chapter 1 Introduction

Economic development is driving the need for increasing amount of energy from the natural environment to meet global needs. Although traditional fossil energies still occupy the largest percentage of the energy consumption structure, governments worldwide are pursuing cleaner energy sources for reducing carbon emissions. Compared with other clean energy such as nuclear energy, wind energy does not produce a significant amount of toxic waste. As the major wind electricity device, wind turbines have been promoted for decades. However, wind farms, which consist of dozens or hundreds of turbines, occupy a lot of land resource or nearshore coastline resource. Since the beginning of this century, a series of floating offshore wind turbine (FOWT) concepts are promoted to work in deep waters where they do not conflict with most human activities.

Offshore floating wind is a growing renewable energy market, it is on the cusp of a huge transformation as it moves from pilot projects to commercial sized wind farms. According to the Floating Wind Joint Industry Project Report (Carbon Trust, 2021), a total of 74.05MW FOWTs are installed in the global wind market by the end of 2020, and it is estimated that the total installed capacity will increase to 125.9MW by 2021 and 127.9MW by 2022. In the long term, the Global Floating Wind Market and Forecast Report (Quest Floating Wind Energy, 2021) published in 2021 shows that the growth of the FOWT nascent market is fast, the potential installed capacity of the market is 180GW with nearly 13000 FOWT units by 2050. Figure 1.1 shows the cumulative global development of floating offshore wind (Carbon Trust, 2021). Figure 1.2 shows the estimated annual installation power capacities of onshore and offshore wind turbines (Global Wind Energy Council, 2021). Table 1.1 introduces decommissioned, fully commissioned and in-construction global floating wind projects (Carbon Trust, 2021).

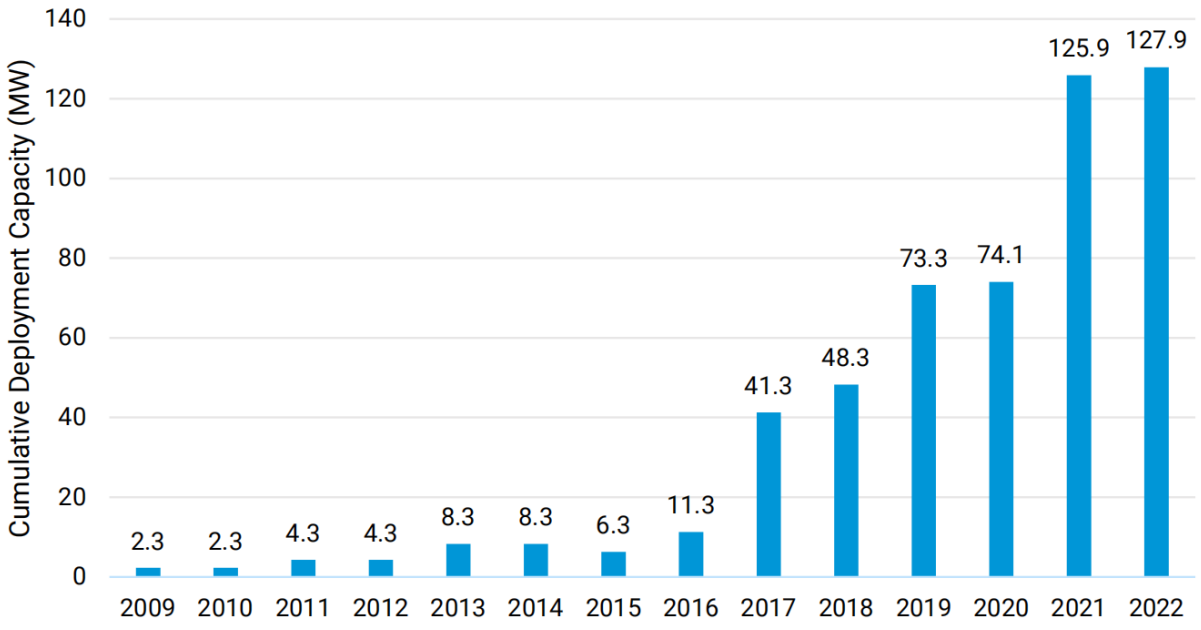

Figure 1.1 Cumulative global development of floating offshore wind

(Carbon Trust, 2021)

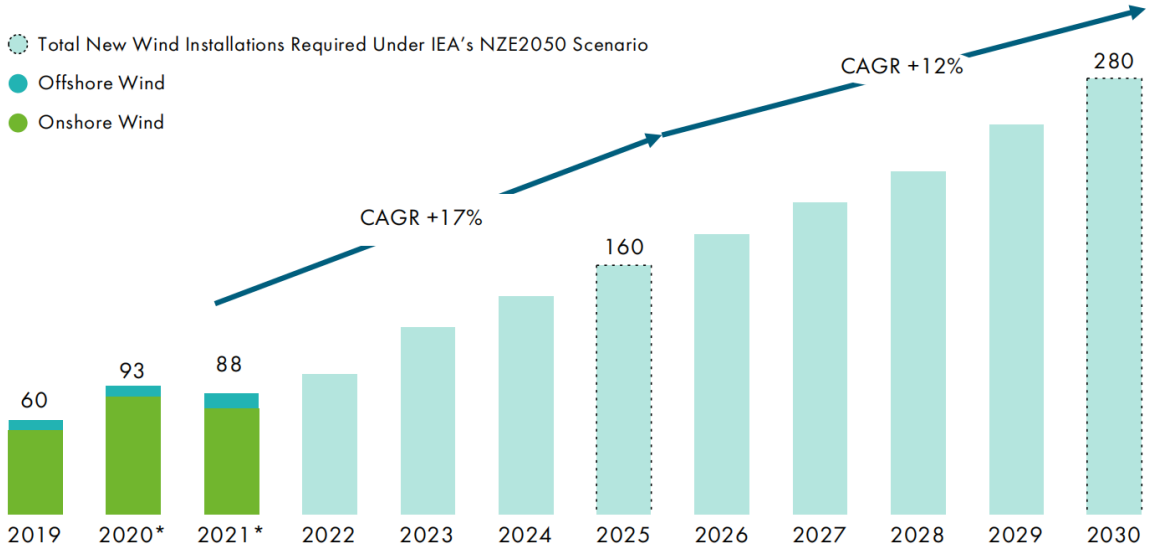

Figure 1.2 Estimated global power capability (GW) of annual wind turbine installations

(Global Wind Energy Council, 2021) (CAGR: Compound Annual Growth Rate)

Project	Country	First power	Project developer	Technology developer	Concept	Total capacity	Turbine rating	Turbine OEM
Hywind I	Norway	2009	Statoil	Statoil	Hywind	2.3MW	2.3MW	Siemens
WindFloat Atlantic Phase 1* (Decommissioned)	Portugal	2011	EDPR, Repsol, Chiyoda, Mitsubishi	Principle Power	WindFloat	2MW	2MW	Vestas
Fukushima Forward-phase 1	Japan	2013	Marubeni Corporation	Mitsui Engineering & Shipbuilding	Semi-Sub	2MW	2MW	Hitachi
Kabashima (Decommissioned)**	Japan	2013	Toda Corporation	Toda Corporation	Hybrid Spar	2MW	2MW	Hitachi
Fukushima Forward-phase 2***	Japan	2015	Marubeni Corporation	Mitsubishi Heavy Industries	V-Shape Semi-Sub	7MW	7MW	Mitsubi-shi
Fukushima Forward-phase 3	Japan	2016	Marubeni Corporation	Japan Marine United	Advanced Spar	5MW	5MW	Hitachi
Sakiyama	Japan	2016	Toda Corporation	Toda Corporation	Hybrid Spar	2MW	2MW	Subaru
Hywind Pilot Plant	UK	2017	Statoil	Statoil	Hywind	30MW	6MW	Siemens
Floatgen	France	2018	IDEOL	IDEOL	Damping Pool	2MW	2MW	Vestas
IDEOL Kitakyushu Demo	Japan	2018	IDEOL & Hitachi Zosen	IDEOL	Damping Pool (Steel)	3MW	3MW	Aerodyn
Kincardine Phase 1	UK	2018	Pilot Offshore, Cobra	Principle Power	WindFloat	2MW	2MW	MHI-Vestas
WindFloat Atlantic 2	Portugal	2019	EDPR, ENGIE, Repsol, PPI	Principle Power (PPI)	WindFloat	25MW	8.3MW	MHI-Vestas
Ulsan Demo	South Korea	2020	Unison, KETEP, Mastek Heavy Industries, SEHO Engineering, University of Ulsan	Mastec Heavy Industries	Semi-Sub	0.75MW	0.75MW	UNISON
Tetraspar Demonstration ****	Norway	2021	innogy SE, Shell, Steisdal OT	Steisdal Offshore Technologies	Tetraspar	3.6MW	3.6MW	Siemens
PivotBuoy - PLOCAN******	Spain	2021	X1Wind	Norvento Seaplace Magnomatics	PivotBuoy	0.22MW	0.22MW	Vestas
Kincardine Phase 2******	UK	2021	Pilot Offshore, Cobra	Principle Power	WindFloat	48MW	9.5MW	MHI-Vestas
DemoSATH******	Spain	2022	Saitec	Saitec	SATH	2MW	2MW	TBC

* *WindFloat 1 decommissioned in 2016. The WindFloat 1 substructure redeployed in the Kincardine phase 1 project in Scotland.*
** *Kabashima 2MW turbine to be moved to location off Fukue Island.*
*** *Fukushima Forward- phase 2 7MW floater was decommissioned in September 2020.The 2MW and 5MW Fukushima Forward floaters are due to be decommissioned in 2021.*
**** *Tetraspar Demonstration: Scheduled to be fully commissioned in July 2021*
PivotBuoy PLOCAN: Scheduled to be fully commissioned in July 2021
Kincardine Phase 2: One WindFloat device (2MW) was installed in 2018, and is producing power. The remaining 5 devices (48MW) are due to be fully commissioned in August 2021
DemoSATH: Scheduled to be fully commissioned in January 2022

Table 1.1 Decommissioned, fully commissioned and in-construction global floating wind projects

(Carbon Trust, 2021)

1.1 Research Background

To secure a global carbon net zero strategy by 2050, powering progress was discussed in the UN Climate Change Conference (COP 26) in the UK in 2021 (United Nations, 2021). Wind is a clean renewable power source from nature and is believed to be beneficial for the net zero target by global governments if it is used reasonably (United Nations, 2021). A wind turbine, an electricity generating device that can produce clean power is believed to play an increasing important role in global energy system (Global Wind Energy Council, 2021). Onshore and offshore wind turbines are two important wind electricity generating devices. Although the development of wind resources has been rapid in recent years, there are limited wind energy coastal development (James & Ros, 2015). To solve the contradiction between the rapidly growing demand for clean energy and the limited resources of lands or the nearshore coastlines, various novel FOWTs which can operate in deep waters are designed (James & Ros, 2015).

Bearings are cast components and are mostly manufactured as standard components following the corresponding industry guidelines or standards. However, for FOWTs, which are novel concepts and are not widely built around the world, their bearings inside are currently same to the ones in the offshore fixed wind turbines. For example, the IEC-61400 guideline which is used for the design of offshore wind turbines, does not consider the floating foundations of wind turbines as influencing factors when it introduces the theoretical methods for designing yaw bearing. It is not surprising that as it focuses on fixed offshore wind turbines, load effect from FOWTs on their yaw bearings is not included. It means that specific consideration of bearing design for novel FOWTs is necessary. Figure 1.3 shows the location of yaw bearing on a wind turbine.

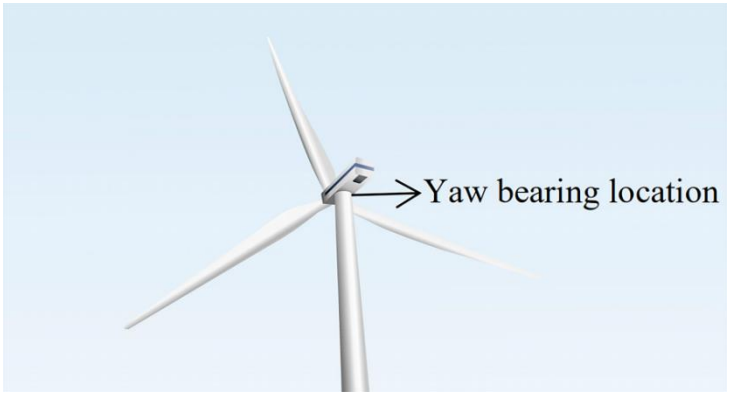

Figure 1.3 Location of yaw bearing

Besides, with the proposal and construction of the new FOWT design concept and the trend of large-scale development of them (Laura and Vicente, 2016), the issues that yaw bearings face change more rapidly. It means that corresponding design of yaw bearing will face some new difficulties by following the traditional theoretical methods, especially because some parameters in these methods are summarized from long-time operation experience. It's difficult to obtain these parameters for the corresponding offshore floating wind turbines as current FOWTs haven't operated for such a long time (Hu, 2018).

For traditional offshore structures, researchers proposed the concept of asset integrity management (AIM) to assess their integrity under operation (Kusumawardhani et al., 2016). AIM was first proposed by American Bureau of Shipping (ABS), Bureau Veritas (BV) and Det Norske Veritas (DNV) in 2006. The objective of AIM is to achieve health management and risk control for high-risk facilities in traditional energy and chemical industry (Bertrand, 2007) (Bertrand, 2007) . Since then, AIM has developed rapidly and is widely applied in offshore energy facilities and equipment such as oil and gas pipelines, offshore drilling platform and so on. However, few AIM methodologies have been implemented and adopted for FOWTs equipment. Thus, a systematic AIM methodology is necessary for future FOWT equipment analysis. In other words, current guidelines and standards for designing and constructing components in wind turbines cannot meet the requirement of FOWTs due to the new complex structure of FOWTs and the complicated operating environment they may be subjected to.

In this research, a systematic methodology for assessing the integrity of yaw bearing for four FOWTs is proposed. It evaluates the yaw bearing under working conditions. Considering the influence of various physical structures of wind turbine foundations and different global environment loads, the methodology provides a base for the AIM for the design, construction, and analysis of operation periods of FOWTs.

1.2 Research Aims and Objectives

This PhD thesis focuses on a systematic methodology for assessing the integrity of yaw bearing which is a key component of AIM for FOWTs. The main research objectives are outlined as follows:

• To develop a systematic methodology for assessing the integrity of yaw bearings in FOWTs.

• To conduct multi-dimensional comparative research of yaw bearings among onshore wind turbines, offshore fixed wind turbines and FOWTs with the consideration of their different support foundations.

• To analyse the influence of the operation environment especially turbulent wind loads on the global dynamic response of wind turbines.

• To compare the differences of two different fatigue life calculations methods: theoretical analysis method and finite element analysis (FEA) method.

• To perform an extended finite element method (XFEM) study for the crack propagation at different working locations in yaw bearings which are subjected to their corresponding damage equivalent loads.

• To compare the results from fracture mechanics analysis method with the ones from the above fatigue life calculation method.

1.3 Thesis Structure

To achieve the above-mentioned objectives, the thesis is organized and divided into eight chapters, summarized as follows:

Chapter 1 introduces the background, research aims and objectives together with the thesis structure.

Chapter 2 presents a state-of-art literature review for this research study. It includes failure analysis for normal rolling bearing from the perspectives of fatigue analysis and fracture mechanics, environmental loads for offshore structure from the aspects of aerodynamic and hydrodynamic loads and the development of asset integrity management for offshore equipment and facilities.

Chapter 3 introduces the wind and wave environmental conditions for wind turbines and the approach for calculating turbulent wind fields.

Chapter 4 describes an approach for obtaining the global dynamic loads for the six wind turbines under turbulent wind fields.

Chapter 5 conducts a fatigue damage equivalent load calculation for a yaw bearing, it includes the complex DEL forces and DEL moments which are applied for next research process.

Chapter 6 introduces a finite element model of yaw bearing that is built to analyze the stress state under the combined loads simplified from the above DEL loads. The global yaw bearing model built in this chapter will also be used for the submodel building work in Chapter 8. Then, this chapter conducts a fatigue life calculation using theoretical analysis method and finite element analysis method respectively. The results are used to be compared with each other and to validate the following SIF results fracture mechanics analysis.

Chapter 7 investigates the fracture mechanics for rolling contact fatigue and introduces the XFEM analysis for the crack propagation in yaw bearing.

Chapter 8 draws conclusions about the work from the former chapters and makes recommendations for future work.

A research flowchart is shown in Figure 1.4.

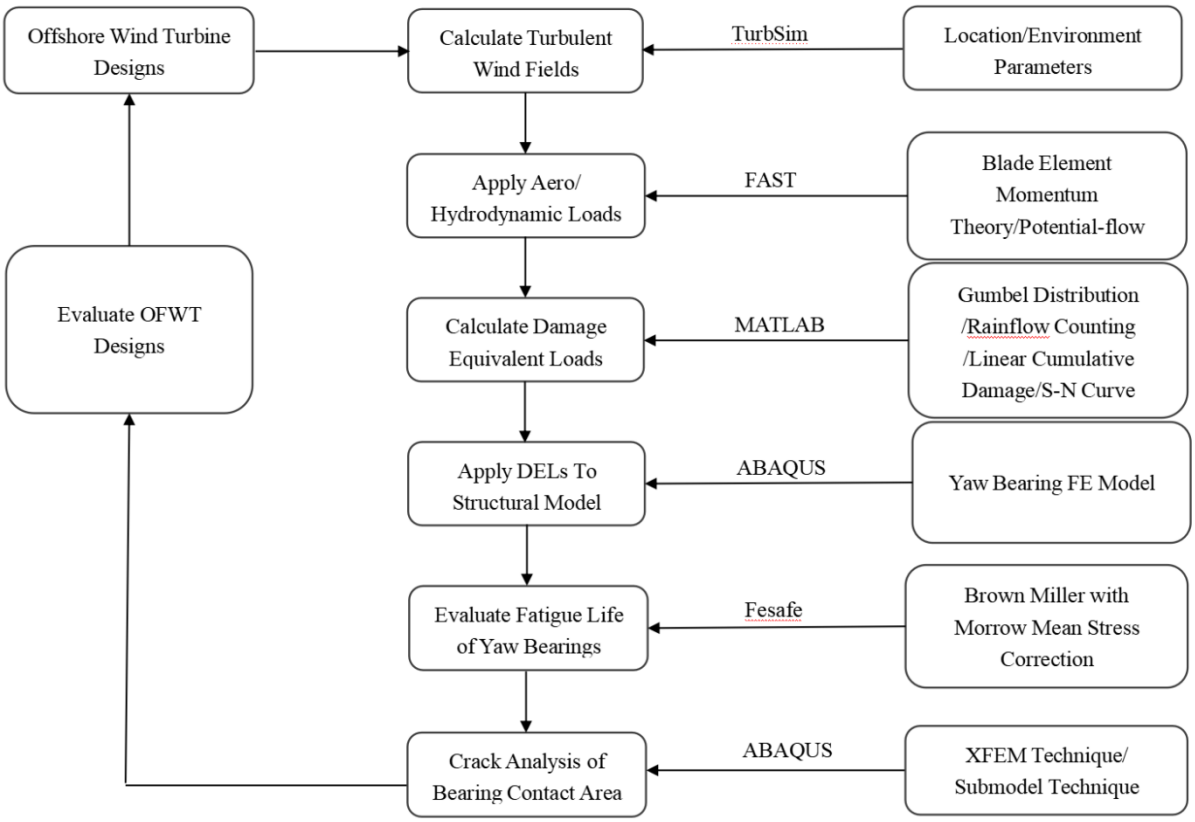

Figure 1.4 Research flowchart of thesis

(TurbSim: a stochastic, full-field and turbulence simulator for generating inflow wind fields. FAST: a fully coupled time-domain analysis code for simulating the dynamic response of wind turbines. ABAQUS: a finite element program for advanced linear and nonlinear engineering analysis applications. Fesafe: a durability analysis software for finite element models)

Chapter 2 Literature Review

2.1 Introduction

As a large normal rolling bearing connecting the nacelle to the tower top, the yaw bearing is a critical component in a wind turbine (He et al., 2018). Despite the fact that the yaw bearing fails less frequently than other components in a wind turbine, its location on the tower top increases the difficulties of maintenance and replacement, resulting in a higher cost of maintenance and replacement than the other components in the nacelle (He et al., 2018). Figure 2.1 and Figure 2.2 show the failure rates for the sub-assemblies of the onshore and offshore wind turbine systems respectively (Dinmohammadi & Shafiee, 2013a, 2013b). Whether onshore or offshore, wind turbines failure exists in the yaw system and its rate is higher for offshore wind turbines. The yaw bearing, which is a major component in the yaw system, is difficult to be replaced or maintain once it fails during operation. It can be speculated that the failure of yaw bearings in FOWTs is going to happen as well as the ones in fixed wind turbines (Dinmohammadi & Shafiee, 2013a, 2013b). Though the failure rates of yaw bearings remain low, once the yaw bearing malfunctions, the wind turbine fails. For the yaw bearings installed in the FOWTs, the maintenance and replacement will both cost much time and money because the operation locations of them are far from land and high-quality operation vessels are required to deal with its surrounding complicated environment.

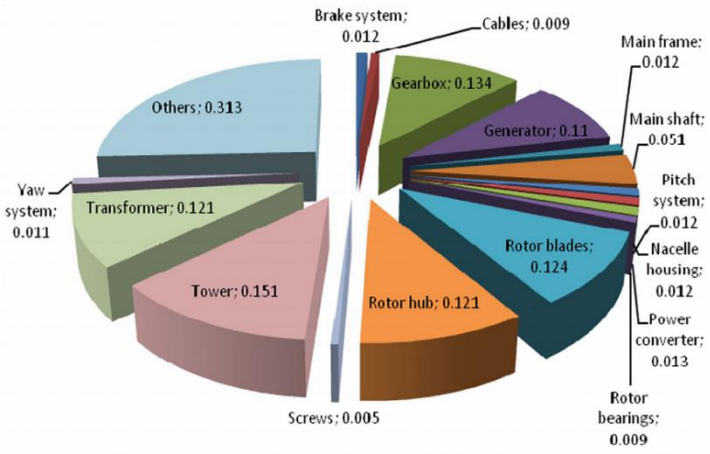

Figure 2.1The failure rates for the sub-assemblies of onshore wind turbine systems

(Dinmohammadi & Shafiee, 2013a, 2013b)

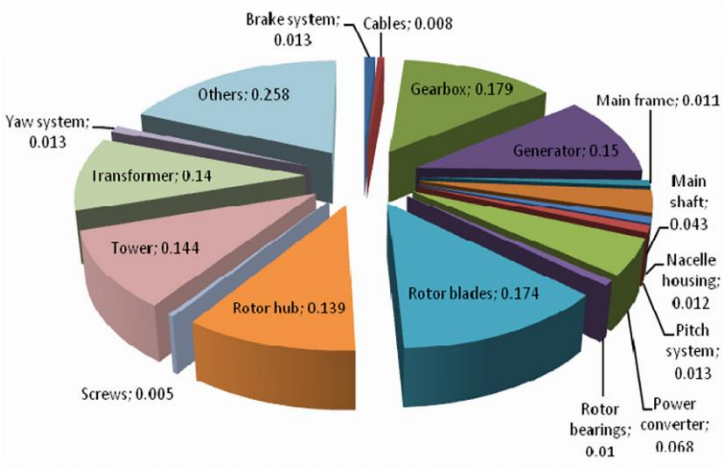

Figure 2.2 The failure rates for the sub-assemblies of offshore wind turbine systems

(Dinmohammadi & Shafiee, 2013a, 2013b)

Yaw bearings are standard components, but because they are installed in different wind turbines, they are exposed to different environmental dynamic loads during their service life. As shown in this research, these dynamic loads significantly affect the fatigue life of a wind turbine yaw bearing. Previous research does not include the influence of dynamic loads on wind turbines where the environment effect is the major focus. In this thesis, research focuses not only on the effect of the environment, but also the effect of the wind turbine foundation on a yaw bearing. Considering both the environment factor and the structure variable, the fatigue lives of yaw bearings on different wind turbine foundations are compared.

To address the issues listed above, this chapter reviews the state-of-art research on rolling bearing failure analysis in Section 2.2, offshore structures' environmental loads in Section 2.3 and asset integrity management Section 2.4.

2.2 Failure Analysis for Normal Rolling Bearing

A yaw bearing should be designed with a high carrying capacity and environmental reliability. As normal rolling bearing, yaw bearing fatigue analysis is an important process in design period. Its fatigue lifetime is limited by the material fatigue which is resulted from the cyclic loads applied on the bearing after a certain number of cycles. This is almost the same as fatigue analysis for other industrial components. Besides, with further related study conducted for decades, researchers have also found some special information and phenomenon for bearing fatigue. The related research is listed as follows:

Lundberg and Palmgren (1947) studied dynamic capacity of rolling bearings and found that the largest orthogonal shear stress in the bearing raceway contributed to the bearing contact fatigue failure (Lundberg & Palmgren, 1947) . Lundberg & Palmgren (1952) defined the bearing's life as the crack initiation life and that represents the foundation of the theory of rolling contact fatigue reliability (Dinmohammadi & Shafiee, 2013a, 2013b).

Morrow (1965) introduced energy-based models by a theory of fatigue based upon cumulative plastic strain energy as a criterion for fatigue damage and elastic strain energy as a criterion for fracture. He found that the fatigue properties of a metal were related to its cyclic stress-strain properties (Morrow, 1965).

Brown and Miller (1973) developed a new theory for multiaxial fatigue with a physical interpretation of the mechanisms of fatigue crack growth. They found that classical theories of fatigue failure cannot correlate experimental data and were dangerous for design (Brown & Miller, 1973).

Ioannides and Harris (1985) developed a new model to predict the fatigue life of a rolling bearing. In their model, the fatigue life of a bearing can be calculated based on different materials and operation conditions with a stress value (Ioannides & Harris, 1985).

Kudish (1986) studied contact frictional stress on fatigue life of elastic solids. Based on independent bearing test results, he found that bearing pitting life is a decreasing monotonic function of the contact friction forces (Kudish, 1986).

Schlicht et al. (1986) found that alternating load stresses and axial stress condition in three directions are the governing parameters which determine bearing crack generation (Schlicht et al., 1986).

Fatemi and Socie (1988) proposed a modification to Brown and Miller's critical plane approach to predict multiaxial fatigue life under both in-phase and out-of-phase loading conditions. The maximum shear strain amplitude and the maximum normal stress on the plane where the maximum shear strain amplitude locates consisted of the components of the modified parameter (Fatemi & Socie, 1988).

Liu and Choi (2008) incorporated the residual stress scatter into the RCF life model. This model was used to predict the fatigue life and they found that the fatigue life was obviously enhanced by the residual stress scatters incorporated in the subsurface (Liu & Choi, 2008).

Glodež et al. (2012) analysed the advantage of stress life and strain life and concluded that stress life was the defining feature in calculating slewing bearing fatigue life (Glodež et al., 2012).

In order to study bearing failure deeply, some researchers tried to explain it using contact mechanics and fracture mechanics.

Based on Hertzian contact theory, Keer and Bryant (1982) studied an angled surface-breaking crack and explained certain aspects of rolling contact fatigue (Kear & Bryant, 1982).

With the assumption that contact fatigue is a reason for subsurface, Kudish (1986) used asymptotic methods and found that the weak dependence of the tangential stress intensity factors (SIFs) at fatigue crack tips on the friction coefficient (Kudish, 1986). Vincent et al. (1998) used the dislocation accumulation theory to develop a model to calculate the fatigue life of bearing material. They studied the related material fatigue process based on the microstructure of material in their model (Vincent et al., 1998).

Ringsberg (2001) developed a strategy for fatigue life prediction of rolling contact fatigue (RCF) crack initiation. The strategy was consisted of elastic-plastic FE analyses, multiaxial fatigue crack initiation models, and comparison of calculated results with experiments and numerical analyses. He found the fatigue life predictions of RCF crack initiation caused by low-cycle fatigue and ratchetting failure can be described by this strategy (Ringsberg, 2001).

Bormetti et al. (2002) studied the subsurface and surface crack origins and their main failure behavior. They defined a crack propagation index as a ratio applied to threshold stress intensity factor for surface and subsurface cracks. They believed that the valuation of this index was useful for determining the favored damage mechanism and evaluating the decisive influence of the hardness distribution (Bormetti et al., 2002).

Göncza et al. (2010) used a finite element method to analyze the initiation and propagation of a raceway fatigue crack. Besides, they performed experiments on the fatigue crack growth parameters for high strength low-alloy steel 42CrMo4. The parameters of the Paris equation C

and m of the steel were experimentally determined at 28 HRc, 45 HRc and 54 HRc (Göncza et al., 2010).

Santus et al. (2012) studied the mechanisms of crushing, spalling, pitting. They found that the characteristic depths and the stress index method can be used to associate specific tests to component design, without any misunderstanding of size effect (Santus et al., 2012).

Deng et al. (2015) studied the subsurface fatigue crack propagation under rolling contact fatigue (RCF) by a three-dimensional model of bearing ring with a subsurface crack inside. The stress intensity factor (SIF) was calculated to evaluate fatigue crack propagation (Deng et al., 2015).

The above studies are related to bearing mechanical fatigue analysis and analysed bearing fatigue life from both the macro aspect and the micro aspect. However, in a practical design approach a yaw bearing is usually specified using industry standards. Several bearing calculation methods in design guidelines are discussed below.

In the American National Standard method, the fatigue life is calculated according to the American National Standards Institute/American Bearing Manufacturers Association (ANSI/ABMA) standard for a ball bearing (American National Standards Institute, 1990a) and ANSI/ABMA standard for a roller bearing (American National Standards Institute, 1990b). In the International Standard method, ISO Standard 281 is used to calculate fatigue lives of ball bearings and roller bearings (International Organization for Standardization, 2008). An integrated life modification factor is a function of the fatigue limit load (accessible for designed bearing from manufacturer catalogue) and the dynamic equivalent axial load (International Organization for Standardization, 2008). In the stress-life method, the fatigue life calculation is similar to the ISO Standard 281 but an integrated life adjustment factor is determined by a fatigue limit stress that is based on the von Mises stress criterion (T.A. Harris & Kotzalas, 2007; Barnsby et al., 2003). The above-mentioned mathematical methods are usually used to demonstrate adequate fatigue life of rolling bearings. The Lundberg-Palmgren theory is the basis of all the three methods. However, some limitations exist in the Lundberg-Palmgren theory, and these also affect the accuracy of calculation for bearing fatigue life. Tedric and Michael (2007) believed that the usage of standard should focus on the limitations that those applications in which the geometries and materials of the bearings used fulfill the standard specifications. In their book, the limitations for operating conditions are stated as follows (Tedric A Harris & Kotzalas, 2007):

• The bearing outer ring is mounted and properly supported in a rigid housing.
• The bearing inner ring is properly mounted on a non-flexible shaft.
• The bearing is operated at a steady speed under invariant loading.
• Operational speed is sufficiently slow such that rolling element centrifugal and gyroscopic loading are insignificant.
• Bearing loading can be adequately defined by a single radial load, a single axial load, or a combination if these.
• Bearing loading does not cause significant permanent deformations or material transformations.
• For bearings under radial loading, mounted internal clearance is essentially nil.
• For angular-contact ball bearings, nominal contact angle is constant.
• For roller bearings, uniform loading is maintained at each roller-raceway contact.
• The bearing is adequately lubricated.

To address some of the issues mentioned above, current standards make some adjustments for bearing design. In the ANSI/ABMA standard, the life modifications are discussed for reliability, bearing steel material, lubrication and flexible supporting structure (American National Standards Institute, 1990a, 1990b).

Current research has deeply studied the methods for bearing fatigue life calculation and explored the contact mechanics and fracture mechanics behind bearing fatigue phenomenon. However, in terms of yaw bearing installed in novel FOWTs, limited research focuses on the external factors such as the response of the flexible supporting structures and the combined variant environment loads. In current design standards mentioned above, the life modifications of flexible supporting structure focus on fixed wind turbines. The consideration about life modifications of floating supporting structures is not included in them. Besides, a complete research of yaw bearing requires the consideration of the environment loads as it can evaluate its lifetime more accurately. Thus, this thesis pays more attention to failure features of yaw bearings that operate in different environment loads with different floating supporting structures.

2.3 Environmental Loads for Offshore Structure

2.3.1 Aerodynamic loads

During a turbine's service life, wind is the major environment source for its aerodynamic loads. It is difficult to predict wind loads for wind turbine systems as wind speed and direction

continuously change in nature. However, researchers around the world have tried to understand and explain the aerodynamic loads on offshore structures by various theories and approaches over the past decades.

It is widely accepted that aerodynamic loads result from the lift forces and drag forces. For offshore wind turbines, the lift forces, skin friction drag, and viscous pressure drag are the major sources of aerodynamic loads. In addition, for FOWTs, their aerodynamic loads are usually calculated by the approaches with well-known blade element momentum (BEM) theory. The BEM theory is developed based on empirical models and corrections factors (Moriarty & Hansen, 2005). Related research about the application of BEM theory is introduced as follows:

Jonkman (2009) proposed a comprehensive simulation tool to model the dynamic response of FOWTs. In which, the aerodynamic loads along with the wind inflow were analysed by the time-domain simulation tool (Jonkman, 2009).

Cordle and Jonkman (2011) introduced an approach to carry out testing and validation of design tools for aerodynamic forces of offshore floating wind turbines. For aerodynamics, AeroDyn in FAST used quasi-steady blade element momentum (BEM) theory or a generalized dynamic inflow model to calculate aerodynamic forces with consideration of tip and hub losses according to Prandtl and skewed-wake corrections. AeroDyn in ADAMS (Automatic Dynamic Analysis of Mechanical System) calculated aerodynamic forces with the same methods above in FAST. SIMO (Simulation of Marine Operations) used BEM theory to calculate the forces on the rotor blades with dynamic inflow effects. The forces on the tower and nacelle were calculated with the drag force in SIMO. Besides, tools like HAWC2 (Horizontal Axis Wind turbine simulation Code 2nd generation), 3Dfloat (an integrated wind turbine simulation software), SIMPACK (a general multibody system simulation software) also used similar methods to calculate aerodynamic loads (Cordle & Jonkman, 2011).

Li et al.（2015）proposed an Aero-Hydro simulation code for aerodynamic loads calculation of an offshore wind turbine. BEM theory was applied in the code with a dynamic wake model to consider the wind unsteadiness caused by platform global motion (Li et al., 2015).

In addition, in terms of the aerodynamic loads of wind turbines which originate from many factors, Burton et al. concluded major features of aerodynamic load and divided them as follows (Burton et al., 2008):

• Deterministic aerodynamic loads: steady (uniform flow), yawed flow, shaft tilt, wind shear, tower shadow and wake effects
• Stochastic aerodynamic forces due to the temporal and spatial fluctuation/variation of wind velocity (turbulence)
• Rotating blades aerodynamics, including induced flows (i.e., modification of the wind field due to the turbine), three-dimensional flow effects and dynamic stall effects
• Dynamic effects from the blades, drive train, generator and tower, including the modification of aerodynamic forces due to vibration and rigid-body motions
• Subsystem dynamic effects (i.e., the yaw system and blade pitch control)
• Control effects during normal operation, start-up and shutdown, including parked conditions

For wind turbines, considering the uncertainty of wind load, partial safety factors were described in wind turbine standards (Germanischer Lloyd., 2010; International Electrotechnical Commission, 2005). Based on partial safety factors, corresponding applications on wind load for wind turbine design were proposed by some researchers, they are introduced as follows：

• Wind turbine blades (Ronold & Christensen, 2001; Ronold et al., 1999; Kong et al., 2005, 2006).
• Wind turbine tower and foundation (Nicholson, 2011).
• Wind turbine drivetrain (Guo et al., 2015; Derks, 2008).
• Other wind turbine systems (Bansal et al., 2002).

It can be found that partial safety factors on the yaw bearing have not been proposed which means the influence of wind load on yaw bearing in wind turbine design is ignored by researchers by now. Furthermore, despite the convenience of application of partial safety factors, Hu pointed out that two major shortcomings of them are obvious (Hu, 2018). First, it is impossible for designers to accurately represent the changes in temporal and spatial wind load. Second, following the design standards incorporated with partial safety factors may result in the conservatism of the results.

Besides, it is widely known that three kinds of wind fields are concluded for wind turbine wind environment during operation: uniform wind field, steady wind field and turbulent wind field. They account for the major aerodynamic loads of components in wind turbine. They are analyzed by some researchers as follows:

Ronold et al. (1999) applied the uniform wind field for wind turbine design. It simplified the aerodynamic modeling of wind turbine (Ronold et al., 1999).

Li et al. (2015) validated an aero-hydro simulation code for offshore floating wind forms with the uniform wind field (Li et al., 2015).

Liu et al. (2017) applied the uniform wind field for the CFD analysis of floating offshore wind turbines (Liu et al., 2017).

Noda and Flay (1999) applied a model to simulate the wind turbine blade fatigue with turbulent wind fields (Noda & Flay, 1999).

Dolan and Lehn (2006) simulated a model of the effect of wind shear and tower shadow on wind turbine 3p torque oscillations (Dolan & Lehn, 2006).

Shen et al. (2011) analyzed the influence of shear flow on wind turbine aerodynamic loads (Shen et al., 2011).

Lubitz (2012) studied the influence of ambient turbulence on performance of a small wind turbine (Lubitz, 2014).

Hu et al. (2016) implemented a dynamic wind load model to analyse fatigue life of composite wind turbine blades. The variable wind load was calculated by a joint distribution of mean wind speed and turbulence intensity (Hu et al., 2016).

Li et al. (2016) investigated the aerodynamic load of a horizontal axial wind turbine under the turbulent wind inflow (Li et al., 2016).

Lee et al. (2017) considered the influence of both the inflow turbulence and the realistic wind field varies in vertical direction (Lee et al., 2018).

As the researches on wind turbine progress, it is obvious that aerodynamic load from turbulent wind field draws more attention of the researchers than the ones from uniform wind field and steady wind field. This is because turbulent wind field is more in line with real wind condition. Thus, turbulent wind field is also adopted in the analysis of aerodynamic load in this thesis.

2.3.2 Hydrodynamic loads

FOWTs are exposed to waves as well as wind. Compared with onshore fixed wind turbines, offshore wind turbines are subjected to not only aerodynamic wind loads, but also hydrodynamic wave loads. The restraining system of foundations in fixed offshore wind

turbines and floating offshore wind turbines are different. Thus, it is necessary to study the hydrodynamic responses of the supporting foundations in wind turbines as they are important parts of the stability of the entire wind turbine system. This section briefly introduces research about hydrodynamic loads on offshore structures.

Waves contribute to the major fluctuating hydrodynamic loads on offshore structures. It is assumed that the sea water is incompressible and inviscid (O. M. Faltinsen, 1990). There are two basic assumptions and concepts related to wave load: kinematic boundary condition, dynamic free-surface condition.

Besides, linear wave theory for propagating waves, stokes wave theory that includes first order and higher order wave elevation, stream function wave theory that is related to wave nonlinearities, statistical waves description that includes wave spectrum, short-term and long-term sea description have been developed by researchers for decades.

Some aspects of the hydrodynamic response for offshore wind turbines which are related to the concept and location specifications are stated by Kaimirad as below (Karimirad, 2014):

- Suitable wave kinematics models
- Hydrodynamic models accounting for water depth, met ocean and design/concept specifications
- Extreme hydrodynamic loading including breaking waves
- Nonlinear wave theories and appropriate corrections
- Slamming, ringing and high-order wave loading
- Stochastic hydrodynamics applying linear wave theories with required corrections
- Slender or large-volume structures (and structural components)

However, for FOWTs, their hydrodynamic loads are usually calculated by potential-flow theory and Morison's equation which is based on a strip theory, or the inclusion of additional damping coefficients and stiffness based on data from experiments (Jonkman et al., 2014).

Jonkman (2009) proposed a comprehensive simulation tool to model the dynamic response of FOWTs. In which, the hydrodynamic loads were calculated with the consideration of hydrostatic restoring, the added-mass and damping, free-surface memory, viscous drag and the incident-wave excitation from linear diffraction (Jonkman, 2009).

Cordle and Jonkman (2011) introduced an approach to carry out testing and validation of design tools for hydrodynamic forces of FOWTs. For hydrodynamics, Hydrodyn in FAST used Airy wave theory with free-surface correction to calculate wave kinematics. The tool adopted linear hydrostatic restoring, added mass and damping contributions from linear wave radiation (including free-surface memory effects), nonlinear viscous drag contributions from Morison's equation, and incident wave excitation from linear diffraction. HydroDyn in ADAMS calculated hydrodynamic forces with the same methods above in FAST. In SIMO, linear Airy wave is used to calculate wave kinematics. The tool adopted added mass and damping contributions, linear and quadratic potential forces including frequency dependent excitation, and slow drift. It included mooring-line forces, viscous drag forces from Morison's equation, and hydrodynamic coupling force models. Besides, tools like HAWC2, 3Dfloat, SIMPACK also used similar methods to calculate hydrodynamic loads (Cordle & Jonkman, 2011).

Ramachandran et al. (2013) studied the consistency between response amplitude operators (RAOs) calculated from Wave Analysis at Massachusetts Institute of Technology (WAMIT) and FAST. They found that WAMIT can be used to verify the modeling of a rigid FOWT in FAST. However, the RAOs for a flexible turbine cannot be calculated by WAMIT. They believed that most of the coupling between turbine and platform is only achieved by using FAST, not achievable by WAMIT, as the turbine flexibility is not included in WAMIT (Ramachandran et al., 2013).

Li et al.（2015）used an aero-hydro simulation code for hydrodynamic loads calculation of an FOWT. Potential flow theory, impulse response theory, potential damping, second-order difference-frequency forces were considered for the calculation (Li et al., 2015).

In addition to codes mentioned above, there are some other for hydrodynamic load simulation. For example, SESAM developed by Det Norse Veritas (DNV) can perform a fully coupled analysis of FOWTs with Sima and HydroD module. OrcaFlex developed by NREL for the design and analysis of marine systems can compute hydrodynamic loads of FOWTs when used in FAST. Flexcom Wind is developed by Wood for simulating hydrodynamic load of FOWTs since its first version launched in 2017. In this thesis, FAST is adopted to simulate FOWTs. FAST is developed much earlier than the others and it has been widely used for hydrodynamic analysis of FOWTs by researchers around the world for a long time. Besides, it has equivalent functions of other simulating codes.

2.3.3 Combined Dynamic loads

For offshore structures, time-domain analysis and frequency-domain analysis are the two major approaches for dynamic loads calculation. Despite the fast analysis speed of frequency-domain analysis, time-domain analysis is more suitable for FOWTs as they are subjected to both wind loads and waves loads. In addition, control, strong coupling of rotor-platform, large deformation, highly linked force-displacement relations, coupling of mooring stiffness and motions also affect the choice of dynamic loads analysis approach (Karimirad, 2014). Thus, time-domain analysis approach is widely used in several numerical tools for combined dynamic loads analysis of wind turbines. As introduced in section 2.3.1 and 2.3.2, SIMA, SIMO-RIFLEX, ADAMS, WAMIT, FAST, HAWC2, 3Dfloat, SIMPACK, SESAM, Flexcom codes are used for aerodynamic, hydrodynamic, or coupling dynamic analysis of wind turbines. However, for time-domain analysis of offshore wind turbines, some aspects that related to time domain are stated as below (Karimirad, 2014):

- Nonlinear hydrodynamic loads
  - Inertial and drag forces accounting for position updating
  - Retardation and memory effects
  - Hydro-elasticity and fluid-structure interactions
  - Current loads
  - Vortex induced vibrations
  - Vortex induced motions
  - Shallow water effects and nonlinear wave kinematics
- Soil-foundation interactions
- Wind and aerodynamic forces
  - Lift and drag excitations considering the relative velocity
  - Aero-elasticity
- Damping
  - Aerodynamic damping
  - Hydrodynamic damping
  - Wave-induced aerodynamic damping
  - Wind-induced hydrodynamic damping
  - Structural damping
  - Soil damping

- Mooring system
- Structural considerations
  - Large elastic deflections
  - Rigid body movement
  - Nonlinear finite elements
- Control and servo loads

These aspects have been well considered in FAST as introduced in the above two sections (Jonkman, 2007).

2.4 Asset Integrity Management

To investigate yaw bearing integrity in a FOWT, a description about asset integrity management (AIM) is introduced in this section. In advance to introducing AIM, the definition of asset is the base of this concept. As AIM applied in industry focuses more on the management of physical assets, thus asset is defined as a physical item or valuable entity for an organization (International Organization for Standardization), 2014). Asset integrity management (AIM) is one of the most important factors for the structure safety during installation and operation (David M, 2011). In the past decades, some serious industrial accidents have happened without the consideration of asset integrity (Ratnayake, 2012). This causes a lot of financial lost to the owners. Besides, for example, for offshore oil and gas industry, a lot of offshore facilities and equipment have exceeded their design life, and are extended after a systematic assessment (the Offshore Division of HSE's Hazardous Installations Directorate, 2020). It saves the assets' owners extra costs. Based on these, AIM for industry facilities and equipment are believed to be important to both their safety and life extension.

With the development of renewable industry, FOWTs is becoming the focus. Compared with traditional fixed wind turbines which are onshore or offshore, floating offshore wind turbines are subjected to more complex environmental loads during their service life due to their various working locations. For wind turbines, yaw bearing is one of the biggest physical components. It is usually designed and manufactured strictly following the industry standards. This draws attention to the fact that whether their service states and service lives vary from each other when they are installed in different FOWTs and when are subjected to different environmental conditions for a long service time. However, there are few applications of AIM for yaw bearings in FOWTs, because they are not as mature as other offshore industry equipment and facilities.

Therefore, this section reviews the development and application of AIM in other industry field especially offshore industry field, which can be referred to support related research on investigation of AIM for yaw bearings in FOWTs in this thesis.

In 2006, ABS (American Bureau of shipping), BV (Bureau Veritas) and DNV first introduced AIM as a new concept for gaining health management and risk control for facilities or equipment with high risk in petrochemical and petroleum industry (Bertrand, 2007). In AIM, risk identification and evaluation are key parts for the facilities and equipment. They include a lot of different analysis approaches, they are mainly divided into five kinds (Tang et al., 2018): Event Tree Analysis (ETA), Hazard and Operability Analysis (HAZOP), Human Reliability Analysis (HRA), Fault Tree Analysis (FTA) and Failure Mode Effect and Criticality Analysis (FMECA). For assessing the equipment or facilities, FMECA approach is adopted to identify and evaluate the risk they may encounter during the life cycle. The objectives of FMECA are described as follows (Tang et al., 2019):

- Discover failure modes for different components in a mechanical system.
- Analyse the reasons for each failure mode
- Analyse the influence from each failure mode
- Determine the probability of the occurrence for each failure mode.

In this research, floating offshore wind turbines are the target mechanical system. Despite the complex mechanical structure of them, their global load response analysis can be carried out by the modules or similar ones as described in section 2.3. For different components, FMECA is mainly used to discover the corresponding local failure modes of them. Besides, AIM approach has also been applied by organizations or companies in other industry fields, they are introduced as below:

The UK Health and Safety Executive (2020) reviewed performance of assets based on their installation types in Key Programme 3 Asset Integrity Programme. They found that mobile rigs performed totally better than fixed installations and fixed production assets were more likely to perform better than floating installations. Meanwhile, these three kinds of assets performed differently in specific area and each of them has its own advantage in local area of the whole asset integrity (the Offshore Division of HSE's Hazardous Installations Directorate, 2020).

ABS AIM team (2021) used 3-D vision for structural tracking. A computer-aided design (CAD) model is turned into a database which is able to store typical vessel condition information by

the 3-D tool. It is capable of tracking ultrasonic thickness measurements and marking up fracture damage or buckling damage in a virtual system. Based on these, related maintenance or replacement plan is proposed (ABS AIM team, 2021).

SGS company (2021) believed that an AIM system fully integrates the design, engineering, and operational integrity. The diagram about what the AIM system SGS provides to their clients is shown in Figure 2.3 below. The system is divided into three parts: design, safeguarding systems, maintenance, and inspection (SGS company, 2021).

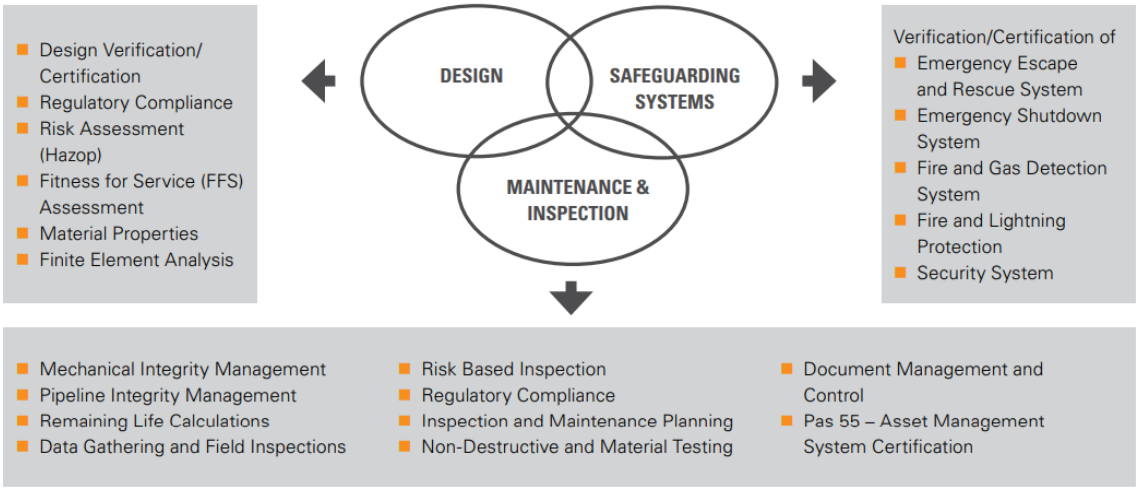

Figure 2.3 AIM system provided by SGS company

(SGS company, 2021)

In addition to practical application in industry fields by organizations and companies, research about AIM is also conducted by scholars around the world.

Ossai et at. (2014) proposed a framework for sustainable AIM which is used for renewable energy generation plants. They found that sustainable AIM can solve the problems resulted from poor AIM, such as increased downtime, high maintenance cost, high repair operation cost and low energy output. In sustainable AIM, an accurate understanding of the demands from stakeholders is beneficial for the efficiency of renewable energy generation (Ossai et al., 2014).

Lazakis & Kougioumtzoglou (2019) assessed the risks related to the activities of installation, operation, and maintenance in a wind farm lifecycle with the usage of failure mode, effects and critically analysis, hazard identification methods. They proposed an integrated risk analysis methodology for main wind turbine components which includes personnel safety,

environmental impact, asset integrity, and operation. In terms of asset, they believed that pitch system is the most sensitive component, as well as yaw system. is the fact that they suffer from higher failure probability also results in lower energy production and less income of the assets' owners. Meanwhile, the authors thought that additional accurate data about the offshore wind industry is beneficial for offshore wind turbine development as the current application of onshore data on offshore wind turbine may result in significant problems(Lazakis & Kougioumtzoglou, 2019).

Leimeister and Kolios (2018) classified the methods that used in the offshore and marine renewable energy fields. Then, they analyzed the applicability, benefits, and limitations to offshore wind turbine systems of these methods. Based on this work, they believed that offshore wind turbine systems are rather complex with various components that need special attention to their working environment. However, they also pointed out the limited experience with novel structures and the lack of reliability data. Other aspects like data confidentiality, time saving, and computing efficiency are believed to challenge the reliability of assessment of offshore wind turbine. Thus, they thought that it is necessary to develop more complex, efficient and flexible tools for the design and operation of offshore wind turbine systems (Leimeister & Kolios, 2018). Ozguc (2020) studied the risk-based inspection (RBI) program which is a part of the AIM for offshore floating structures such as floating production storage and offloading (FPSO) and floating liquefied natural gas (FLNG). He developed a semi-quantitative risk assessment tool for offshore floating structures. Besides, he provided a detailed user guideline about the RBI program. Based on the program, he found that the extent and cost of the detailed generic inspection is probably to be reduced due to the following aspects (Ozguc, 2020):

• Risk which is resulted from a wrong survey focus is reduced.
• Survey time is reduced by the selection of critical connections.
• Local non-destructive evaluation and thickness measurements is reduced and more focused.

Zulkifly and Mohd (2013) believed that current performance of asset integrity has not meet the requirements of assets' owners as the similar incidents occur again and again in the offshore industry. Thus, they proposed an indicator system for identifying measurable asset integrity performance which provides integrated view on the health status of the offshore assets. They studied five different floating offshore facilities in Malaysia with this risk-based integrity indicator methodology to verify its applicability in real life. Finally, they thought that this

methodology is beneficial for making decisions between maintaining the current asset conditions or requiring more monitorization on assets (Zulkifly & Mohd, 2013).

Kusumawardhani et al. (2016) studied the challenges that AIM practices face in the oil and gas industry for their further development in the future. The fluctuation in oil and gas market is the major research point in their study. By analysing data about offshore installations from other studies, practical interviews, online questionnaire with related industry experts in different regions in the world, they found that most of the challenges are similar and repeated without the consideration of the geographical locations of assets. Thus, it is necessary to study the root cause that affect assets' integrity and sometimes the causes are resulted from the defects occurred during operation. The defects may occur due to some factors such as environmental conditions, basic design, operating conditions and so on. Figure 2.4 shows the factors which affect the degradation of an offshore installation (Kusumawardhani et al., 2016).

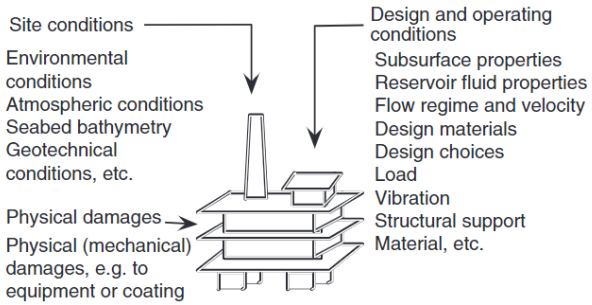

Figure 2.4 Factors affecting the degradation of an offshore installation (Kusumawardhani et al., 2016)

Nielsen and Sørensen (2014) proposed a method which is based on the Markov decision process for offshore wind turbines. Damage model with failure probability is necessary for the method. The value of failure probability is uncertain in assets' lifecycle as the damage size of defect in assets is changeable with operation time. They also mentioned that a fracture mechanical model can be used for fatigue research and the value of model parameters can be calibrated by the design model which is based on S-N curve. The model is applied with the monitoring and inspection results of assets for future decision (Nielsen & Sørensen, 2014).

Freiburger et al (2017) introduced new guidelines for asset integrity management of mechanical assets. Compared with the guidelines for mechanical integrity system, the major change in their research is terminology, such as asset integrity versus mechanical integrity and systems versus

equipment, safety-critical systems, asset management tools and so on. They also described failure modes, damage mechanisms and life cycle in the research (Freiburger et al., 2017).

Based on the above studies conducted by scholars around the world, AIM has been widely used in different industry fields. No matter in traditional petrol energy platforms or renewable clean energy facilities, the base of their AIM research is assets' life cycle and the analysis tools adopted in the different phases of assets' entire management process. This will be briefly introduced in the next two sections.

2.4.1 Asset life cycle

Different assets have different life cycles, it is better to assess an asset life before they enter the design phase or market. Its failure during the operation will lead to overwhelming cost of time and money. Taking into consideration of every stage of asset and usage of the data generated from the asset operation at different stages is beneficial for a long service life and low operation and maintenance cost. In order to introduce asset management process clearly, the concept of asset life cycle is proposed for people to understand intuitively. Three options from different asset consulting and management companies are introduced as below.

Gocodes company (2020) in the USA proposed six stages of asset life cycle which are concluded as follows: planning, procurement or acquisition, deployment or installation, utilization, maintenance, disposal (Gocodes company, 2020).

AssetInfinity company (2019) in India believed that five stages can be analyzed in asset's life cycle: procurement, deployment, utilization, maintenance, disposal (AssetInfinity company, 2019).

UpKeep company (2021) in the USA divided asset life cycle into four stages: create or acquire, utilize, maintain, renew or dispose (UpKeep company, 2021).

Despite that asset life cycle is divided into different kinds of phases in different approaches, the core targets of these approaches are the same: assessing the integrity of an asset and deciding whether it fails to operate as normal. An asset, no matter it has simple or complex structure, it must perform effectively and efficiently to support reliable and safe operation. Thus, it is important to deliberate on the operating environment for an asset to achieve better operating

target. To achieve the target, tools that are used to analyse an asset at different phases are essential and introduced in next section.

2.4.2 Asset integrity tools

To assess life cycle for an asset, essential tools used at different stages of life cycle are not to be ignored (Dana Vanier, 2001). For offshore oil and gas exploration and development (Renard, 2013), Bureau Veritas (BV) developed an open Web-based system named VeriSTAR AIMS for AIM system team to work in real time online, this system contains almost the full analysis tools for AIM. An example of finite element method (FEM) model used in the system is shown in Figure 2.5 (Renard, 2013).These tools are integrated in the system to support each step in an asset's life cycle, and they are divided as below:

• Structural FEM analysis tool:
This analysis tool is used to build a finite element global structural model for future stress calculation and further fatigue life study.

• Hydrodynamic and mooring analysis tool:
It considers the environment conditions and mooring system condition for the offshore asset. It works with the structural FEM analysis tool for the load analysis and fatigue life calculation of the asset.

• Inspection tool:
In the system, its main target is to support the whole system along the integrity management cycle. The inspection tool is based on a system tree of the asset which is predefined. The characters of asset decide the configuration of the system tree. All the information gained from the asset is inserted into the corresponding sub module of system tree. For users, it is easy to inspect and manage their assets by a graphical interface of the tool. Some important information such as the name, location, expiration data and classification notations are included in the inspection tool.

• Documentation and data management tool:
VeriSTAR AIMS software allows co-users to get access to each step of the integrity cycle at any given time online. Thus, information or data of different facilities and equipment is stored securely on the Internet. Relevant tool about documentation and data management is designed in the whole system. This tool includes the information of detailed report for users to manage

asset integrity. Data about physical size of different facilities or equipment, asset operating states, finite element analysis results and so on is also included in the tool.

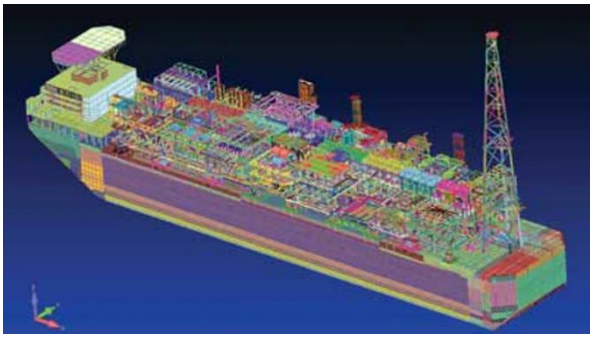

Figure 2.5 Typical FEM model of an integrated hull and topsides FPSO

(Renard, 2013)

Specifically for pipelines, Agrawal from Gail company (Agrawal, 2021) introduced a pipeline integrity management system. The integrity system is first described from a life cycle perspective which is shown in Figure 2.6 and then it is divided into three parts as below (Agrawal, 2021):

• Design and engineering tool:
Based on ASME B 31.8 & API (American Society of Mechanical Engineers, 2005), a software tool for safety and integrity of pipeline in the selection of materials, processes and technology is included.

• Manufacturing & construction tool:
For manufacturing and construction, the system includes quality management system (QMS) tools such as quality assurance (QA) and quality control (QC) plan, risk management tools and project quality index (PQI).

• Operation & maintenance tool:
In terms of operation and maintenance of pipeline, electronic data management system

GIS mapping of pipeline network and risk management matrix are included in the system.

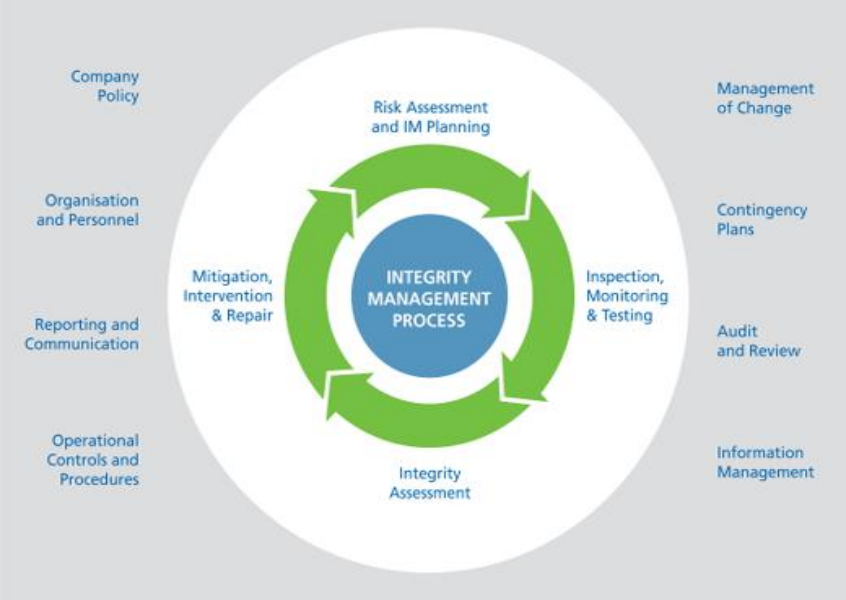

Figure 2.6 Integrity management system for pipeline

(Agrawal, 2021)

Based on the classification and description above, it can be found that during the process of exploration and development of oil or gas, there are various tools to assess the integrity of equipment or facilities according to different purposes of usage. The study on the tools used in AIM process is beneficial for the design and application of methodology proposed in this thesis. In this thesis, some tools are used to assess the influence of environment difference and supporting foundation difference on yaw bearing. First, tools such as TurbSim and FAST are mainly used to obtain data about environment condition, combined dynamic load. Then, MATLAB is used to carry out further analysis of the data. Finally, ABAQUS and Fesafe are used as design and engineering tools to conduct FEM analysis.

2.5 Summary

Offshore wind turbine systems are very complex with dependent, repairable, or redundant components, dynamic characteristics, and non-linearities. Furthermore, they require special consideration regarding the severe offshore site conditions, implying several uncertainties in the motion and stress response of the system due to unknown and complex environmental impacts, as well as non-linearities. However, there is little experience with novel structures and lack of reliable data. Besides, in terms of ethical and economic aspects, such as data confidentiality, as well as time and computational efficiency, certain standards must be met. These factors challenge the reliability assessment of offshore wind turbines (Leimeister &

Kolios, 2018). The offshore wind turbines are subjected to higher environmental and power utilization stresses than onshore turbines resulting from the marine environment. Therefore, they have higher failure rates (Karyotakis & Bucknall, 2010), which is the reason why onshore failure models are not appropriate for modeling the O&M and performance of offshore turbines (Laura，Castro Santos & Vicente，Diaz-Casas, 2016).

For a mature industrial asset, there are a lot of AIM methods of assessing its integrity during its lifecycle. However, FOWT is a novel concept proposed by researchers no more than two decades. Thus, with the combination of AIM methods adopted in other mature industry fields such as FPSO or pipeline that mentioned above and wind turbine design rules or standards for its components, a novel and systematic methodology is proposed in this thesis for investigating the AIM of yaw bearings in FOWTs. Yaw bearings in FOWTs are under development and not as mature as other industrial assets. An example of yaw bearing which is the largest slewing bearing component in wind turbine is used as the research target. It represents the concept of asset in the following content of this thesis. The characteristics of this methodology are concluded as follows:

• As a brand new mechanical system, FOWT is subjected to new working environment. It means that the AIM methods applied in relevant or similar industrial fields may face limitation and is not applicable for this new mechanical system.

• In the current existing AIM methods, data resulted from the practical operation phases of mechanical system is used for analysing and evaluating its fatigue life. However, the methodology for investigating the AIM of yaw bearings in FOWTs in this thesis is designed to conduct an analysis of fatigue life in the design phase and to provide the foundation for systematic anticipation for the future practical operation.

• The methodology is believed to be used as a reference for other components of new mechanical system in its design phase.

• The methodology in the thesis is used to discover the gap between theories and practices of AIM in FOWTs.

Chapter 3 Environmental Conditions

During a wind turbine's service life, wind is the major environment load source. As a jointing element in the wind turbine, the yaw bearing is exposed to different wind conditions and subjected to different turbulent wind loads. In this research, the same turbulent wind is chosen for the wind environment condition for both onshore and offshore wind turbines for comparative purposes. The Kaimal spectrum is chosen to represent usual wind turbine operation under turbulent wind fields (Jonkman & Buhl Jr, 2005).

Besides, compared with an onshore wind turbine, offshore wind turbines are subjected to waves as well as wind. In this work, the yaw bearings are subjected to hydrodynamic wave loads as well as wind loads. The Pierson-Moskowitz spectrum is chosen (Jonkman & Buhl Jr, 2005) .

3.1 Wind Condition

3.2 Kaimal Spectrum

Aerodynamic loads normally consist of steady loads, periodic loads and randomly fluctuating loads. In this paper, a dynamic load analysis is based on a randomly fluctuating load. The leading stochastic aerodynamic loads result from turbulence (Matha, 2010). The turbulent velocity undulations are assumed to be a random vector field. The components of the random vector field have zero-mean Gaussian statistics. On the basis of the Kaimal spectral and the exponential coherency model, power spectral densities are used to describe the components of wind velocity (Jonkman, 2016). The equation below gives the power spectra densities (Jonkman, 2016):

$$\frac{S_k(f)}{{\sigma_k}^2} = \frac{4fL_k/V_{hub}}{\left(1+\frac{6fL_k}{V_{hub}}\right)^{5/3}} \qquad \text{Equation 3.1}$$

where f is the component frequency, k is the velocity component direction index (i.e.1= longitudinal, 2 = lateral, and 3 = upward); S_k is the component spectrum with single-sided velocity; $\sigma_k$is the standard deviation of velocity component. L_k is the integral scale parameter velocity component.V_{hub} is wind speed in hub centre.

Based on measurements of a flat homogeneous terrain in Kansas, the turbulence spectral parameters of the Kaimal spectrum are described in Table 3.1 (Jonkman, 2016).

Velocity component index k	1	2	3
Standard deviation σ_k	σ_1	$0.8\sigma_1$	$0.5\sigma_1$
Integral scale L_k	$0.8\Lambda_1$	$2.7\Lambda_1$	$0.66\Lambda_1$

Table 3.1 Kaimal turbulence spectral parameters

(Jonkman, 2016)

where σ_1 is standard deviation of velocity component direction index, Λ_1 is integral scale of velocity component direction index.

The Kaimal spectrum is selected for all turbines in this study to produce a direct comparison of fatigue life of yaw bearings in different wind turbines.

3.2.1 Turbulent wind field

This work utilizes the TurbSim code which contains the IEC Kaimal spectural model. This model differs from the original Kaimal spectrum in that it uses alternate turbulence component variance ratios and equations for the upward velocity component (Jonkman, 2016). This work performs a numerical simulation of a full–field flow and the results in the IEC Kaimal spectural model using FAST (Kelley & Jonkman, 2005). The parameter HubHt is set as 90 meters as it is the height of turbine hub where the turbulence is generated (Jonkman et al., 2009), on the basis of IEC61400-1 guidance (International Electrotechnical Commission, 2005), the grid points of full-field wind file with normal turbulence model are set as 41×41.

Three different average inflow wind velocities 10m/s, 12m/s, 14m/s are set as input parameters in TurbSim to generate the full-field turbulent wind field. The rated hub wind velocity is 11.4 m/s (Jonkman et al., 2009). These turbulent wind velocities were selected as they are within the rated cut in wind speed 3m/s and cut out wind speed 25m/s and represent the largest operation time of the wind turbine (Harris et al., 2009).

3.3 Wave Condition

The wave conditions used in this research are not as complex as the wind conditions. For a clear analysis comparison, a single wave condition is considered in this paper as described below.

3.3.1 Pierson-Moskowitz spectrum

The Pierson-Moskowitz spectrum is chosen for this analysis as it is a fully developed spectrum for marine structure hydrodynamic analysis and it is fully coupled in FAST code (Jonkman, 2007). By contrast, the Joint North Sea Wave Project (JONSWAP) spectrum is used in limited situations (Jonkman, 2007). Besides, it is defined by the IEC 61400-3 standard (International Electrotechnical Commission, 2009). This wave spectrum is specified by a linear random wave model defined by a two-parameter spectral formulation. The spectrum is applicable to a fully developed sea state and is often used to conduct a fatigue analysis of a marine structure (Jonkman et al., 2014).

The following formulation describes the spectral density of the surface elevation:

$$S_{PM}(f) = 0.3125{H_s}^2{f_p}^4\, exp\left(-1.25\left(\frac{f_p}{f}\right)^4\right) \qquad \text{Equation 3.2}$$

where H_s is significant wave height and f_p is wave peak frequency. In this thesis, the significant wave height is set as 5 meters and wave peak frequency 1/12.4 as they are common sea conditions that wind turbines will be subjected to under operation (Zhang & Wang, 2015).

A location in the northern North Sea is selected as the reference point to obtain the ocean environmental conditions. This site is located at 61º 20′ N latitude, 0º 0′ E longitude on the prime meridian northeast of the Shetland Islands, which are northeast of Scotland (Jonkman & Buhl Jr, 2005). The location is chosen as extreme wind and wave conditions exist here, and it can cover most of the working environment conditions that wind turbines will face in the future. Figure 3.1 shows the location of the selected reference point.

Figure 3.1 Selected reference point

3.4 TurbSim Code

TurbSim is a random, full-field, turbulent-wind simulator. A statistical model is used to simulate time-domain three-component wind velocities at points in a 2D vertical rectangular grid. The grid is fixed in space in TurbSim. The output of the code is usually used as input in FAST (Jonkman & Buhl Jr, 2005) which is an inflow wind-based code. The combination of the turbulent wind fields resulting from TurbSim with Taylor's frozen turbulent assumption from FAST is used to obtain wind speed locally in time and space (Jonkman, 2016).

As introduced above, Kaimal spectra is used to describe wind in this research using a frequency approach. In TurbSim, the frequency domain spectra are transformed to a time domain series by an inverse Fourier transform method (Jonkman, 2016).

Although this method is used to simulate a hypothesized stationary process, it can also be applied to kinetic components using the AeroDyn module (David et al., 2002) in FAST to combine coherent turbulent structures with a generated time series. The process of a TurbSim simulation with AeroDyn is illustrated in Figure 3.2 (Jonkman, 2016). The figure shows that TurbSim uses a transformation from the frequency domain to time domain producing wind output compatible with InflowWind (Jonkman, 2016). Besides, optional coherent structures are written to a separate file and superimposed in AeroDyn v13 which require a full field background (Jonkman, 2016) .

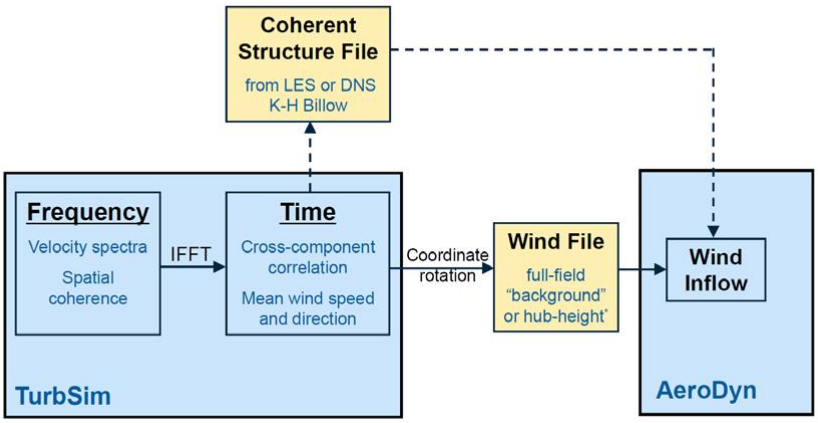

Figure 3.2 TurbSim simulation method

(Jonkman, 2016)

3.5 Turbulent Wind Field Results

Three different average inflow wind velocities are set as input parameters in TurbSim to generate the full-field turbulent wind filed, corresponding to 10m/s, 12m/s, 14m/s, since the rated hub wind velocity is 11.4m/s (Jonkman et al., 2009). The three full-field turbulent wind fields are shown in Figure 3.3 to Figure 3.5. They are short time-series wind fields with 600 seconds to couple with the wave conditions. The random seeds of the three wind fields are the same to avoid their influence on the following research.

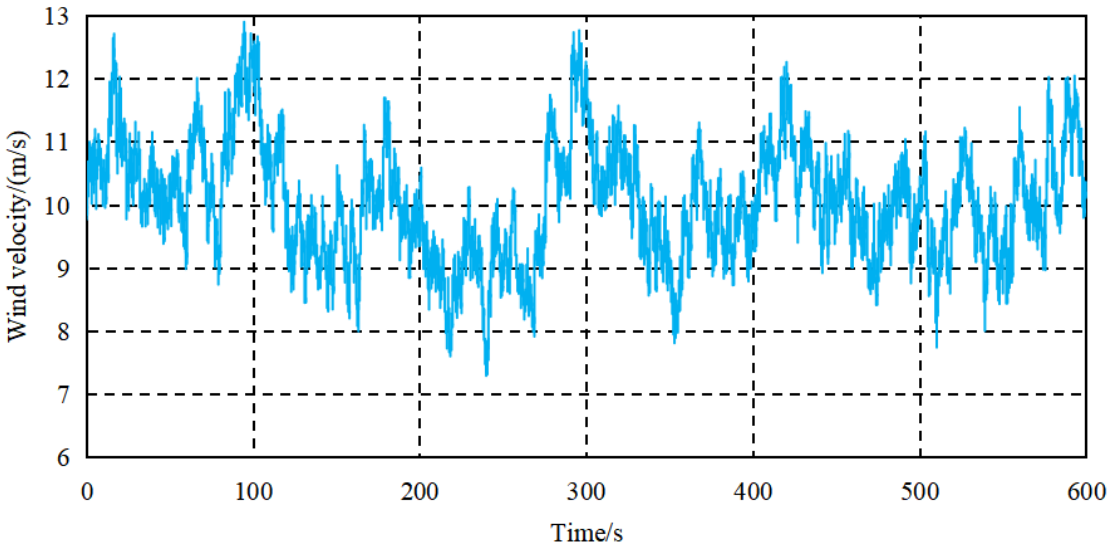

Figure 3.3 Time series plots of wind velocity of 10m/s

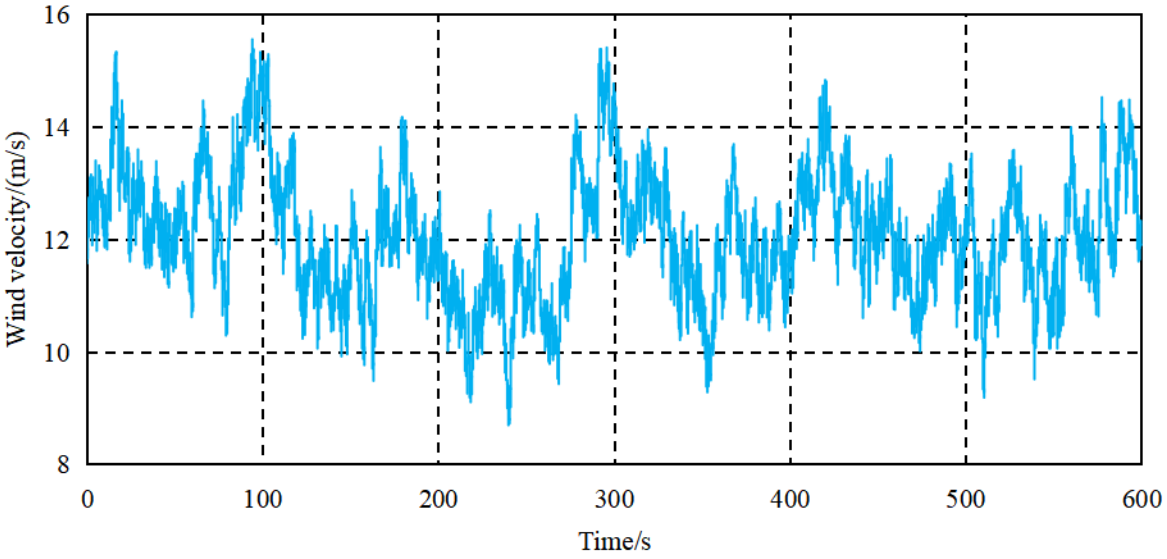

Figure 3.4 Time series plots of wind velocity of 12m/s

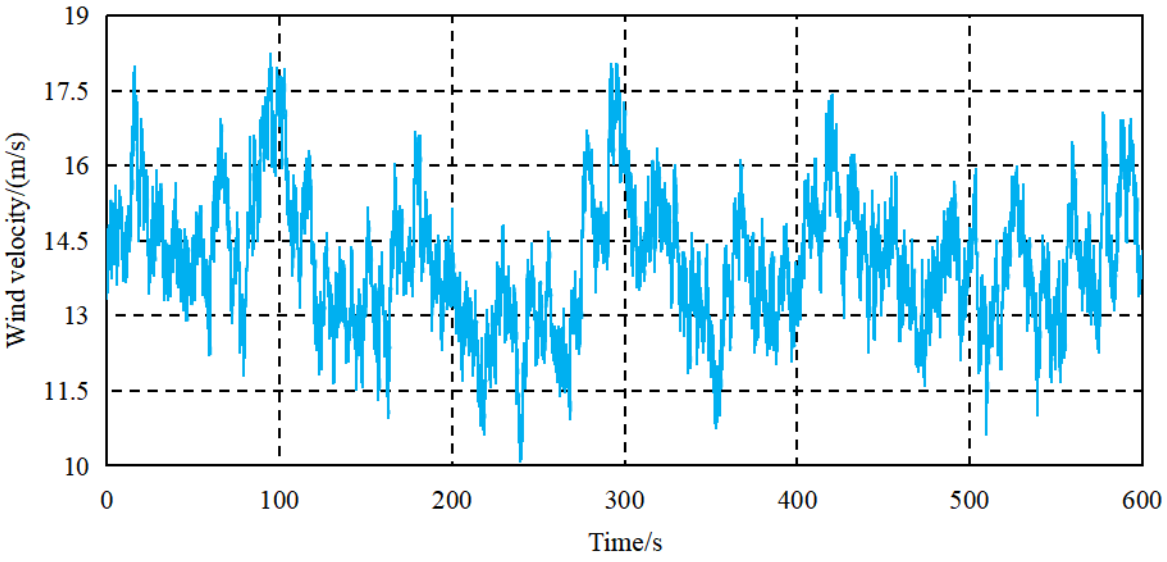

Figure 3.5 Time series plots of wind velocity of 14m/s

Chapter 4 Global Dynamic Loads

4.1 Fast Code

The dynamic response of the wind turbine yaw bearing is analysed by a time domain simulation code FAST (Jonkman & Buhl Jr, 2005) . This analysis fully couples AeroDyn which is an aerodynamic module; HydroDyn which is a hydrodynamic module; ServoDyn control which is an electrical dynamic module; and ElastoDyn which is a structural dynamic module (Jonkman & Buhl Jr, 2005).

4.1.1 AeroDyn module

AeroDyn is a time-domain wind turbine aerodynamics module which has been coupled in the FAST code to conduct an aero-elastic simulation of onshore and offshore turbines. AeroDyn is also able to be used as a standalone code to simulate aerodynamic response of wind turbines (National Renewable Energy Laboratory, 2021a).

For calculating aerodynamic loads on both the blades and tower, blade element momentum (BEM) and generalized dynamic wake (GDW) theories are used in the AeroDyn module. In the aerodynamic analysis process, tip losses, hub losses, tangential induction in BEM theory calculation and the Bessoes-Leishman dynamic stall correction are utilized (Manwell et al., 2009). These theories are chosen to meet the requirement of the time-domain aerodynamic load calculation of wind turbines.

4.1.2 HydroDyn module

HydroDyn module is a time-domain hydrodynamics module in the FAST wind turbine code. It is coupled with other modules to enable aero-hydro-servo-elastic simulation of offshore wind turbines. HydroDyn is developed for both fixed and FOWTs.

HydroDyn module can generate regular, irregular, short-crested and long-crested waves, as well as full wave kinematics and wave elevations. For finite depth, waves are generated analytically with first order theory which sometimes is termed Linear Airy alone or the combination of first order and second-order wave theory in this module (National Renewable Energy Laboratory, 2021d). HydroDyn only analyses wave kinematics in the domain between still water level (SWL) and flat seabed. It does not include wave stretching and higher wave theories. Fast

Fourier Transforms (FFTs) are used to conclude all the components of wave frequency to save computational cost (National Renewable Energy Laboratory, 2021d).

Besides, potential-flow theory is used to model the loads on the substructures and their components whose sizes are similar to a typical wavelength. Potential-flow theory and strip theory are combined using a hybrid model in the HydroDyn module and used to calculate the offshore wind turbine hydrodynamic loads. For substructures or their components which are smaller than a typical wavelength, strip theory is applied. Morison's equation for added-mass, viscous-drag components and distributed fluid inertia is contained in the strip theory loads. These theories are chosen to meet the requirement of the time-domain hydrodynamic load calculation of wind turbines.

4.1.3 ServoDyn module

To control the wind turbines in specific conditions, several basic methods are used in the ServoDyn Module. They are pith control, generator and torque control, the high-speed shaft (HSS) brake, nacelle-yaw control and tuned mass damper (National Renewable Energy Laboratory, 2021e). To speed up the calculation time, the high-speed shaft (HSS) brake, nacelle yaw control and tuned mass damper are neglected. The torque control, pitch control and generator control are chosen to be implemented. These are set up to meet the requirement of the combined time-domain load calculation of wind turbines. Besides, the choices are simply the computing process.

4.1.4 ElastoDyn module

In order to define and configure the structural model parameters of wind turbines, ElastoDyn module is coupled in FAST. The module considers the geometries and options of tower, nacelle, drivetrain and blades. Besides, initial conditions for the wind turbine structure are set by this module (National Renewable Energy Laboratory, 2021c). This research focuses on the dynamic loads on structures, thus ElastoDyn is only used to consider the gravity, initial conditions, mass and inertia and some other structural parameters related to the dynamic analysis of wind turbines. Besides, for onshore wind turbine, BeamDyn module can be used to replace the ElastoDyn module for the blade dynamics in FAST code (Jonkman & Jonkman, 2016).

4.1.5 Other modules

SubDyn module is a time-domain structural-dynamics module that developed for multimember fixed-bottom substructures which are created by the National Renewable Energy Laboratory (NREL). This module is coupled into the FAST aero-hydro-servo-elastic computer-aided engineering (CAE) code. SubDyn is used to support the following offshore wind substructures: monopiles, tripods, jackets, and other non-floating lattice-type substructures. Onshore fixed and offshore fixed wind turbines are also included in the module (National Renewable Energy Laboratory, 2021f).

SubDyn bases on two important engineering analysis models: a linear finite-element beam (LFEB) model by a frame, and a dynamics system reduction with the combination of Craig-Bampton (C-B) method and static-improvement method (SIM). The second mode is applied to reduce the mode quantity that is used to get an accurate solution (National Renewable Energy Laboratory, 2021f).

For every time step, the FAST code transfers loads and responses among SubDyn, HydroDyn and Elastodyn by using a coupling hydro-elastic interaction (National Renewable Energy Laboratory, 2021f). Besides, another important module is BeamDyn. It sometimes can be replaced by ElastoDyn as introduced in Section 4.1.4.

BeamDyn module is also developed by National Renewable Energy Laboratory (NREL) and it is a time-domain module for the structural dynamics of slender structures. This module is coupled with other modules introduced above in FAST code to model structural dynamics of blade. It is able to model composite wind turbine blades which are deformed largely in initial twisted and curved conditions (National Renewable Energy Laboratory, 2021b).

4.2 Wind Turbine Model

Six different supporting systems are selected to support the same NREL 5MW wind turbine, a horizontal-axis wind turbine which was developed by National Renewable Energy Laboratory (NREL) of the U.S. Department of Energy. The tower-top coordinate system is shown in Figure 4.1 (Jonkman & Buhl Jr, 2005). The parameters of the NREL wind turbine are shown in Table 4.1 (Jonkman & Buhl Jr, 2005). In the thesis, the tower-top coordinate system translates and rotates with the movement of the platform. However, it does not yaw with the wind turbine nacelle. Six different wind turbine platforms are chosen as the supporting foundations. Onshore

and monopile supports are conventional land-based wind turbine platforms. The ITI barge is a preliminary barge concept developed by the Department of Naval Architecture and Marine Engineering at the Universities of Glasgow and Strathclyde in conjunction with ITI Energy (Robertson & Jonkman, 2011). The Tension Leg Platform is designed by Massachusetts Institute of Technology (MIT) and NREL (Robertson & Jonkman, 2011). It will be referred to as TLP in this paper. The spar platform is an OC3-Hywind spar buoy developed within the Offshore Code Comparison Collaboration (OC3), which is a project operated under Subtask 2 of the International Energy Agency (IEA) Wind Task 23 (Robertson & Jonkman, 2011) and will be referred to as spar in this thesis. The UMaine semisubmersible is a generic model of a semisubmersible created by the University of Maine DeepCwind project and will be referred to as semi-submersible in this thesis (Robertson & Jonkman, 2011) . For these six kinds of wind turbines, the same yaw bearings are all mounted on the top of towers. The varying supports give rise to different motions. As a result, the yaw bearings of the different wind turbines respond differently to the same wind environment. The six NREL 5MW wind turbine concepts are shown in Figure 4.2 (Robertson & Jonkman, 2011).

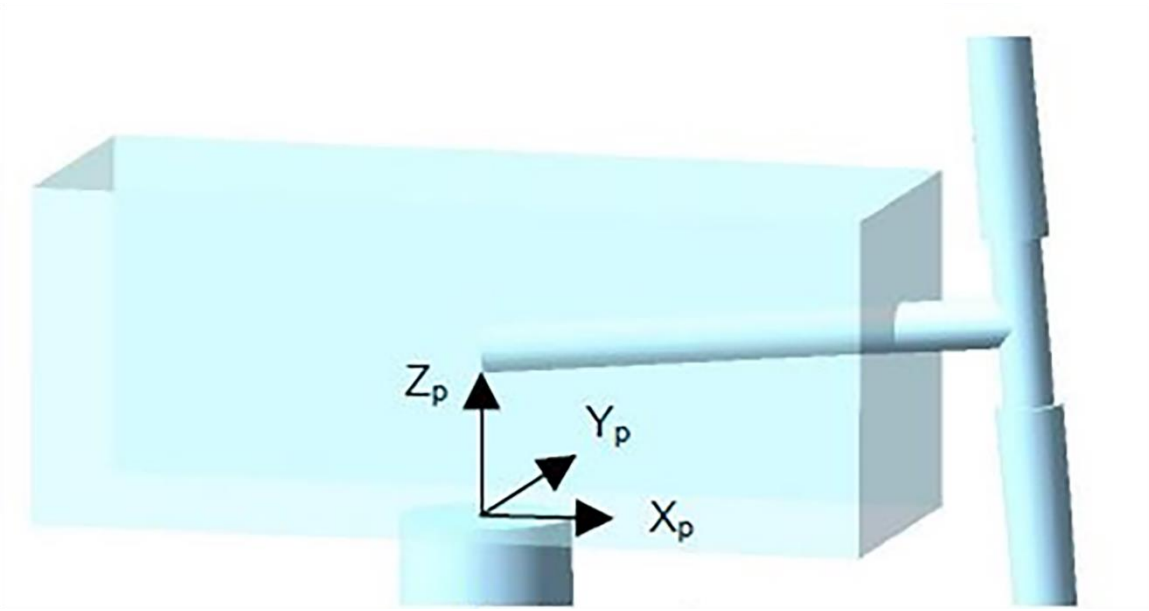

Figure 4.1 Tower-top coordinate system

(Jonkman & Buhl Jr, 2005)

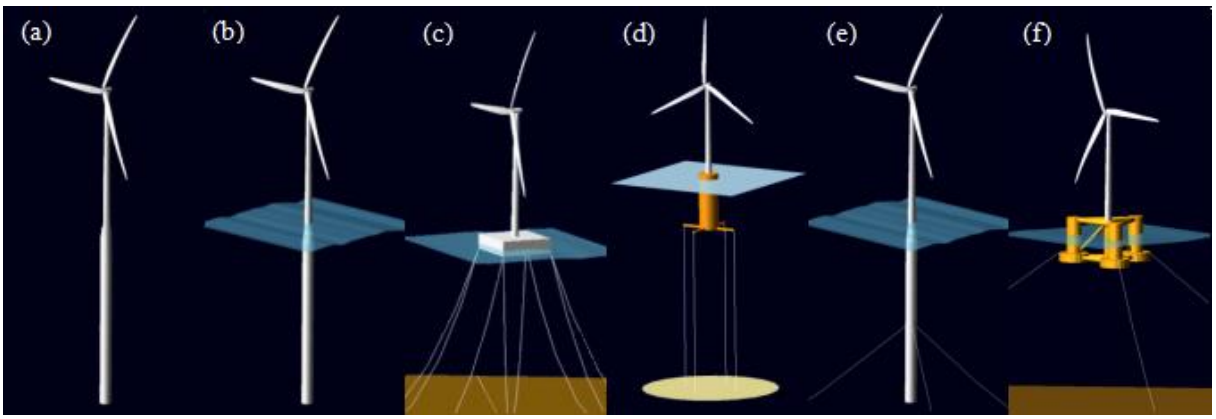

Figure 4.2 Computer model of the six NREL 5MW wind turbines

((a)onshore,(b)monopile, (c)ITI barge, (d)TLP, (E)spar, (f)semisubmersible)

(Robertson & Jonkman, 2011)

Item	Description
Wind turbine class	IEC61400-3, IB
Rating	5 MW
Rotor orientation, configuration	Upwind, 3 blades
Rotor, hub diameter	126 m, 3 m
Hub height	90 m
Cut-in, cut-out wind speed	3 m/s, 25 m/s
Rated wind speed	11.4 m/s
Cut-in, rated rotor speed	6.9 rmp, 12.1 rmp
Rated tip speed	80 m/s
Overhang, shaft tilt, precone	5 m, 5 ˚, 2.5 ˚
Rotor mass	110 t
Nacelle mass	240 t
Tower mass	347.46 t

Table 4.1 The specification of NREL 5MW turbine

(Jonkman & Buhl Jr, 2005)

4.3 Time Series Dynamic Load Result

In this section, the time series loads of yaw bearing on the case study wind turbines are calculated. Three representative turbulent wind fields are applied. To ensure calculation accuracy, the first five percent of the time series load are omitted. Figure 4.3 to Figure 4.8 show the X-direction, Y-direction, Z-direction forces and X-direction, Y-direction, Z-direction moment of the yaw bearing at 10 m/s. Figure 4.9 to Figure 4.14 show the X-direction, Y-direction, Z-direction forces and X-direction, Y-direction, Z-direction moment of the yaw bearing at 12 m/s. Figure 4.15 to Figure 4.20 show the X-direction, Y-direction, Z-direction forces and X-direction, Y-direction, Z-direction moment of the yaw bearing at 14 m/s. To reduce the calculation error, the first five percent of the whole-time history is ignored.

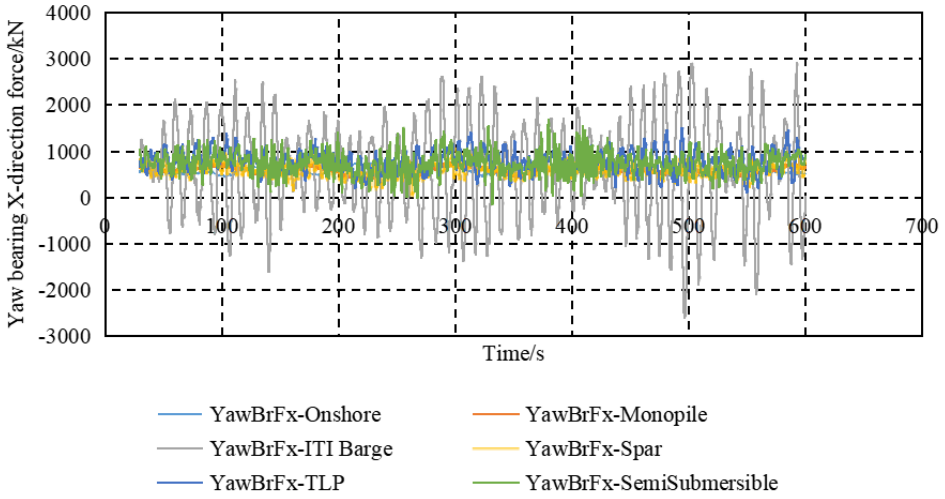

Figure 4.3 Yaw bearing X-direction force at 10m/s for six wind turbines

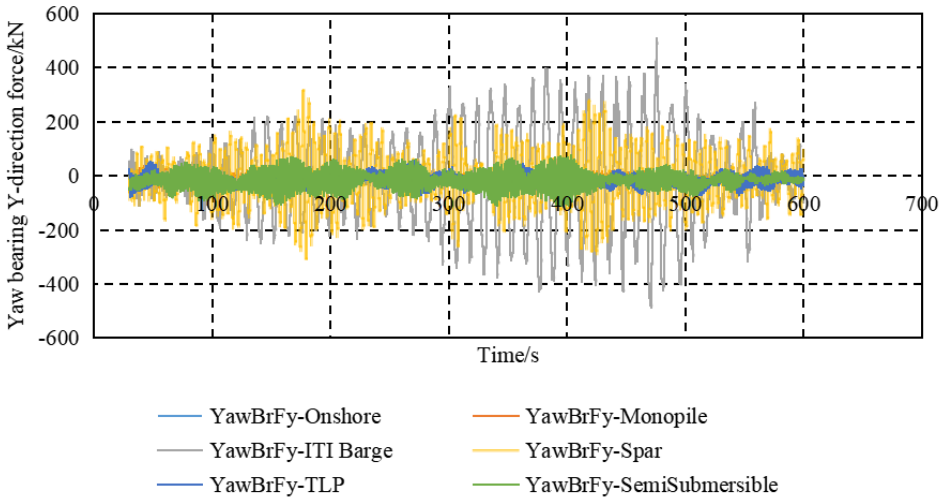

Figure 4.4 Yaw bearing Y-direction force at 10m/s for six wind turbines

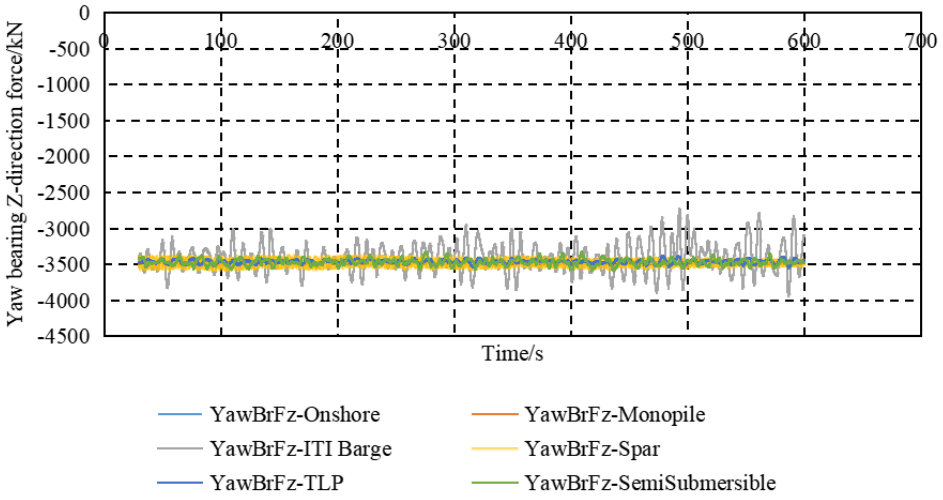

Figure 4.5 Yaw bearing Z-direction force at 10m/s for six wind turbines

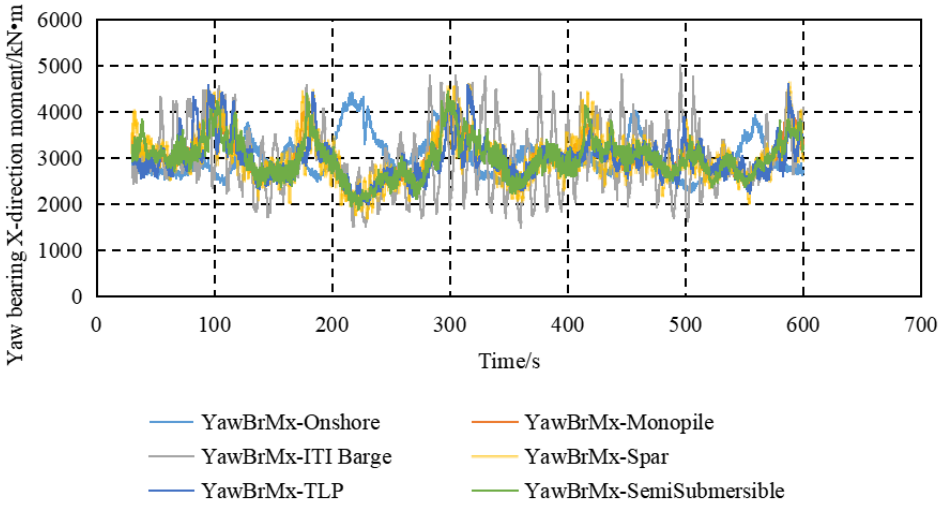

Figure 4.6 Yaw bearing X-direction moment at 10m/s for six wind turbines

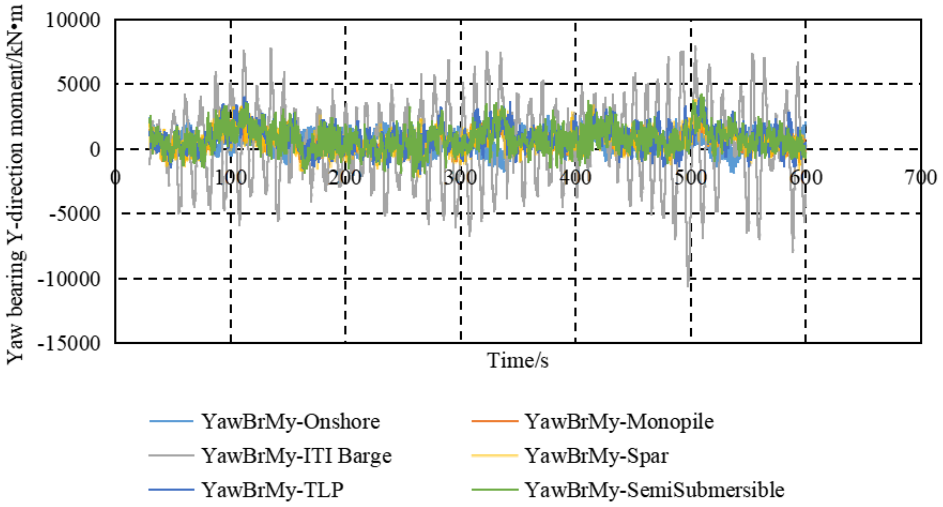

Figure 4.7 Yaw bearing Y-direction moment at 10m/s for six wind turbines

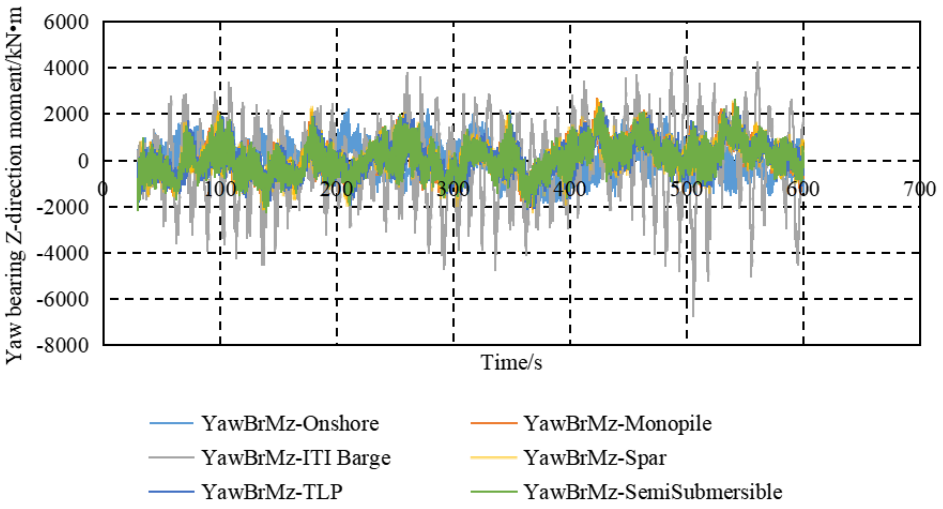

Figure 4.8 Yaw bearing Z-direction moment at 10m/s for six wind turbines

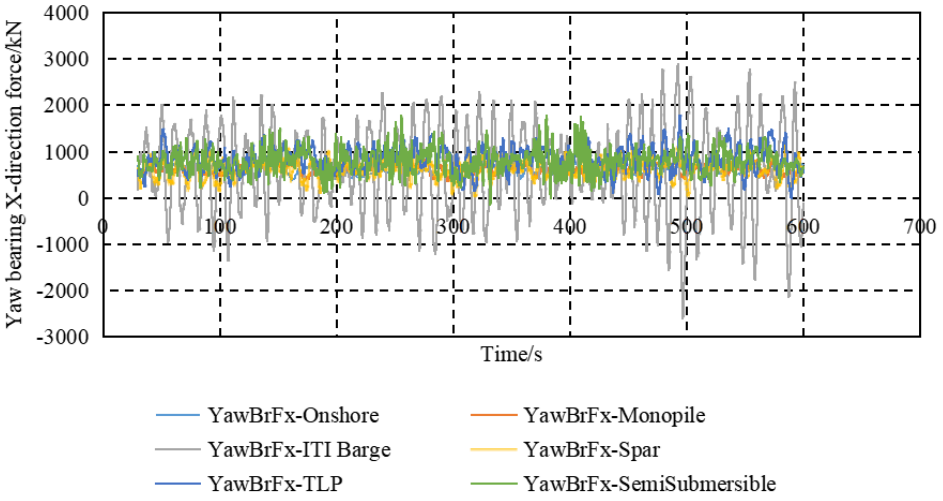

Figure 4.9 Yaw bearing X-direction force at 12m/s for six wind turbines

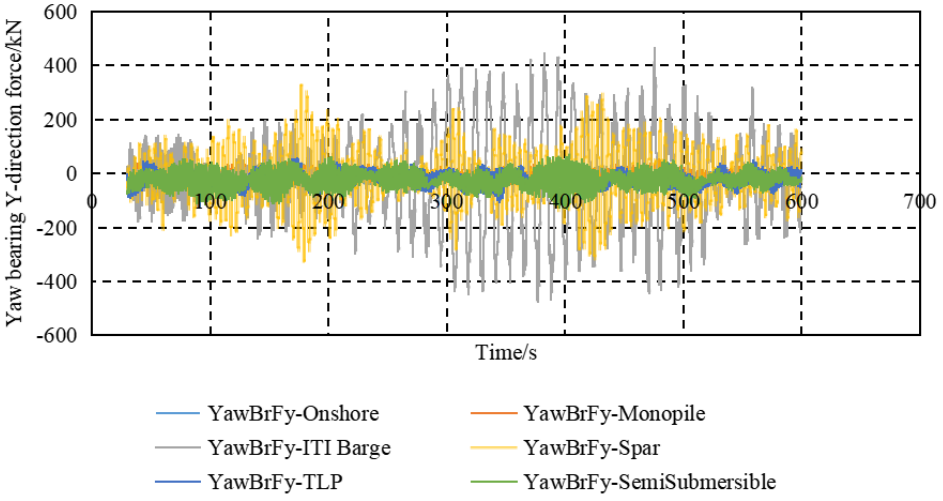

Figure 4.10 Yaw bearing Y-direction force at 12m/s for six wind turbines

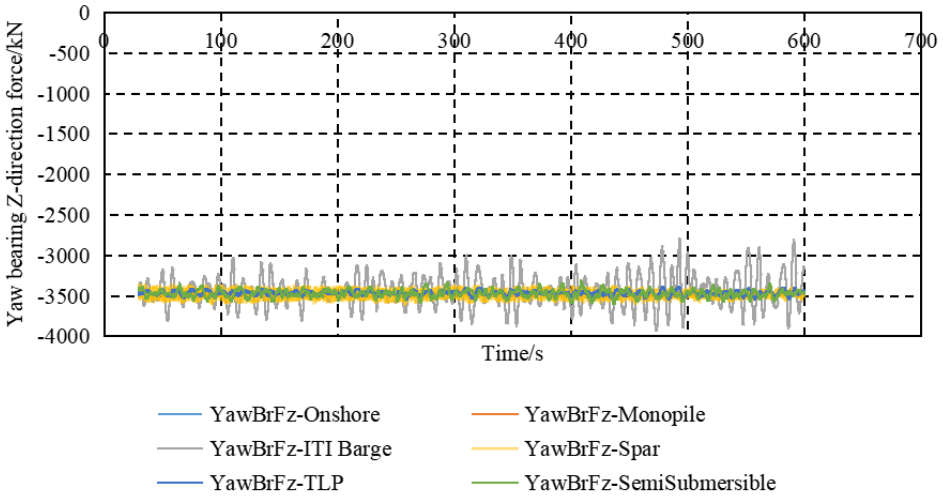

Figure 4.11 Yaw bearing Z-direction force at 12m/s for six wind turbines

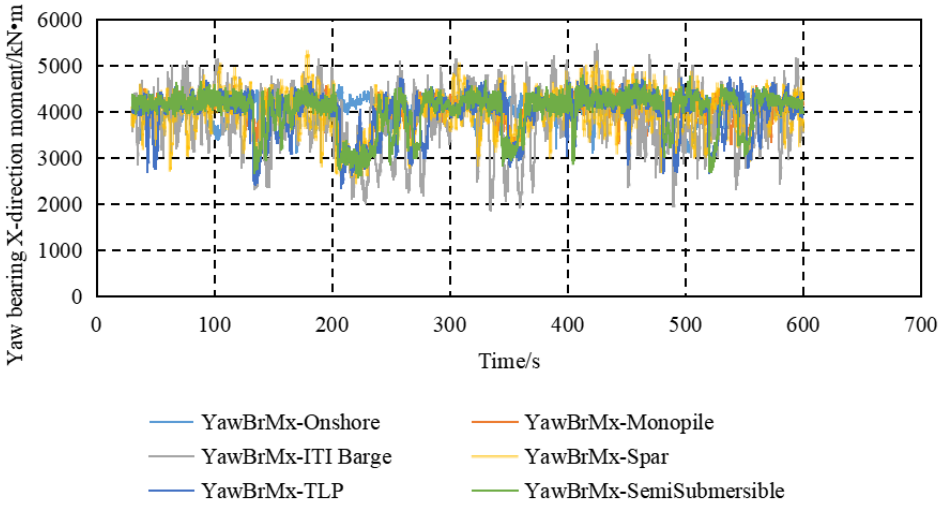

Figure 4.12 Yaw bearing X-direction moment at 12m/s for six wind turbines

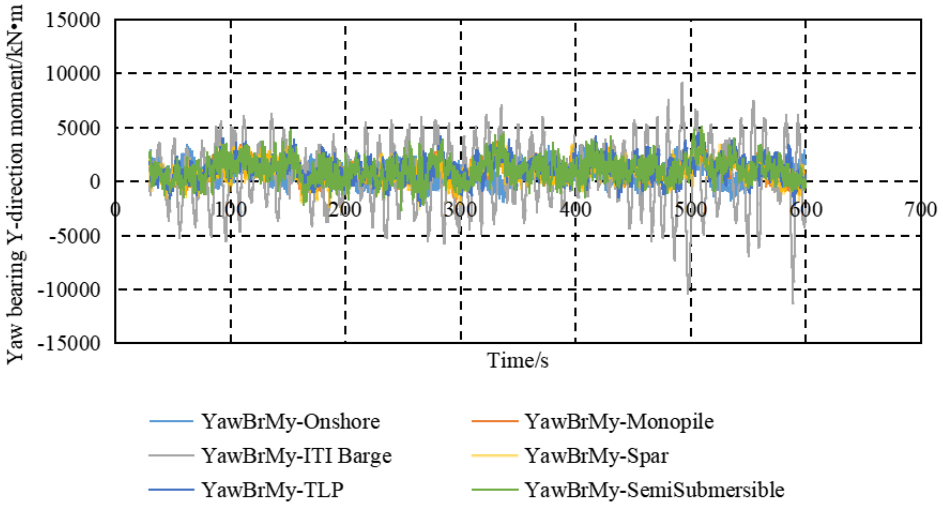

Figure 4.13 Yaw bearing Y-direction moment at 12m/s for six wind turbines

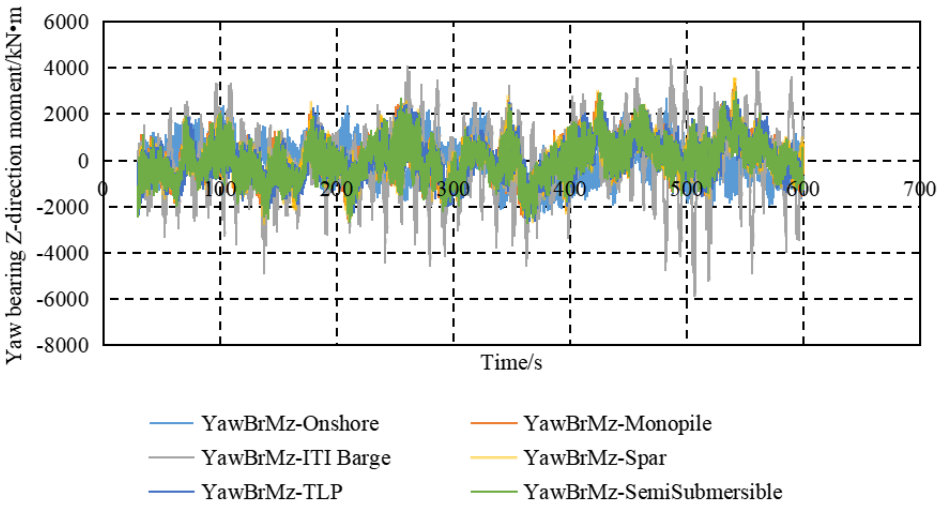

Figure 4.14 Yaw bearing Z-direction moment at 12m/s for six wind turbines

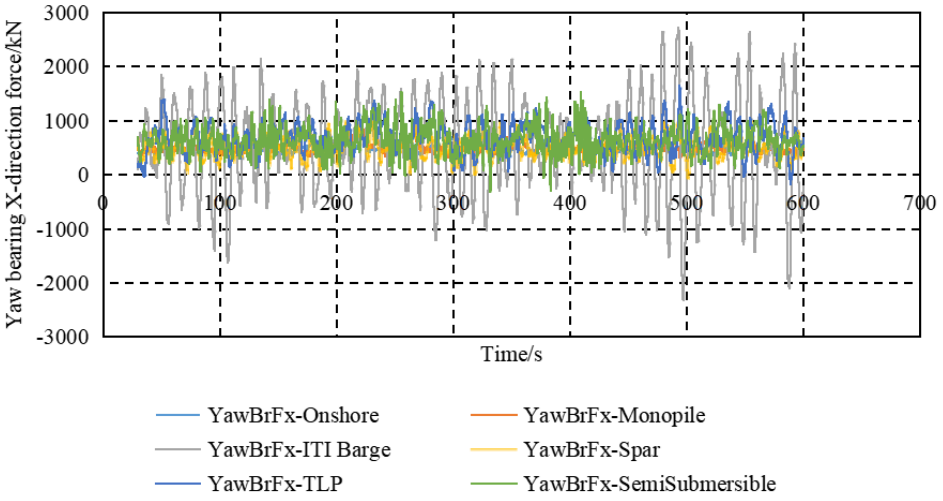

Figure 4.15 Yaw bearing X-direction force at 14m/s for six wind turbines

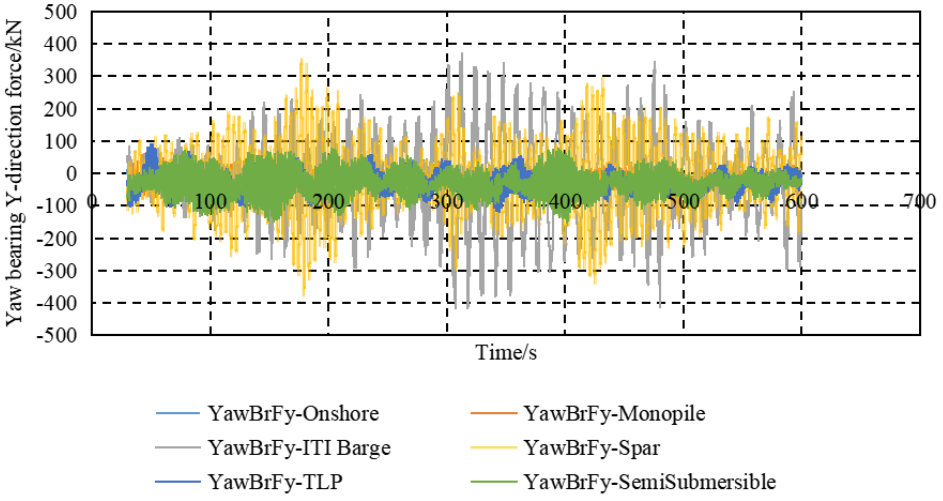

Figure 4.16 Yaw bearing Y-direction force at 14m/s for six wind turbines

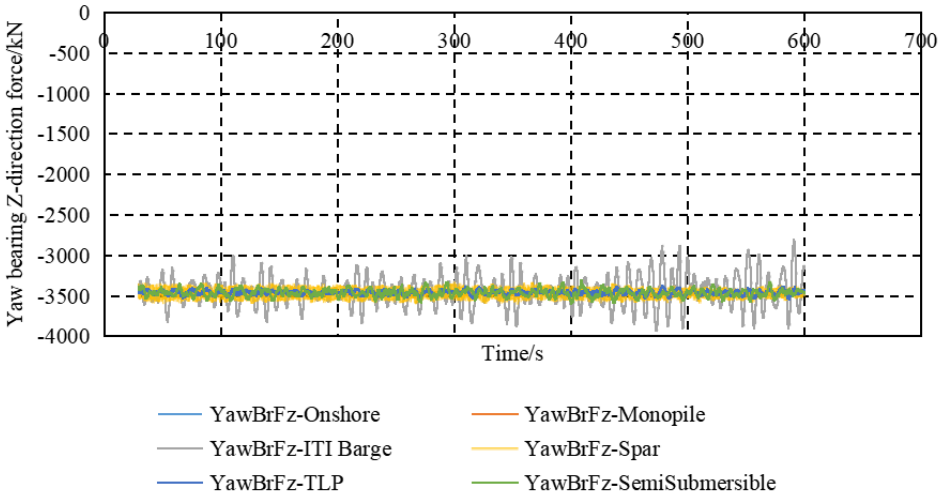

Figure 4.17 Yaw bearing Z-direction force at 14m/s for six wind turbines

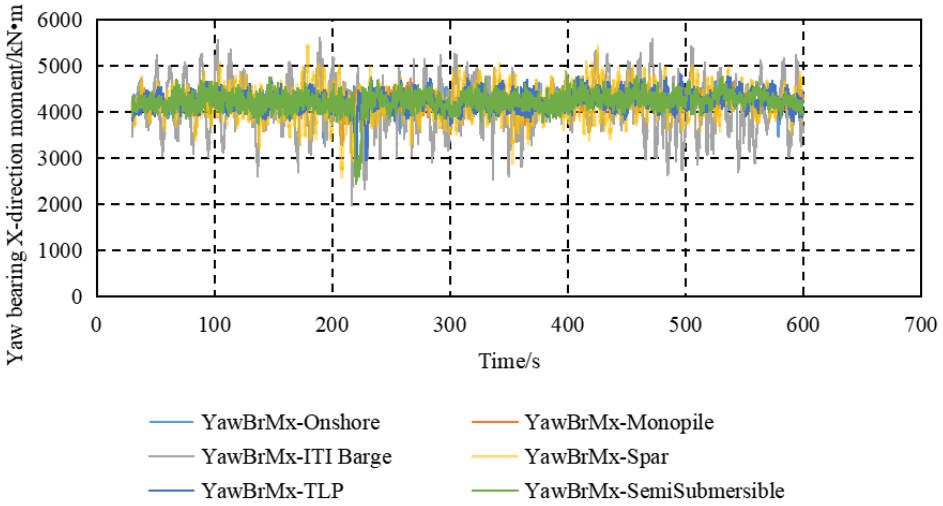

Figure 4.18 Yaw bearing X-direction moment at 14m/s for six wind turbines

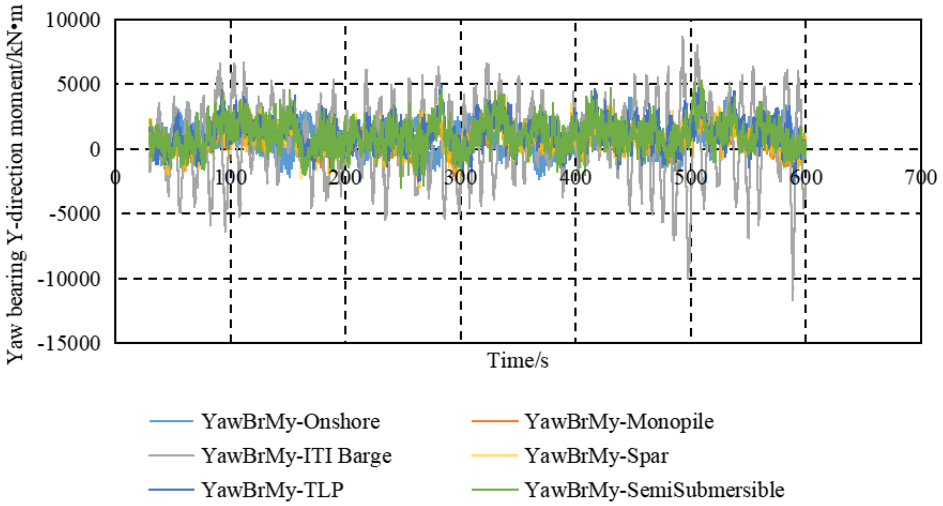

Figure 4.19 Yaw bearing Y-direction moment at 14m/s for six wind turbines

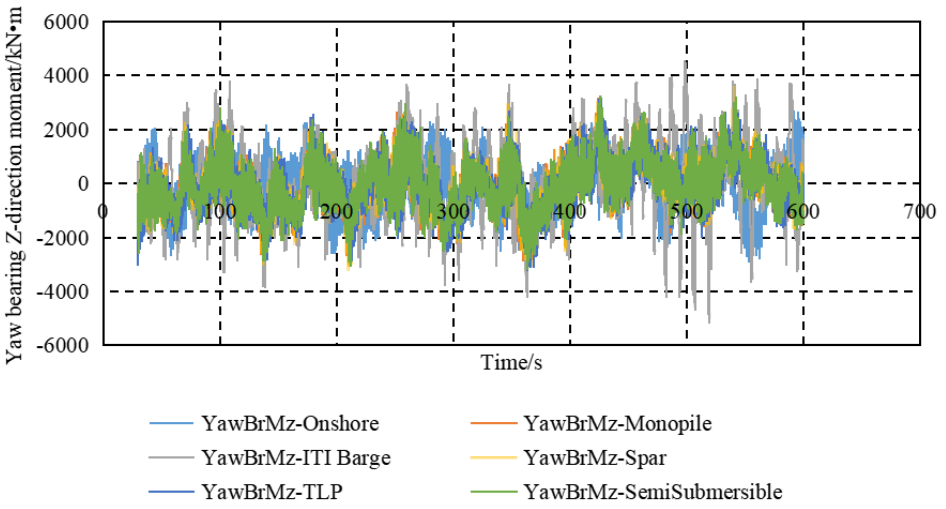

Figure 4.20 Yaw bearing Z-direction moment at 14m/s for six wind turbines

Chapter 5 Damage Equivalent Load

5.1 Damage Equivalent Load Theory

In the design process of a yaw bearing, fatigue loads are important because they are the main reason for bearing failure (Harris et al., 2009).

Annex G of the IEC-61400-1 onshore wind turbine design standard (International Electrotechnical Commission, 2005) and the IEC-61400-3 offshore wind turbine design standard (International Electrotechnical Commission, 2009) can predict fatigue damage equivalent loads resulting from short-term dynamic loads. The Block-Maximum method and Gumbel distribution method are combined to generate the ultimate loads of the yaw bearing. Then, the damage equivalent load is estimated by the combination of a rain flow counting algorithm, the linear cumulative damage law and S-N curve theory (Moriarty et al., 2004).

The equations below show the Gumbel distribution function $F(x;\mu,\beta)$and density function $f(x)$:

$$F(x;\mu,\beta) = e^{-e^{-\frac{(x-\mu)}{\beta}}} \qquad \text{Equation 5.1}$$

$$f(x) = \frac{1}{\beta} e^{-\frac{(x-\mu)}{\beta} - e^{-\frac{(x-\mu)}{\beta}}} \qquad \text{Equation 5.2}$$

where x is the ultimate load, μ and β are Gumbel distribution parameters.

The Block-Maximum method is used in the wind turbine exceeding probabilistic function:

$$F = \left(1 - \frac{1}{p_f}\right)^{\frac{1}{N}} \qquad \text{Equation 5.3}$$

where p_f is the wind turbine failure probability. The design life for wind turbine is 20 years (Harris et al., 2009). This means there are 1051200 groups of 10-minute periods during the design life and therefore p_f is no more than $1/1051200$. N is the block number of short-term dynamic loads. 10 groups of 10 minutes short-term dynamic loads are generated for each turbulent wind model. $10N$ maximum array M are then fitted with a Gumbel distribution (Moriarty et al., 2004).

The ultimate load L_{ult} can then be estimated by:

$$L_{ult} = \mu - \beta\, ln(-ln(F)) \qquad \text{Equation 5.4}$$

On the basis of Miner's cumulative damage rule, the total damage D on the wind turbine is:

$$D = \sum_i \frac{n_i}{N_i(L_i^{RF})} \qquad \text{Equation 5.5}$$

where n_i is the cycle count of the i^{th} load, N_i is the cycle number to failure of the i^{th} load, L_i^{RF} is the cycle load range about a fixed load-mean value.

The relationship between the load range and the number of cycles of failure is expressed by an S-N curve with a Goodman correction equation:

$$N_i = \left(\frac{L_{ult} - |L^{MF}|}{\frac{1}{2}L_i^{RF}}\right)^m \qquad \text{Equation 5.6}$$

$$L_i^{RF} = L_i^R \left(\frac{L_{ult} - |L^{MF}|}{L_{ult} - |L_i^M|}\right) \qquad \text{Equation 5.7}$$

where L^{MF} is the fixed load-mean, m is the Whöler exponent, and $m = 3$ for yaw bearing loads (Harris et al., 2009).

The fatigue damage equivalent load DEL with constant amplitude are calculated by:

$$D = \sum_i \frac{n_i}{N_i} = \frac{n^{eq}}{N^{eq}} \qquad \text{Equation 5.8}$$

$$n^{eq} = f^{eq} T \qquad \text{Equation 5.9}$$

$$N^{eq} = \left(\frac{L_{ult} - |L^{MF}|}{\frac{1}{2}DEL}\right)^m \qquad \text{Equation 5.9}$$

$$DEL = \left(\frac{\sum_i \left(n_i (L_i^{RF})^m\right)}{n^{eq}}\right)^{\frac{1}{m}} \qquad \text{Equation 5.10}$$

where f^{eq} is DEL frequency, T is the time of time series load, n^{eq} is the total equivalent fatigue counts for time series load, N^{eq} is the equivalent number of cycles until failure for the time series load.

To obtain accurate results and minimise the time cost, fatigue damage equivalent load DEL_{agg} is analysed with an aggregate array of 10 groups of time series dynamic loads:

$$DEL_{agg} = \left(\frac{\sum_j \left(\sum_i \left(n_i \left(L_i^{RF} \right)^m \right) \right)}{\sum_j n_j^{eq}} \right)^{\frac{1}{m}} \qquad \text{Equation 5.11}$$

Examples of damage equivalent loads are shown in the following sections. The damage equivalent loads are different for each wind velocity. The results of ITI barge are the maximum among all wind speeds, for which the force is about two times larger than the fixed turbine and the moment is approximately one and half times larger.

5.2 Damage Equivalent Load Result

Fatigue damage equivalent loads for yaw bearings are calculated from the time-series loads. They are divided into DEL forces and DEL moments in Sections 5.2.1 and 5.2.2. Besides, a group of short-term dynamic loads of an onshore wind turbine at 10m/s is shown in the form of a rain flow matrix. Figures 5.1, 5.2, 5.3 show the short-term dynamic forces on the yaw bearing in onshore wind turbine at 10m/s in the X-, Y- and Z- directions respectively. Figures 5.4, 5.5, 5.6 show the short-term dynamic moments on the yaw bearing in onshore wind turbine at 10m/s in the X-, Y- and Z- directions respectively.

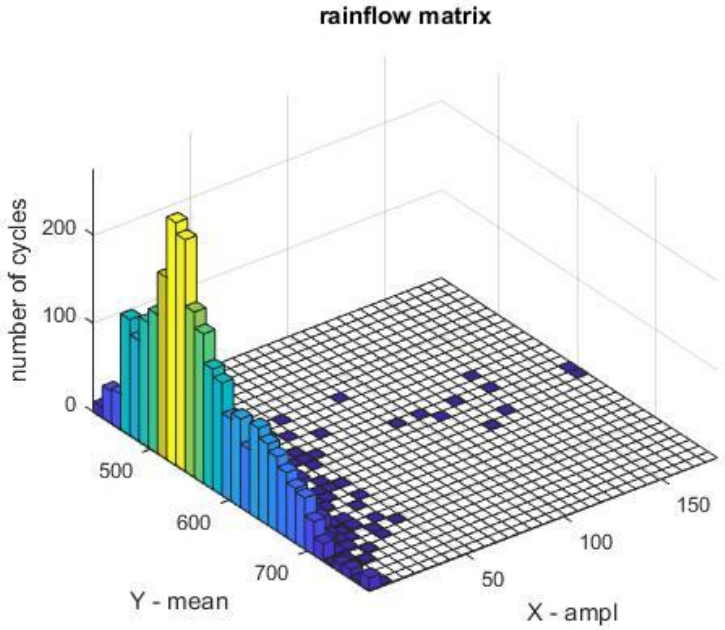

Figure 5.1 A short-term dynamic X-direction force of onshore wind turbine at 10 m/s

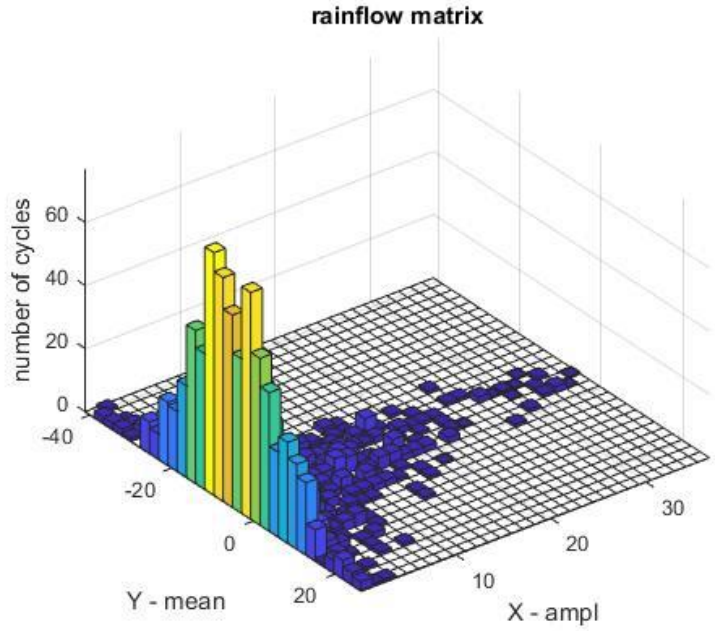

Figure 5.2 A short-term dynamic Y-direction force of onshore wind turbine at 10 m/s

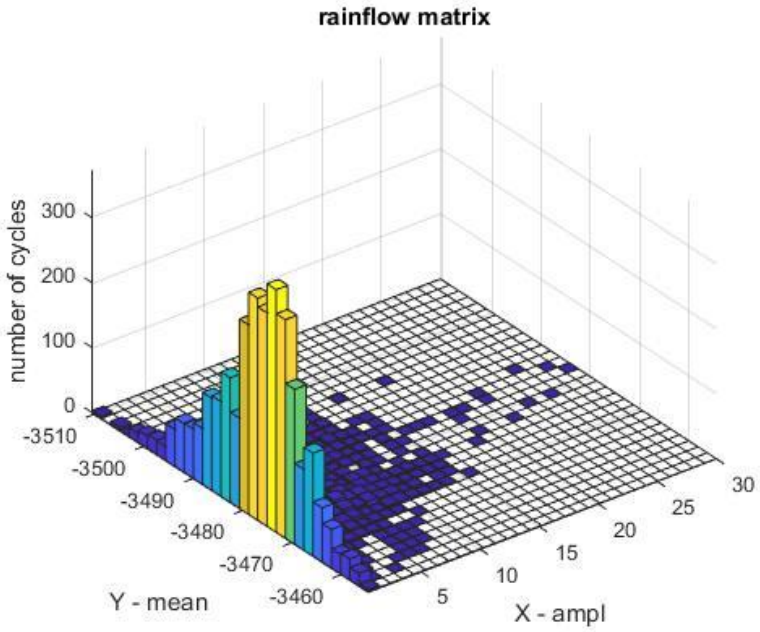

Figure 5.3 A short-term dynamic Z-direction force of onshore wind turbine at 10 m/s

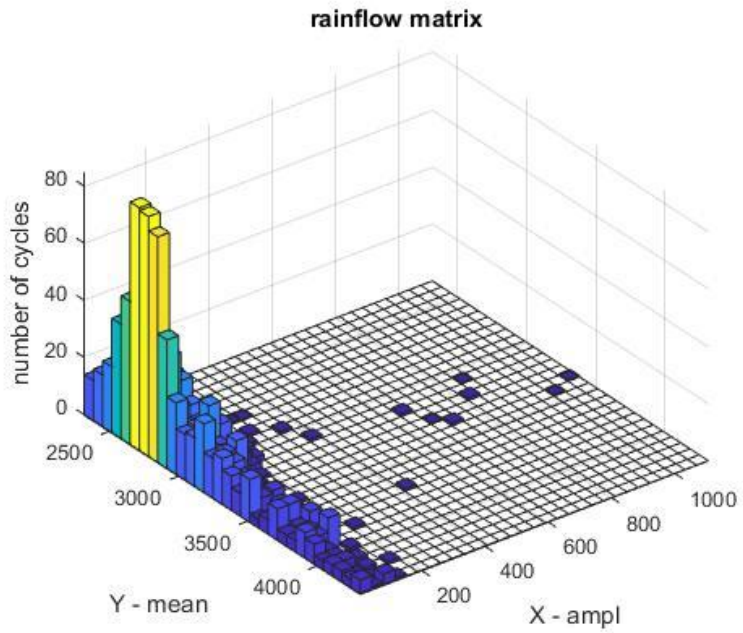

Figure 5.4 A short-term dynamic X-direction moment of onshore wind turbine at 10 m/s

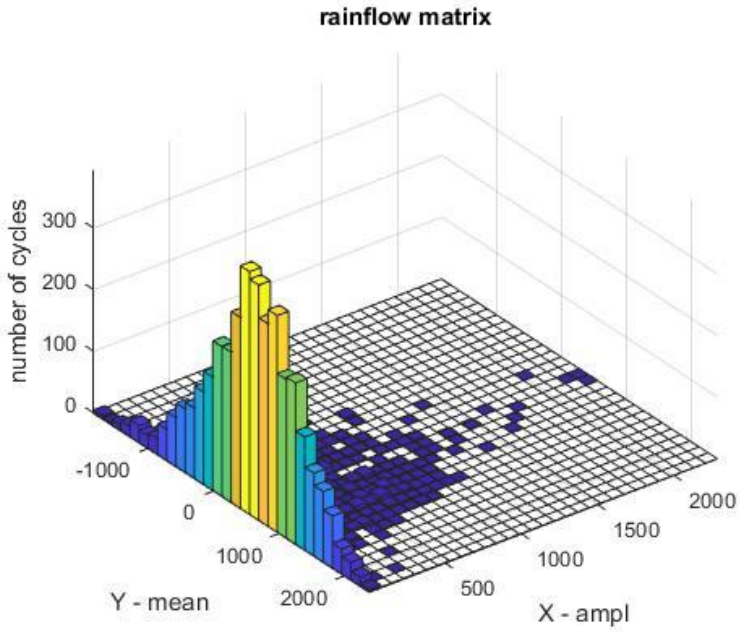

Figure 5.5 A short-term dynamic Y-direction moment of onshore wind turbine at 10 m/s

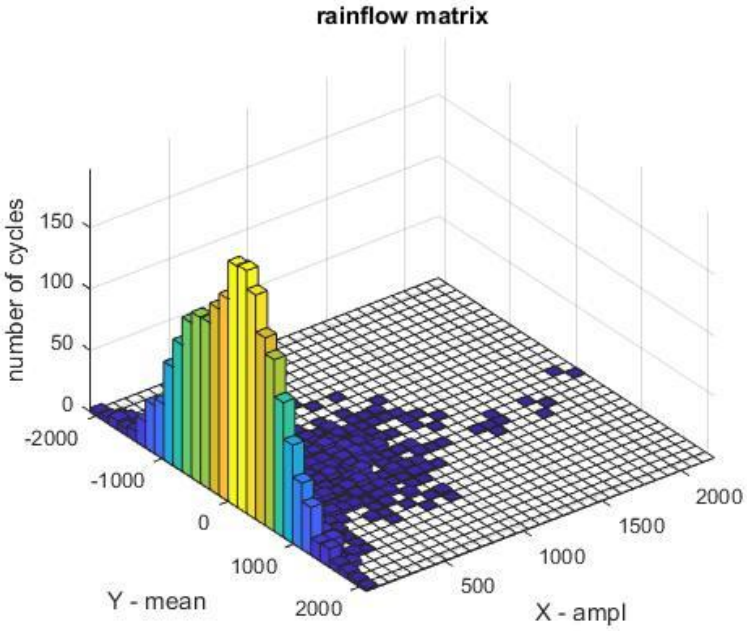

Figure 5.6 A short-term dynamic Z-direction moment of onshore wind turbine at 10 m/s

5.2.1 Damage equivalent force

Damage equivalent forces of yaw bearing for the six wind turbines at all three wind conditions are calculated and compared below. Figures 5.7, 5.8, 5.9 show the damage equivalent forces on the yaw bearing in onshore wind turbine at different wind velocities in the X-, Y- and Z-directions respectively.

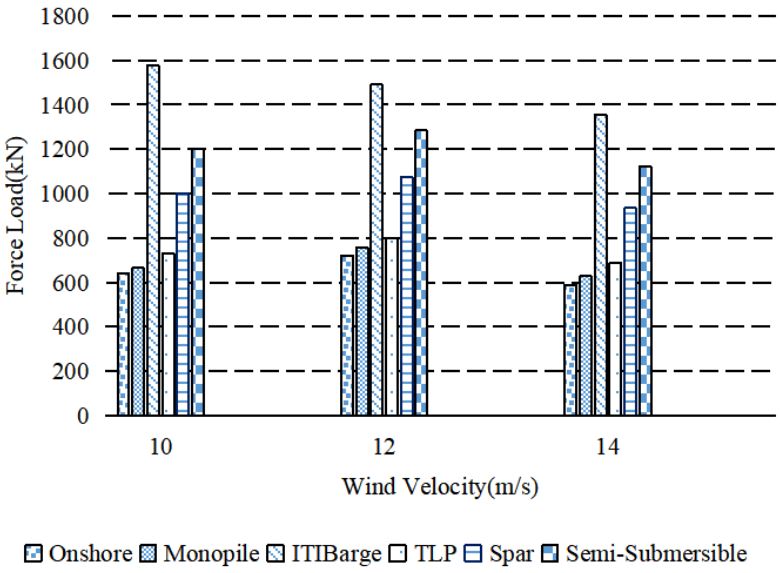

Figure 5.7 Damage equivalent force in X-direction

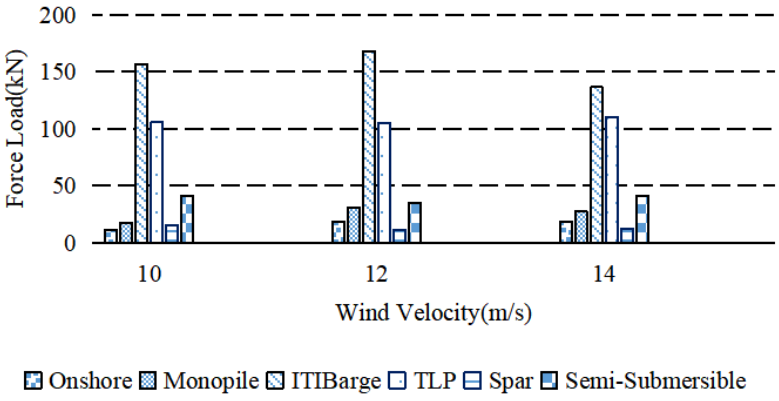

Figure 5.8 Damage equivalent force in Y-direction

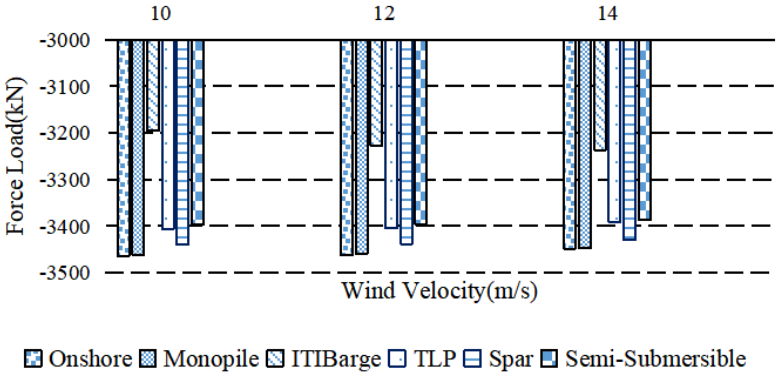

Figure 5.9 Damage equivalent force in Z-direction

5.2.2 Damage equivalent moment

Damage equivalent moments of yaw bearing for the six wind turbines at all three wind conditions are calculated and compared below. Figures 5.10, 5.11, 5.12 show the damage equivalent moments on the yaw bearing in onshore wind turbine at different wind velocities in the X-, Y- and Z- directions respectively.

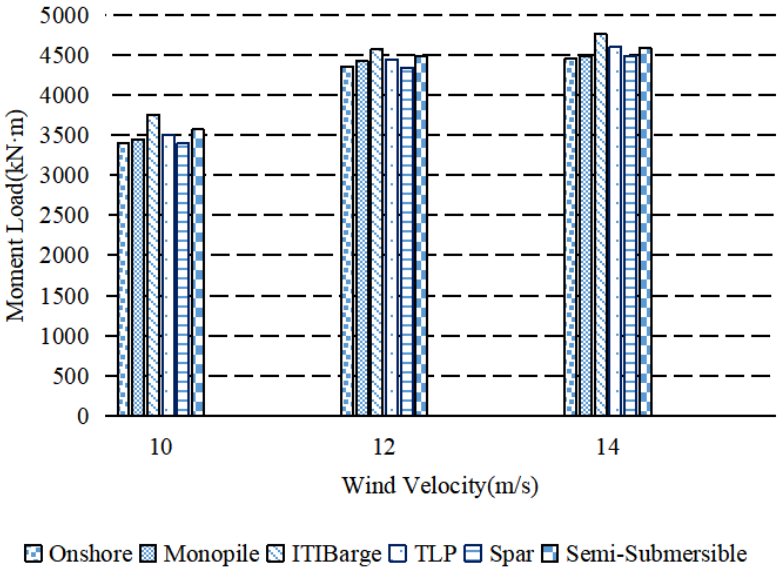

Figure 5.10 Damage equivalent moment in X-direction

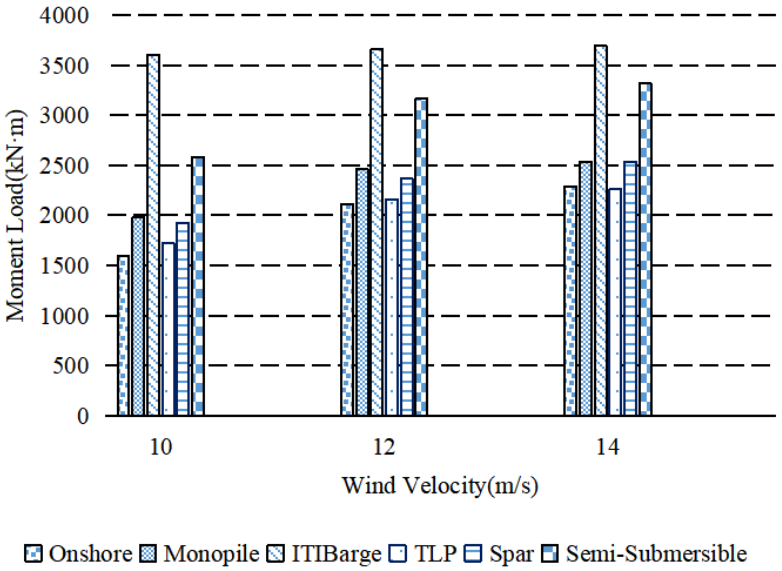

Figure 5.11 Damage equivalent moment in Y-direction

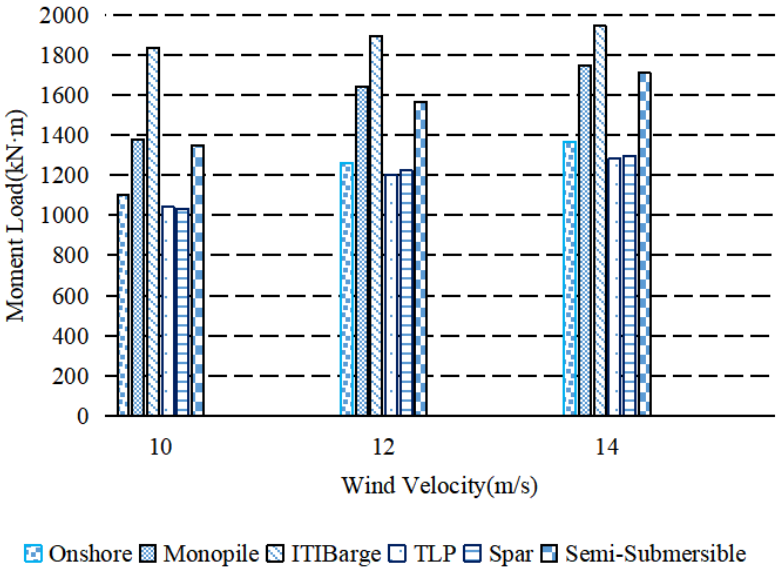

Figure 5.12 Damage equivalent moment in Z-direction

5.3 Summary

In this section, the damage equivalent loads of yaw bearing at different working conditions are calculated. The results show that:

•The damage equivalent loads on a yaw bearing in an onshore wind turbine are smaller than in offshore wind turbines, except in the Z-direction force.

•The forces on the ITI Barge wind turbine are significantly larger than the other wind turbines, except in the Z-direction force.

•The results of ITI Barge wind turbine and TLP wind turbine are significantly larger in the Y-direction force than other wind turbines.

•The results of ITI Barge wind turbine and Semi-Submersible wind turbine are significantly larger in the X-direction force and in the Y-direction moment.

•The results of Onshore wind turbine and Monopile wind turbine are similar in all direction forces and in the X-direction moment.

•In terms of forces in all directions, the results of the TLP wind turbine are similar in different wind velocities.

•In terms of forces in all directions, the results of the Spar wind turbine are similar in different wind velocities.

•The moment results of the TLP wind turbine increase with wind velocity in all directions.

•The moment results of the Spar wind turbine increase with wind velocity in all directions.

•All the wind turbines show smaller forces in the Y-direction and larger forces in the Z-direction.

•All the wind turbines show smaller moments in the Z-direction and larger moments in the X-direction.

•Within different wind velocities, the X-direction moments in different wind turbines are similar.

•All the wind turbines show a similar pattern of load fluctuation within the different wind velocities.

Based on the calculations in this section, it is necessary to conduct further and detailed analysis of the yaw bearing with a more precise method to study more deeply the reason for the difference in fatigue life. Six DELs are dealt with different methods based on the design guidelines by NREL (Harris et al., 2009). In the guidelines, F_r is radial load, F_a is axial load and M is moment. F_x, F_y, F_z are the damage equivalent forces in the X-, Y-, Z- directions respectively. M_x, M_y, M_z are the damage equivalent moments in the X-, Y-, Z- directions respectively. In this research, F_x, F_y are converted into F_r, and F_z is equivalent to F_a. M_x, M_y are converted into M and M_z is neglected as the moment in this direction is not used for the fatigue theoretical calculations in current design guidelines. The fatigue life of yaw bearings under different working conditions is considered as a major aspect of this research and is introduced in detail in the next chapter.

Chapter 6 Fatigue Life

The damage equivalent loads calculated in Chapter 5 are applied to the yaw bearing FE model to calculate fatigue life in this chapter. The fatigue life results are compared to the ones calculated by a code-based approach. A solid element model of the yaw bearing was created in ABAQUS (Dassault Systems, 2017). The ABAQUS implicit dynamic solver is chosen for the analysis. The load is applied linearly to the required level. The greatest challenge of the global yaw bearing finite element model is convergence issue. For the computational efficiency of the analysis, a symmetrical semi-circle yaw bearing model is built. There are 64 rolling balls in the half model, and they are contacted with inner ring and outer ring separately, thus totally 128 contact pairs exist in the yaw bearing model.

6.1 Yaw Bearing Data

To meet the assembly requirements for both the onshore and offshore wind turbines, a single yaw bearing suitable for all the wind turbine case studies was selected. The ball material is GCr15 and ring material is 42CrMo following research conducted by Göncza et al. and He et al. (Göncza et al., 2010; He et al., 2018). The structure of the yaw bearing is shown in Figure 6.1.

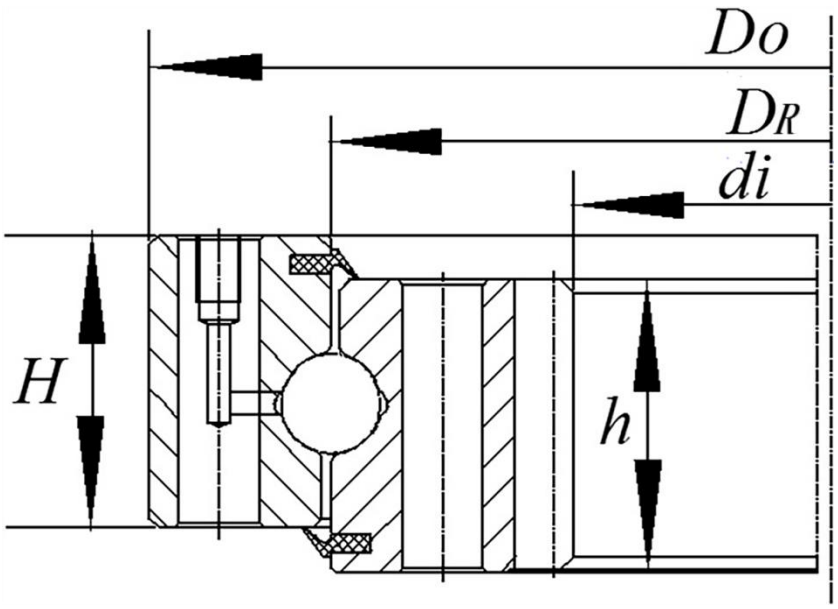

Figure 6.1 Structure of the yaw bearing

where D_O is outer ring diameter, D_R is raceway centre diameter, d_i is inner ring diameter, H is outer ring height, h is inner ring height.

The parameters of yaw bearing are shown in Table 6.1.

Parameter	Value
D_O (mm)	3776
D_R (mm)	3322
d_i (mm)	3550
H (mm)	162
h (mm)	162
i	1
D_w (mm)	75
r (mm)	11.668
α (°)	45
Z	128

Table 6.1 Parameters for yaw bearing

where i is row number, D_w is ball diameter, r is groove curvature radius, α is contact angle, Z is ball number.

The material properties for balls and two rings are shown in Table 6.2 (He et al., 2018).

	Ball	Ring
Material	GCr15	42CrMo
E (GPa)	207	212
v	0.3	0.3
K' (MPa)	1173	5808
n'	0.0932	0.1550
$\sigma_f{}'$	1511	2425
$\varepsilon_f{}'$	1.3943	0.1167

Table 6.2 Material properties for ball and ring

where E is Young's modulus, v is poissons ratio, K' is cyclic strength coefficient, n' is cyclic strain hardening exponent, $\sigma_f{}'$ is fatigue strength coefficient, $\varepsilon_f{}'$ is fatigue extension coefficient.

6.2 FEA Model

In this section, a finite element analysis (FEA) model is built with the yaw bearing data introduced above.

6.2.1 Model building and case running

The element sizing is chosen to ensure accuracy whilst keeping computation times manageable. A refined element size of 4mm is chosen to mesh the contact area of the ring raceway and ball surface (He et al., 2018). The element size is set as 20mm in other parts of the rings following (He et al., 2018). The two element sizes are chosen for the accuracy of results and efficiency of calculations. The element type for the model is C3D8R which is suitable for contact calculation. The element shape is Hex-dominated. The Medial Axis Algorithm is chosen for this FE model.

The DEL loads are applied to the FE yaw bearing model. To achieve convergence of the model, loads are applied step by step. The boundary conditions represent the working conditions of the yaw bearing. A fully fixed restraint is applied to the bottom of the inner ring and an asymmetrical constraint is set at the sections of rings. The rolling balls are restricted to only move in three degrees of freedom but are free to rotate. Differing from other fixed structures in a wind turbine, the interaction within the yaw bearing is important. The contact between the rolling balls and rings are set as general contact with small sliding. The friction coefficient in tangential behaviour is 0.05. The coordinate system of the loads is shown in Figure 6.2. The steps of forces applied on FE model are shown in Figure 6.3. The nondimensional load history is shown in Figure 6.4.

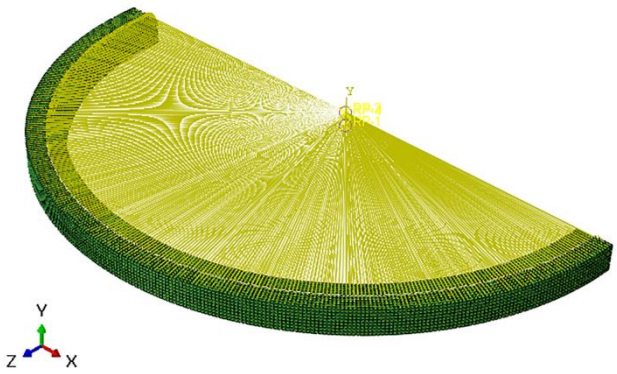

Figure 6.2 Yaw bearing FE model

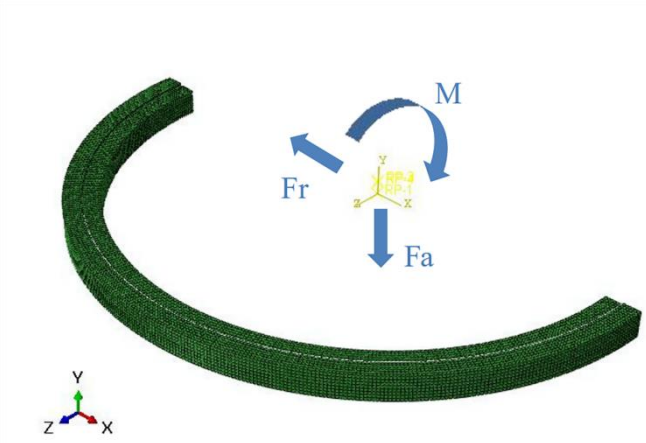

Figure 6.3 Loads coordinate system

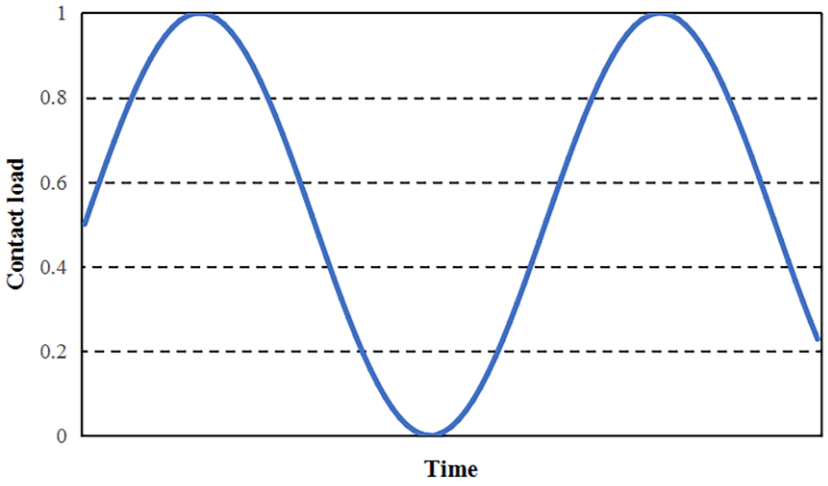

Figure 6.4 Load history applied in yaw bearing

Considering the accuracy and comparability, yaw bearings are assumed to be installed in six different wind turbines (onshore, monopile, ITI barge, TLP, spar and semi-submersible) that were run. Each of the six wind turbines is assumed to work in three different turbulent wind fields (10m/s, 12m/s and 14m/s) separately. Thus, there were totally 18 cases in this thesis. These cases results are introduced in Section 6. 3.

6.3 Stress Result

This section presents the results of the stress analysis for the yaw bearing with DEL loads from six different wind turbines under working conditions of three different turbulent wind fields. The von Mises stress results for onshore wind turbine at 10m/s which is the base case, and ITI barge wind turbine at 14m/s which is the worst case are shown as examples below. Thus, stress distribution patterns of these two cases are shown below. The stress patterns of other cases are not shown in this section due to the similarities in the patterns of the above two cases.

For the case of onshore wind turbine at 10 m/s, Figure 6.5, Figure 6.7, Figure 6.9 show the von Mises results for the rolling balls, outer ring and inner ring respectively.

For the case of ITI barge with wind turbine at 14 m/s, Figure 6.6, Figure 6.8, Figure 6.10 show the von Mises results for the rolling balls, outer ring and inner ring respectively.

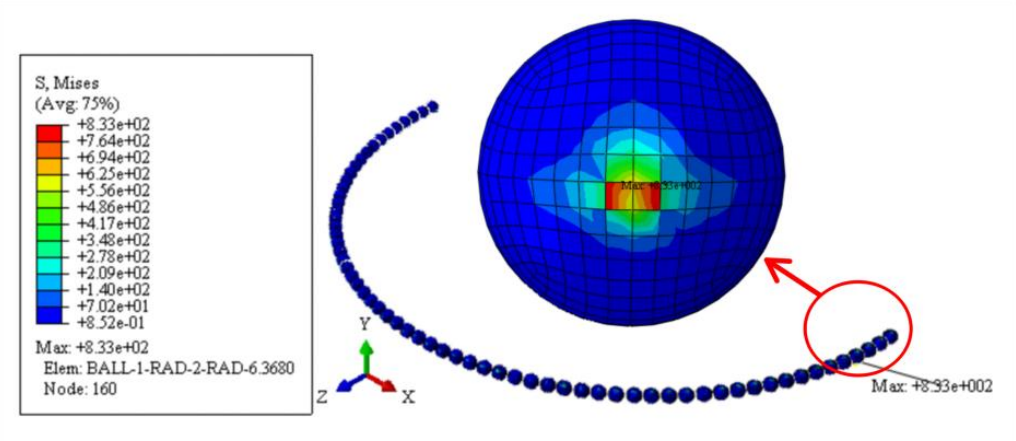

Figure 6.5 Yaw bearing rolling balls von Mises stress of onshore wind turbine

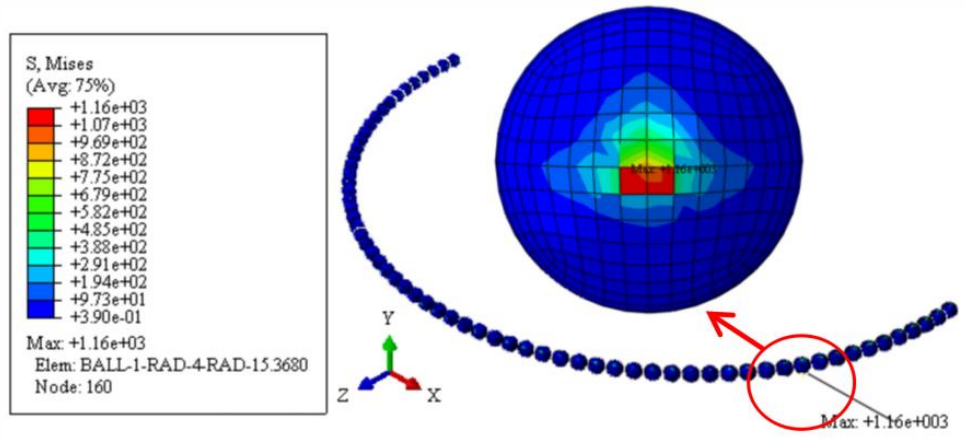

Figure 6.6 Yaw bearing rolling balls von Mises stress of ITI barge wind turbine

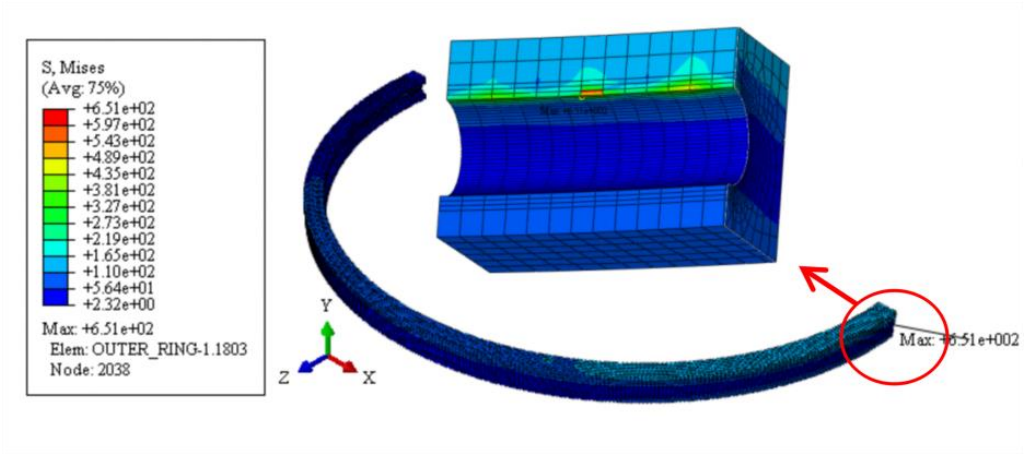

Figure 6.7 Yaw bearing outer ring von Mises stress of onshore wind turbine

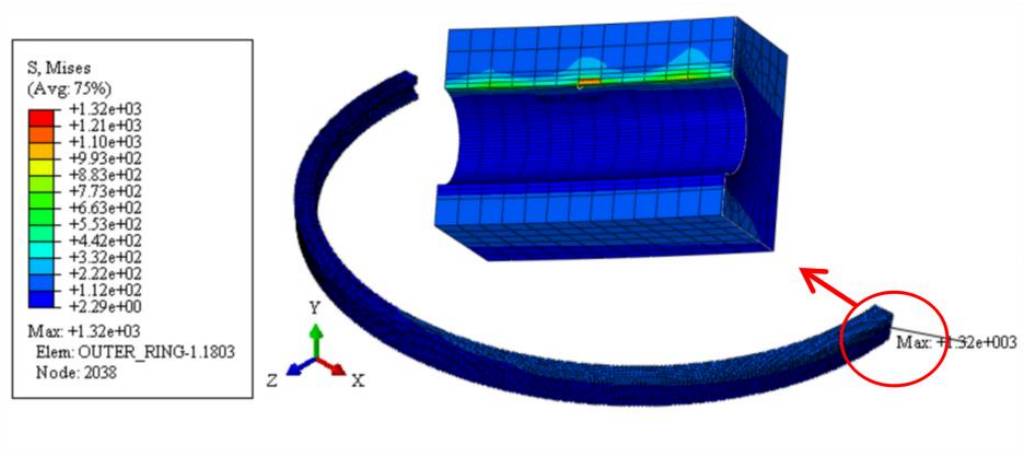

Figure 6.8 Yaw bearing outer ring von Mises stress of ITI barge wind turbine

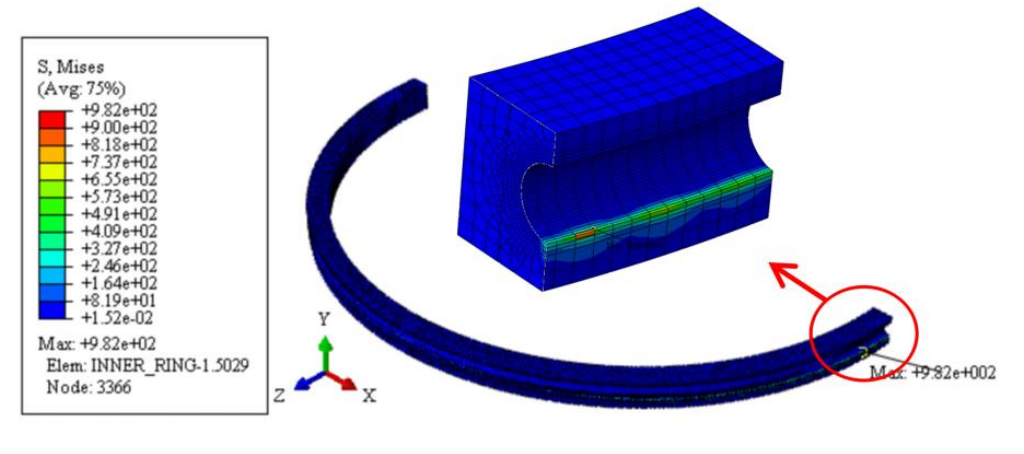

Figure 6.9 Yaw bearing inner ring von Mises stress of onshore wind turbine

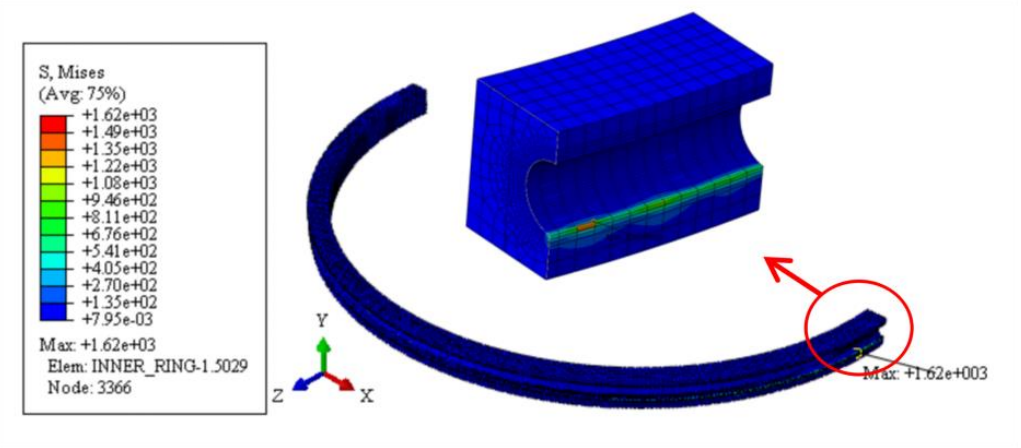

Figure 6.10 Yaw bearing inner ring von Mises stress of ITI barge wind turbine

6.4 Fatigue Life Model

In this section, a code-based approach and a FEA approach for fatigue life calculation of yaw bearing are introduced below. The fatigue life results are also compared below.

6.4.1 NREL method

As introduced in Section 2.2, several standards for slewing bearing fatigue lives are compared. Based on these, a code-based approach for the yaw and pitch bearings by the National Renewable Energy Laboratory is used to calculate the fatigue life of the yaw bearing (Harris et al., 2009). In this method, the basic rating life L_{10} (for 10^6 revolutions) of the yaw bearing is:

$$L_{10} = \left(\frac{C_a}{P_{ea}}\right)^3 \qquad \text{Equation 6.1}$$

where C_a is the basic dynamic axial rating load, described by:

$$C_a = 3.647 f_{cm} (i \cos\alpha)^{0.7} Z^{2/3} {D_w}^{1.4} \tan\alpha \qquad \text{Equation 6.2}$$

where f_{cm} is material parameter described by Harris et al. (2009). P_{ea} is dynamic equivalent axial load, as indicated in equation:

$$P_{ea} = 0.75F_r + F_a + \frac{2M}{D_R} \qquad \text{Equation 6.3}$$

where F_r is radial load, F_a is axial load, M is moment load.

6.4.2 FEA method

As discussed in Section 2.2, several rolling contact fatigue (RCF) theories are introduced and compared. In this section, one of the most common methods is used to calculate the fatigue life of yaw bearing based on the stress results.

The ball material GCr15 and ring material 42CrMo are ductile. The Brown Miller method is usually recommended for the fatigue analysis of ductile material (He et al., 2018). In this method, material data and critical plane techniques are used to calculate the strain spectrum of targeted finite element model. Then, the spectrum is used for the fatigue analysis of finite element model under non-uniform loading conditions. In this thesis, the applied damage equivalent loading history on yaw bearing belongs to this condition. However, when it assumes that fatigue damage is resulted from strain, the Brown Miller method ignores the effect of mean stress. The Morrow mean stress correction method is widely used in practice (He et al., 2018). The elastic stress is corrected with the subtraction of mean stress in every cycle in the method. For the accuracy of fatigue life prediction, the Brown Miller with Morrow mean stress correction fatigue method is chosen to calculate the results of yaw bearing in this thesis. The method is contained in the software FEsafe. LOGLife which represents fatigue life in log scale is used to show the result. To be consistent with the stress distribution patterns which are shown in Section 6.23, examples of LOGLife cycle results for onshore wind turbine at 10 m/s result are shown in Figure 6.11, Figure 6.13 and Figure 6.15, and examples of LOGLife cycle results for ITI barge wind turbine at 10 m/s are shown in Figure 6.12, Figure 6.14 and Figure 6.16.

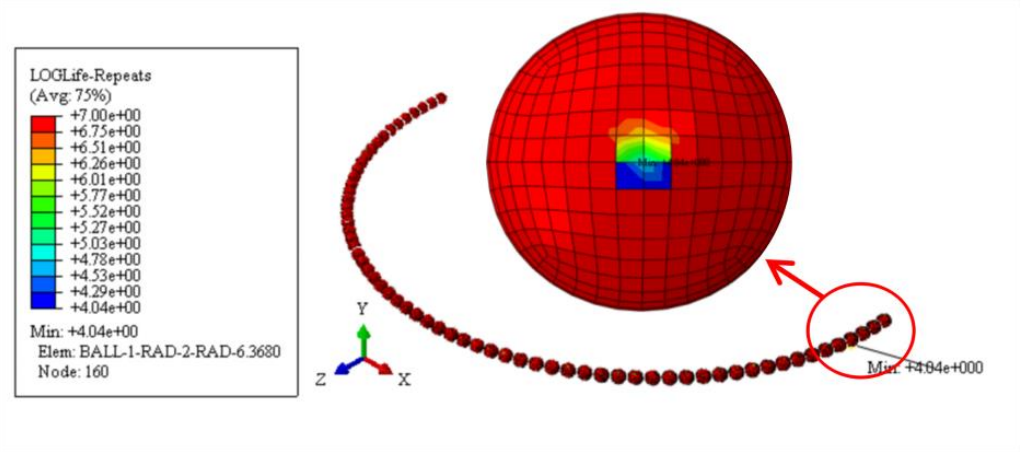

Figure 6.11 Yaw bearing rolling balls LOGLife cycle of onshore wind turbine

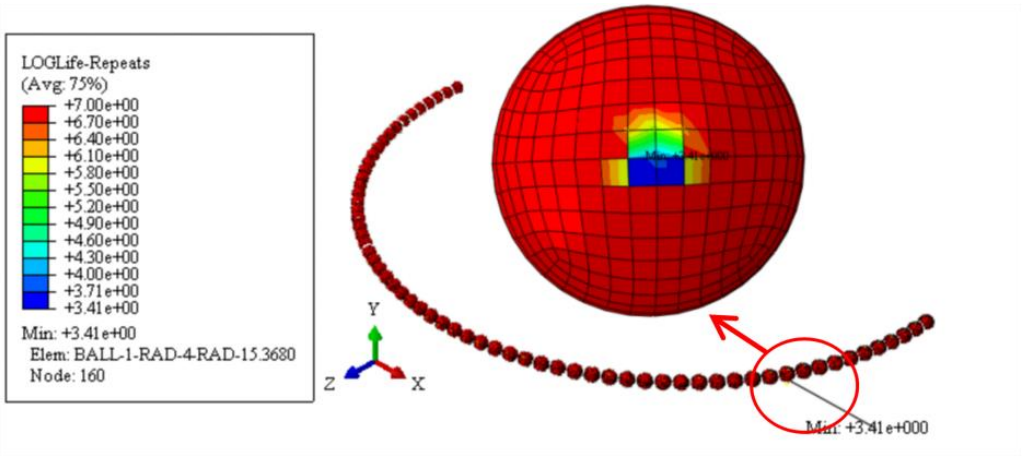

Figure 6.12 Yaw bearing rolling balls LOGLife cycle of ITI barge wind turbine

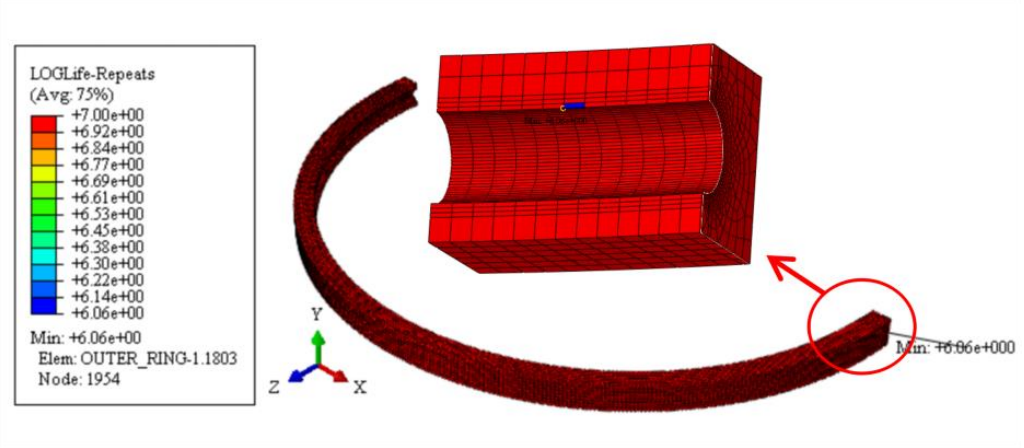

Figure 6.13 Yaw bearing outer ring LOGLife cycle of onshore wind turbine

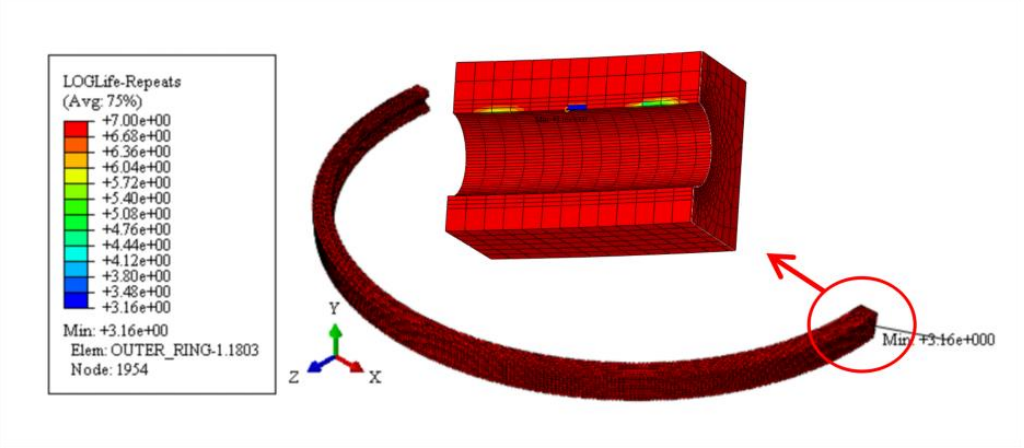

Figure 6.14 Yaw bearing outer ring LOGLife cycle of ITI barge wind turbine

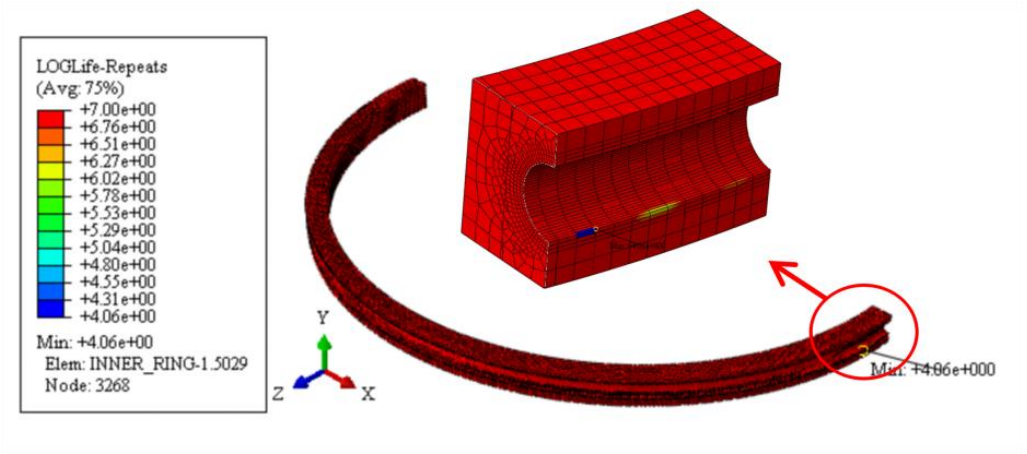

Figure 6.15 Yaw bearing inner ring LOGLife cycle of onshore wind turbine

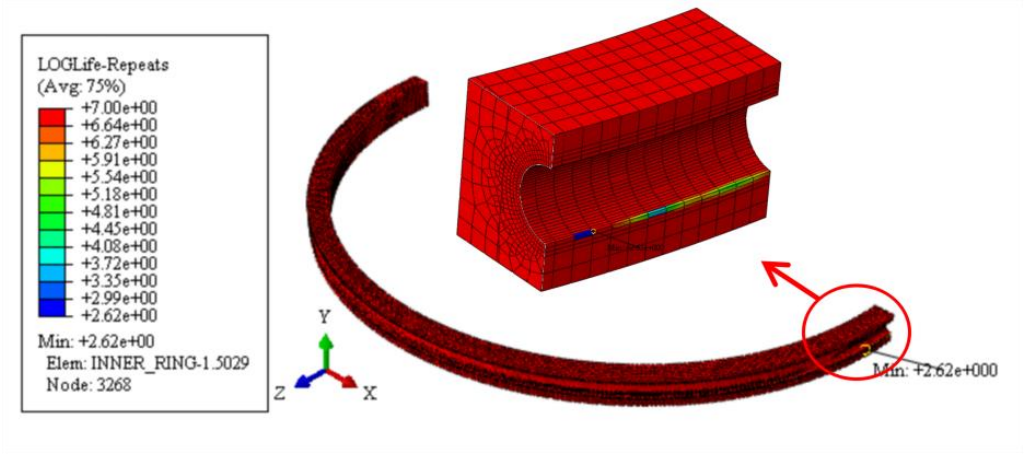

Figure 6.16 Yaw bearing inner ring LOGLife cycle of ITI barge wind turbine

6.4.3 Fatigue life comparison

The NREL fatigue life and the FE simulation fatigue life for the yaw bearing at different working conditions are shown below. Figures 6.17, 6.18, 6.19, 6.20 show the yaw bearing theoretical fatigue life, fatigue life of rolling ball, fatigue life of outer ring and fatigue life of inner ring respectively.

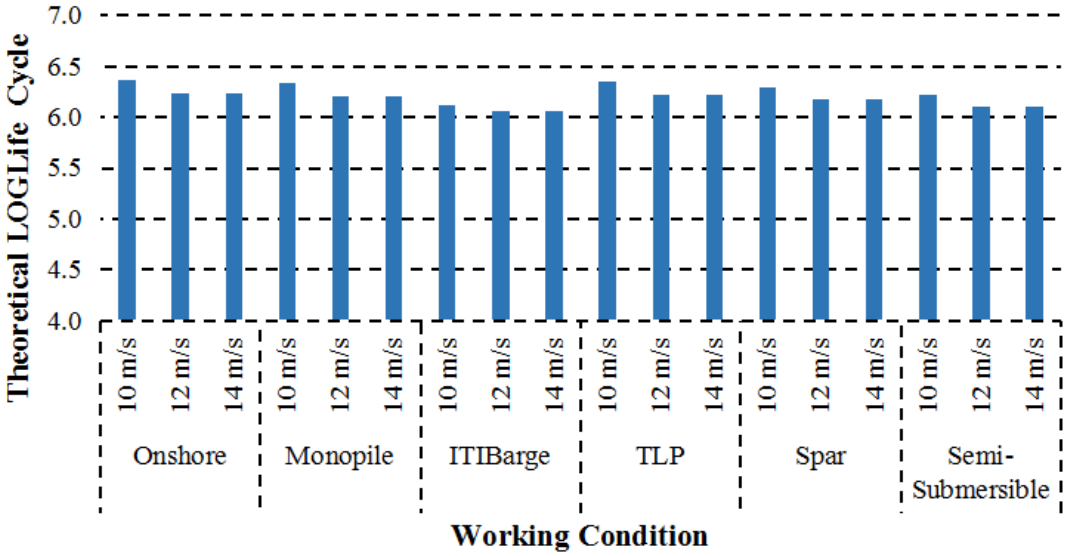

Figure 6.17 Yaw bearing theoretical fatigue life

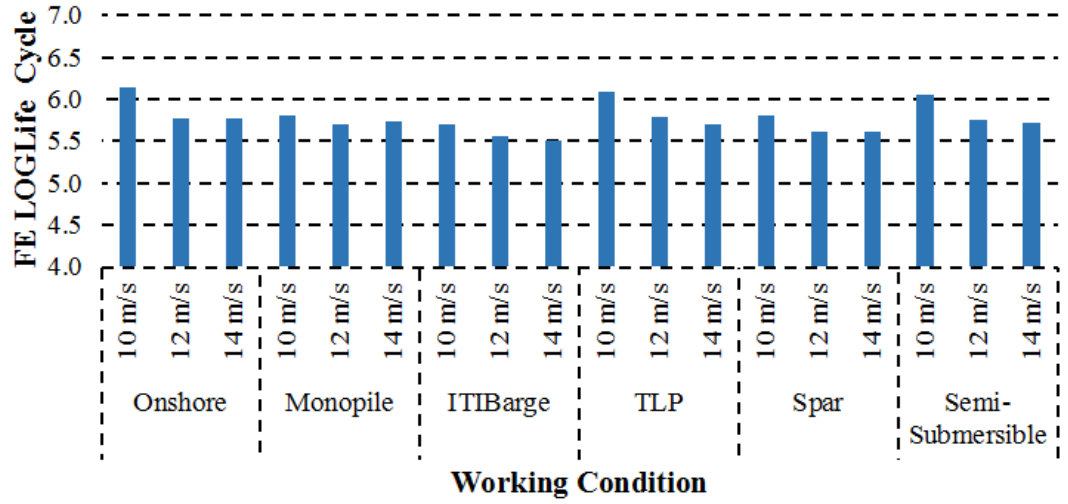

Figure 6.18 Yaw bearing fatigue life of rolling ball

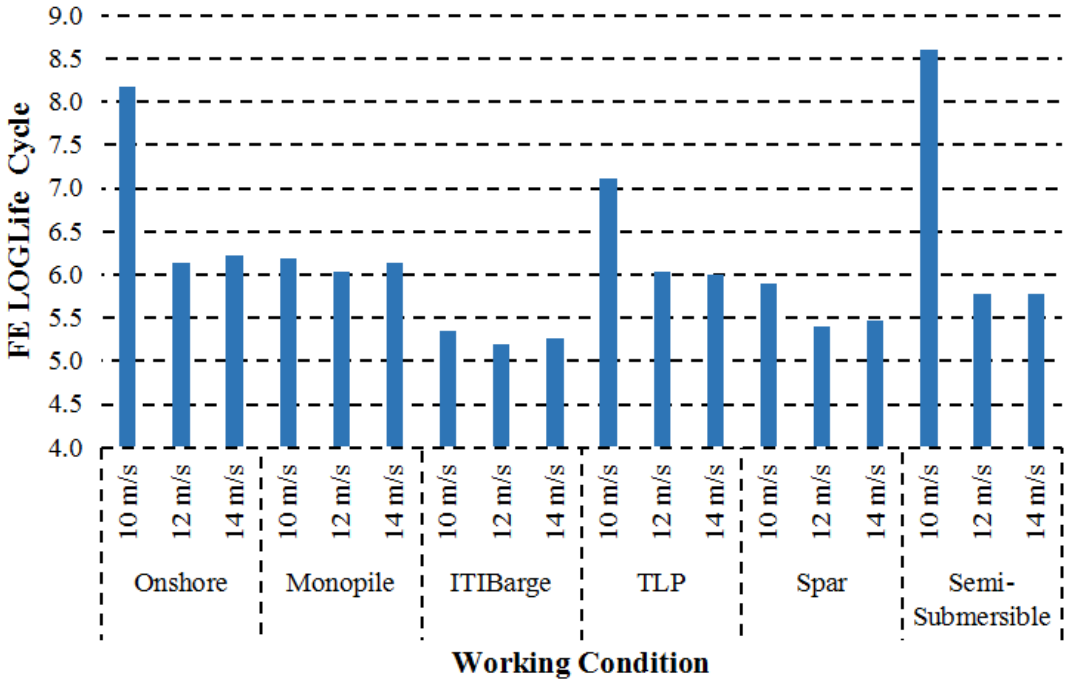

Figure 6.19 Yaw bearing fatigue life of outer ring

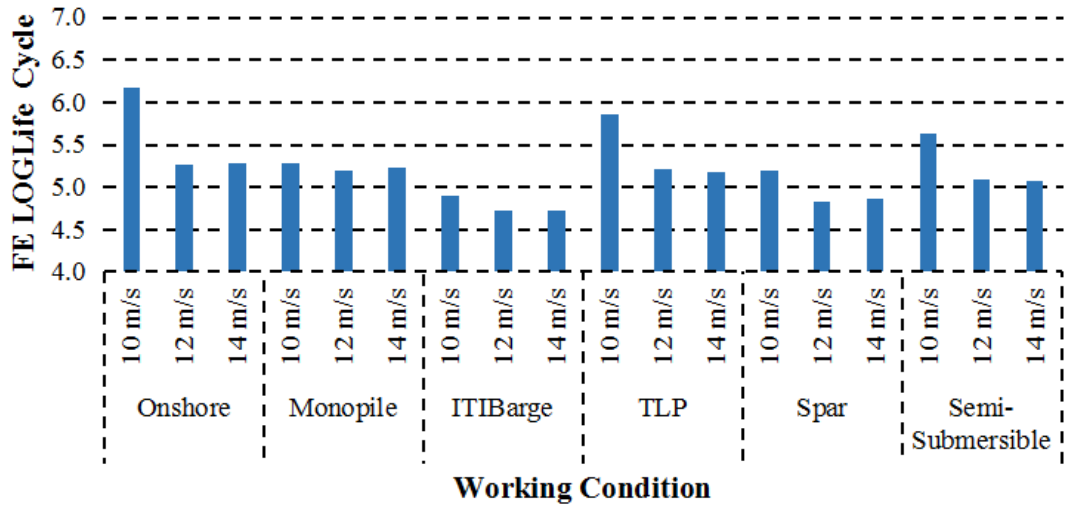

Figure 6.20 Yaw bearing fatigue life of inner ring

6.5 Discussion

In this section, the stress results and life results are discussed first as below:

•The results show that the maximum stress point and the minimum life point are at the same location in the yaw bearing for all cases. The results of the other wind turbines show identical patterns in that the maximum stress points concentrate in a small area in the FE model. The maximum stress point and minimum life point are also at same location for all wind turbines. However, the failure of this small area in FE analysis does not represent the failure of whole yaw bearing. This is because the yaw bearing rotates with changes in wind direction. As a result, the concentrated area of stress will change.

•For the rolling balls, they rotate with the nacelle when the wind direction changes. Thus, the contact areas amongst the rolling balls and rings change frequently. The stress concentration point of the rolling balls is thus changed. As a result, the lifetime of rolling ball calculated in FE model is limited. In this thesis, considering the actual operating conditions and the fact that the rolling balls rotate during operation, the life of the static rolling ball model is assumed to be multiplied by the number of rolling balls.

•For the outer ring, it rotates with the nacelle during operation to adjust the direction of the wind turbine blades to face the wind inflow. The maximum contact stress point in the outer ring is therefore always in the same location.

•For the inner ring, it is fixed to the tower top, but the wind direction changes during operation. As a result, the location of the maximum contact stress in the inner ring changes. This thesis supposes the location of the inner ring is fixed according to the location of rolling balls or changes slightly and slowly; to correct this, the life of inner ring is also multiplied by the number of rolling balls.

Besides, the fatigue life compassion results in Section 6.3.3 show that wind speed has a significant influence on the fatigue life. The results are discussed as below:

• For each wind turbine, the fatigue life at 10 m/s is the longest and the result at 12 m/s is almost the same as it is at 14 m/s.

• The fixed wind turbine, onshore and monopile wind turbines have similar fatigue lives across the wind speeds.

• The fatigue life of ITI barge is the lowest at all wind speeds compared with the other wind turbines. For the floating wind turbines, their fatigue lives vary from each other at separate wind

speeds. The fatigue life of the ITI barge is the lowest with the semi-submersible second lowest. The fatigue life of TLP is the longest and the spar is the second longest.

The FE results vary greatly from each other. In general, they can be divided into two major parts: infinite fatigue life and finite fatigue life.

From the fatigue life results, in the cases of onshore at 10 m/s, TLP at 10 m/s and spar at 10 m/s, the fatigue life of outer bearing is infinite. This is because the stress range is smaller than the fatigue strength.

Examining the finite fatigue life results, the yaw bearing FE model is divided into three major parts: inner ring, outer ring, rolling ball. The results also show that wind speed affects yaw bearing fatigue life.

• For all three parts of the yaw bearing, the fatigue lives of the floating wind turbines are shorter compared to the fixed ones. As wind speed increases, fatigue life shortens. By contrast, the fatigue lives of fixed wind turbines are stable at all wind speeds. It shows that the floating wind turbine arrangement has a significant impact on the fatigue life of the yaw bearing. The high stability of wind turbine structures is beneficial to their yaw bearings. Fixed wind turbine foundations are more stable than floating ones.

• For all the wind turbines, the fatigue life of the inner ring is the lowest at all wind speeds.

• For rolling balls, the fatigue life at 10 m/s is the longest and the result at 12 m/s is similar to that at 14 m/s. It shows that the wind environment has a major impact on the rolling balls.

• For all three parts of the yaw bearing, the fatigue lives of the ITI barge are the lowest and the semi-submersible's fatigue lives are the second lowest at all wind speeds. This correlates with results from NREL where the ITI barge and semi-submersible are shown to have lower stability suggesting there is a direct link between the dynamic response of the FOWT and the fatigue life of the yaw bearing.

• For fixed wind turbines, except the onshore wind turbine, the fatigue life results at 10 m/s of the rolling balls, inner ring and outer ring are similar. Fixed wind turbine support foundations only sway slightly at all wind speeds and hence their change in stability is limited.

• For the floating wind turbines, the fatigue lives of the TLP are the longest and are the closest ones to the fixed wind turbine. It shows that the TLP support foundation is the most beneficial to fatigue life of the yaw bearing because of its favorable dynamic characteristics in waves.

As it is expensive to repair and replace a yaw bearing when it is in working conditions, its fatigue life should be considered. This is especially important for FOWTs which are usually located in deep waters.

6.6 Summary

From Chapter 3 to Chapter 6, a fatigue life analysis of the yaw bearing for six wind turbine concepts is completed. A set of wind inflows are set and are separately coupled with wave conditions to generate dynamic loads. Damage equivalent loads are then calculated from these time-domain dynamic loads. The damage equivalent loads are applied to an FE model of the yaw bearing to calculate fatigue life and compared to a code-based approach. Using the same wind turbine specifications and typical environmental data for all analyses enabled an apples-to-apples comparison of the results. Based on these, some important findings are concluded as below:

•The analysis shows that the NREL calculation method is conservative compared to the FE method for fixed wind turbines and less suitable for FOWTs. This is because the NREL method uses modified parameters based on onshore wind turbines. The effect of different foundations for FOWTs are not included in the model.

•Different foundations for wind turbines directly affect the dynamic loads of the yaw bearing. This results in a difference between the FE fatigue lives and the NREL fatigue lives. This work also suggests that the fatigue lives of the three parts of yaw bearing are different and should be considered separately in theoretical fatigue life calculations and design guidelines.

•The stress concentration point and low fatigue life point are found on a full-size FE yaw bearing model. However, the failure modes and failure processes of yaw bearings are not investigated. To design yaw bearings with high reliability, their failure mechanisms will be considered in the following work. This work provides the foundation for following research for developing more robust methods to evaluate the fatigue state of yaw bearings in offshore wind turbines especially in FOWTs.

Chapter 7 Fracture Mechanics

The yaw bearing is a kind of low-speed heavy-duty slewing bearing. For slewing bearings, alternating loads contributes to their cyclic contact between the rings and rolling elements. This kind of contact relationship shows by a slow swinging state of the bearing. Lubricant and grease which are used to reduce friction and provide cushioning will possibly overflow from the trench of the contact area. As a result, the crack will occur and propagate in the bearing (Md & Mohd, 2013; JAD analysis, 2015). A typical example of fatigue fracture failure phenomenon of slewing bearing is shown in Figure 7.1 (JAD analysis, 2015).

Figure 7.1 A fatigue fracture failure phenomenon of slewing bearing

(JAD analysis, 2015)

This chapter presents a crack propagation analysis for yaw bearings using an XFEM comparative study. This study is based on the results from Chapter 3 to Chapter 6. The focus is on the SIF calculation of the targeted-location crack. The NREL 5WM wind turbine nacelle is again chosen to be installed in six different wind turbine foundations. Based on a global FEA model, a fatigue life analysis of the yaw bearing for each wind turbine was investigated separately in Chapter 6. In this chapter, the six chosen wind turbines are also chosen as target wind turbines. A novel XFEM yaw bearing model coupled with a sub-model which is based on the global FEA yaw bearing model in Chapter 6 is built in ABAQUS. The stress results and LOGLife results representing fatigue life in log scale are used to set the crack in the novel model. The original crack size is set according to the maximum stress area in the global FEA yaw bearing model. The location of the crack is also decided by the depth of the element whose fatigue life is minimum in the global yaw bearing model. This chapter studies the influence of different working conditions on the same initial crack in the yaw bearing.

For a large diameter bearing, the linear elastic fracture mechanics (LFEM) theory is usually used as the high strength bearing material which is defined as linear elastic (Göncza et al., 2010) . The SIFs, which represent the strengths of stress singularities at the crack tip, are decided by the infinitesimal elasticity solution of the problem (Erdogan & Sih, 1963). Sub-surface cracks are initiated in the area of largest contact stresses when high quality surface with good lubrication is present. Fatigue crack propagation under contact loading ultimately leads to pitting and consecutively to the failure of the contact surfaces (Göncza et al., 2010).

It is widely accepted that fatigue cracks are initiated by shear stresses. Both experimental and theoretical research illustrate that fatigue cracks propagate in the direction determined by the local stress field after short crack initiation period (Kudish & Burris, 2000). Now, it is common sense that there is nothing different in the general mechanisms between tensile fatigue and contact fatigue. Thus, contact fatigue can follow the same crack propagation laws for general tensile fatigue (Kudish & Covitch, 2010).

In terms of SIF calculation, there are two traditional numerical methods divided by the kinds of loading on the crack: tensile loading and compressive loading. These numerical methods can solve the problem for a single load case and the SIF results can be used to verify the results from corresponding finite element method. However, in the case of a global yaw bearing with practical complex loads, finite element analysis is considered as the best method to deal with the SIF calculation as it has the advantages of high processing efficiency and broad applicability (Santus et al., 2012).

For decades, finite element analysis for SIF calculation evolved into two research directions: two-dimension analysis and three-dimension analysis. In the two-dimension analysis, starting from the end of the last century, some researchers attempted to calculate the SIF of a crack in two-dimension plane (Hearle & Johnson, 1985; Komvopoulos, 1996; Xu & Komvopoulos, 2013; Aditya A. & Farshid, 2017). A lot of research perspectives concerning SIF calculation have been adopted since then. They are mainly concluded as: cyclic loading, lubricant contamination, contact friction, material defect, material characteristic, crack propagation mode, crack size and location and so on (Kudish & Covitch, 2010). With the rapid development of finite element software and computer processing capability, three-dimension analysis has become available and get increasingly popular. In addition to the research focusing on two-dimension analysis, more research perspectives are adopted by researchers in three-dimension analysis. For example, the corresponding SIF calculation for crack face friction and crack tip

point angle. However, there is limited research about the complex loading influence on the crack and that is what this chapter presents.

For single loading, SIF values for different fracture modes are described below. In the following equations, a is crack size, β is crack orientation angle, v is Poisson's radio, σ is the stress, f_c is friction coefficient. K_I, K_{II}, K_{III} are the SIF value for fracture mode I, mode II and mode III. In these fracture modes, the normal stress contributes to the K_I, the shear stress contributes to the K_{II} and K_{III}.

For single tensile loading, the SIFs are described as (François et al., 2019):

$$K_I = 2\sqrt{\frac{a}{\pi}} \cdot \sigma \cdot \cos^2(\beta) \qquad \text{Equation 7.1}$$

$$K_{II} = 2\sqrt{\frac{a}{\pi}} \cdot \sigma \cdot \frac{1}{2-v} \cdot \sin(2\beta)\cos(\theta) \qquad \text{Equation 7.2}$$

$$K_{III} = 2\sqrt{\frac{a}{\pi}} \cdot \sigma \cdot \frac{1-v}{2-v} \cdot \sin(2\beta)\sin(\theta) \qquad \text{Equation 7.3}$$

For single compressive loading, the SIFs are described as (François et al., 2019):

$$K_I = 0 \qquad \text{Equation 7.4}$$

$$K_{II} = 2\sqrt{\frac{a}{\pi}} \cdot \sigma \cdot \frac{1}{2-v} \cdot \cos(\theta) \cdot [2f_c \cdot \cos^2(\beta) - \sin(2\beta)] \qquad \text{Equation 7.5}$$

$$K_{III} = 2\sqrt{\frac{a}{\pi}} \cdot \sigma \cdot \frac{1-v}{2-v} \cdot \sin(\theta) \cdot [2f_c \cdot \cos^2(\beta) - \sin(2\beta)] \qquad \text{Equation 7.6}$$

For a simple contact pair with tensile or compressive loading condition, such as a small local segment of the yaw bearing with one rolling element and the corresponding bearing ring contact part, the above two numerical analysis methods can be used to calculate the SIF of a crack inside. The SIF result of numerical analysis method can be used to validate the corresponding result from local finite element model.

However, for large yaw bearing with complex loading conditions, an experiment method is usually used to achieve related data such as vibration data, ultimate load, fatigue life and so on (François et al., 2019). For an initial crack in the yaw bearing, it is difficult to observe the condition inside directly. To solve the problem, a novel XFEM yaw bearing model coupled with submodel technique which is built in ABAQUS is shown in this chapter. Complex load combinations are applied to the model. The submodel technique is used to improve the efficiency of computing. The XFEM technique is used to build the initial crack in the yaw bearing.

7.1 Submodel Technique

The submodel technique is applied widely in FEM. This technique is used to study a small component or local region of a global model with refined mesh which is based on an interpolation of the solution from a relatively coarse and undeformed global model (Dassault Systems, 2017). Due to its refined mesh, compared with analyzing a global model, the analysis guarantees more accurate and detailed data about the targeted critical area. Besides, submodel technique is used to drive a local region of the global model with the usage of nodal displacement or element stress results from the global model. Thus, it can save computing resources and modeling time when a series of comparative analysis about different local regions of same global model is required.

There are two basic classifications of submodel technique: node-based submodeling and surface-based submodeling. Node-based submodeling is the more common and general method. It interpolates the global model results such as displacement, pressure degree of freedom or temperature onto the nodes of the submodel. In addition, the second classification of submodel technique, surface-based technique interpolates global model results onto the integration points of submodel on the surface facets based on the driven element (Dassault Systems, 2017).

In this research, to be coupled with the crack analysis of XFEM-based technique which will be introduced below, the node-based technique in submodel technique is adopted to transfer the displacement in the global model. The submodel element type in this research is the same as the global yaw bearing model. Thus, in terms of the node-based submodel technique in the research, a solid-to-solid element type is adopted for the three-dimensional submodel and global model. The three-dimension sub-model of yaw bearing is shown in Figure 7.2.

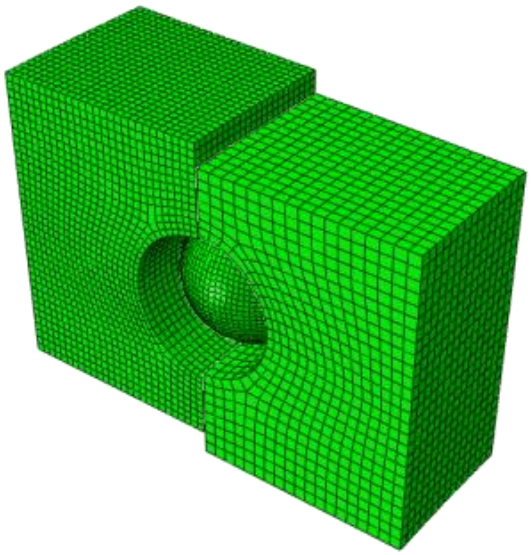

Figure 7.2 Three-dimension submodel of yaw bearing

As for processing steps of a node-based submodel analysis, they are concluded as the following four steps (Dassault Systems, 2017):

- Run a global analysis with the preservation of results surrounding the boundary of submodel
- Define the entire set of driven nodes in the submodel
- Specify the actual nodes and degrees of freedom which is to be driven in all steps to define the time variation of the driven variables in the submodel
- Perform the submodel analysis with the above driven variables for the solution.

In terms of the global model and submodel used in the research, there are some other points should be paid special attention to. They are as follows:

- The global model in the research is a large yaw bearing model with a large amount of contact pairs. It should be noted that the global elements used to drive the submodel are required to be specified. As the contact interface exists in the global yaw bearing model, more than one element could encompass a driven node's location and the contact segments may have coincident nodes temporarily. Thus, this research specifies an appropriate subset of the global model element to avoid the unnecessary contact elements to drive the submodel. Figure 7.3, 7.4 show two pairs of subset elements which drive the outer ring segment and inner ring segment of a submodel separately.

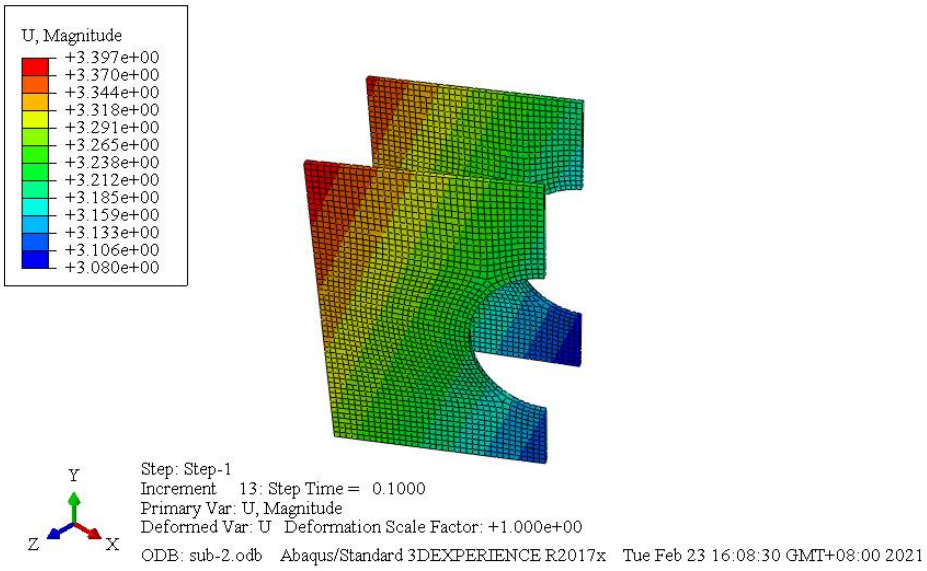

Figure 7.3 A pair of subset elements of outer ring segment in a submodel

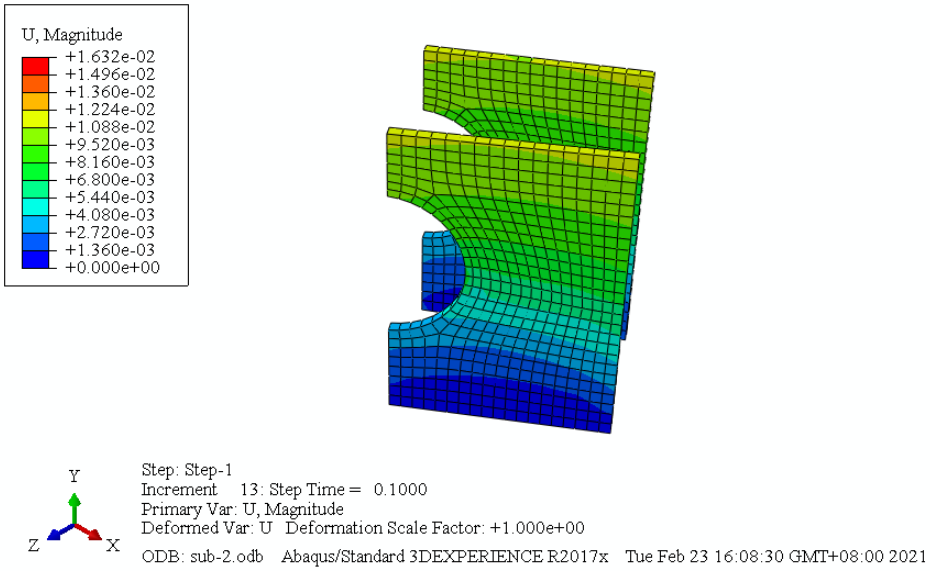

Figure 7.4 A pair of subset elements of inner ring segment in a submodel

• To minimize the file sizes, this research only requests output from the global models which are used to drive the submodel.

• Another requirement about the output between the global model and submodel is its frequency. The same frequency of node output is chosen for all nodes that involved in the interpolation. Thus, it is important to choose an appropriate frequency for both models since the beginning of global model building.

• The last point is about element set. In this research, the global model is a three-dimensional model. Thus, the submodel is also three dimensional with the same element type and is built within the boundary nodes of global mode for the calculation of interpolation between nodes.

7.2 XFEM Technique

XFEM is the abbreviation of extended finite element method. It is a numerical technique which is based on the conventional finite element method and the partition of unity method. It is capable of modeling discontinuities problems in mechanics, such as crack problem. It enables the presence of discontinuities in an element using displacement functions to enrich degrees of freedom. In terms of crack problems, XFEM techniques allow the crack to be independent of the internal geometry and physical interfaces. The crack in a model can be analyzed by XFEM technique without meshing issues as it does not need re-meshing to match the geometry of discontinuities (Dassault Systems, 2017). In detail, crack analysis in XFEM can be divided into two kinds: a stationary crack in a model or a crack that grows along an arbitrary path in a model. In the area of fracture mechanics, XFEM has been a popular calculation method to analyze the SIF for a stationary crack in a structure. In a stationary crack analysis, XFEM technique has some advantages. As the model mesh is generated independently from a crack, it eases the building a stationary crack in a meshed model without partitioning of geometry. Besides, the application of singular crack tip enrichment improves convergence rate for the computing process of a stationary crack. For an XFEM stationary crack analysis, some related specifications should be defined, they are introduced as follow (Dassault Systems, 2017): crack domain, initial crack location, and contact interaction property. These are shown in Section 7.3.1 below.

7.3 Model Analysis

7.3.1 Model building and case running

Compared with initial crack size, the diameter of the global yaw bearing model is rather large. For the accuracy and efficiency of modeling, the submodel technique is adopted to analyze the local contact area.

In this chapter, a small local segment of the yaw bearing with one rolling element and the corresponding bearing ring contact part are chosen as the submodel. To match the global model precisely, the submodel is cut and taken from the global model. Meanwhile, the objectives of

the submodel, such as materials, sections, amplitudes, interaction properties are copied from the global model. The instance type for the submodel should change from dependent mesh on part to independent mesh on instance. The outer ring part of the submodel is meshed with 4.5mm elements which is similar to the element size of the refined contact area of the global yaw bearing model in Chapter 6. The rolling ball is meshed with 4mm and the inner ring part of the submodel is meshed with 6mm. In addition to the above-mentioned adjustments, some other unimportant adjustments are not detailed here for brevity. The original parameters of yaw bearing are described in Chapter 6. This process is computationally heavy as the global model includes a lot of contact pairs. However, the other submodels at different locations of the global model can be easily built by rotating this submodel position. This makes the analysis process more efficient.

The displacement of a submodel is shown in Figure 7.5. The locations of the four submodels of the yaw bearing are shown in Figure 7.6. They are located at Points A, B, C and D. To study the crack propagation in yaw bearing, Point D, the location of maximum stress is chosen. To study the influence of location on crack efficiently, the other three points are chosen as representative points and are spaced equally. The stress results of the global model with submodel in this chapter are compared and verified by the original global model in Chapter 6.

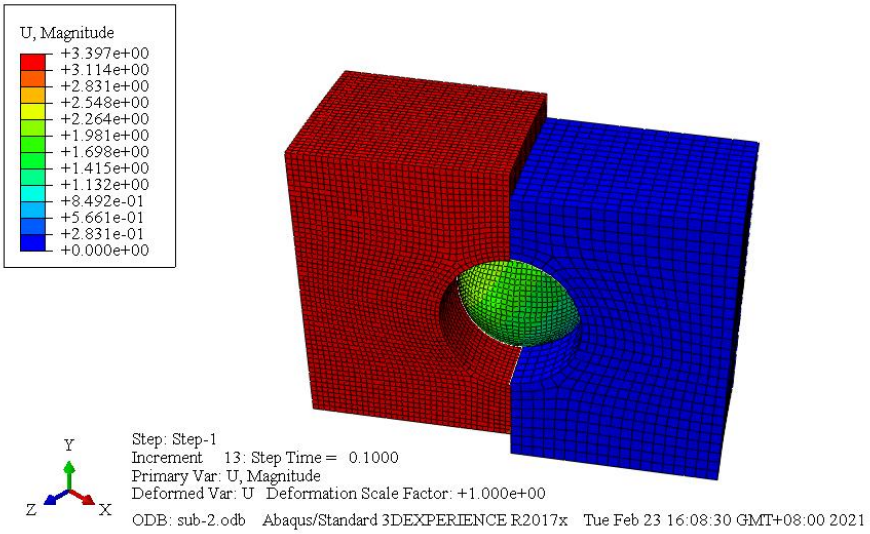

Figure 7.5 The displacement of a submodel

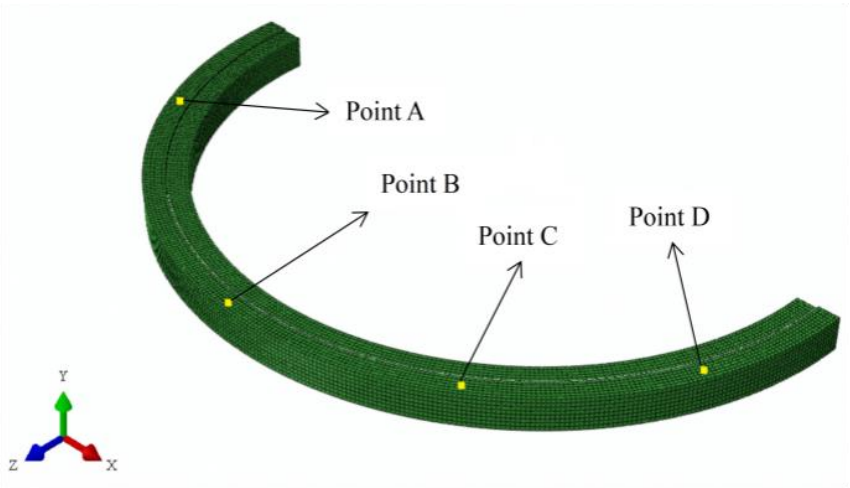

Figure 7.6 The locations of four submodels in yaw bearing

Initial cracks at different locations in the global model are analyzed with the corresponding submodels. An initial crack plane is created and inserted into the raceway contact surface. The plane is located at the position where the maximum shear stress area occurs as it is where fatigue crack failure phenomenon usually occurs. The initial crack plane is perpendicular to the contact surface, and it is assumed that the initial crack grows at this angle. The initial crack plane is set with length of 6mm as the area of maximum shear stress occupies approximately the same space. The initial crack is located at a depth of 2mm from the contact surface as this is the area of maximum shear stress. A sketch of initial crack location is shown in Figure 7.7. The location of initial crack in shear stress result of yaw bearing in onshore wind turbine at 10m/s is shown in Figure 7.8.

Since XFEM is a built-in tool in ABAUS with the advantage of simulating discontinuities and singularities independently of the mesh (Dassault Systems, 2017), the mesh refinement studies are much simpler. There is no need to re-mesh the sub-model segment of the global yaw bearing model. XFEM technique makes the computing process for SIFs of a series of cracks time-saving and high-efficient.

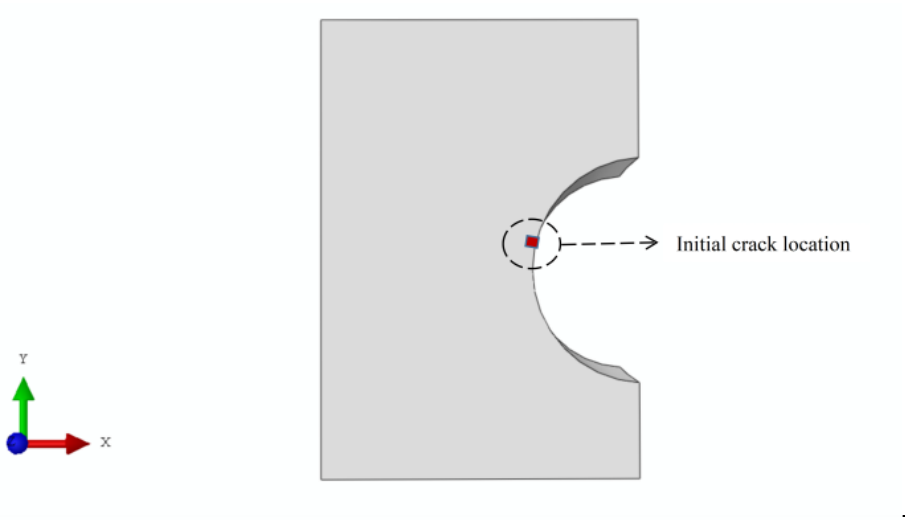

Figure 7.7 The sketch for initial crack location

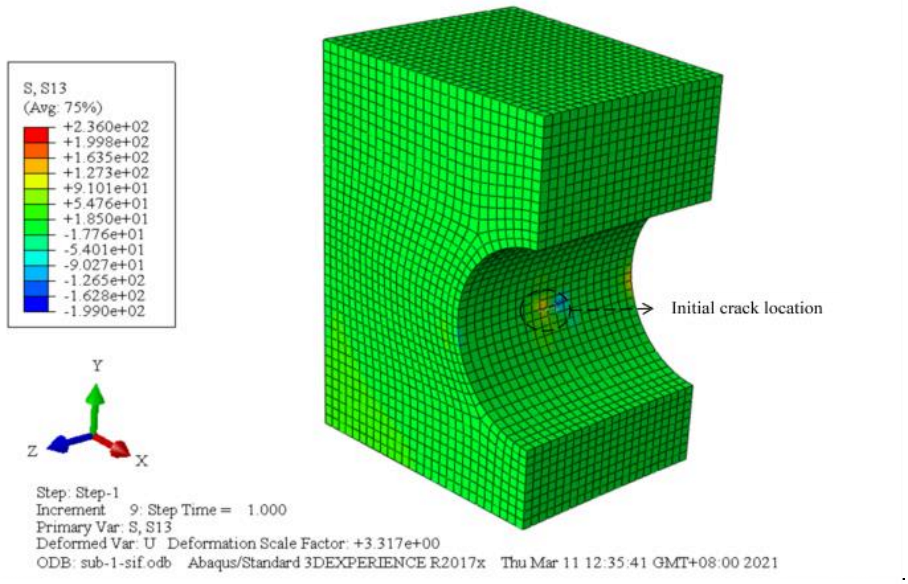

Figure 7.8 The initial crack location in the shear stress result

7.3.2 XFEM results

The research shows that both fracture mode I and fracture mode II exist in yaw bearings. The characteristics of a crack in yaw bearing are analyzed by the parameter SIFs: K_I , K_{II} . Toughness values of 42CrMo K_{IC} were found by Vera et al : 340±10 MPa√(mm (raceway), 1390±100 MPa√(mm (transition), 1380±110 MPa√(mm (core) (Vera et al., 2022). Compared with the SIF simulation results then fracture failure is believed to happen. The SIFs of cracks at different locations with different wind speeds in yaw bearings are shown from Figure 7.9 to

Figure 7.14. Figure 7.9, 7.10 and 7.11 show yaw bearing K_I results with the same initial defect in different wind turbines at 10m/s, 12m/s and 14m/s respectively. Figure 7.12, 7.13 and 7.14 show yaw bearing K_{II} results with the same initial defect in different wind turbines at 10m/s, 12m/s and 14m/s respectively. The character Onshore in Figure 7.9 represents the condition that yaw bearing in onshore wind turbine operating at the wind speed of 10 m/s. The other characters in the remaining figures have similar meanings.

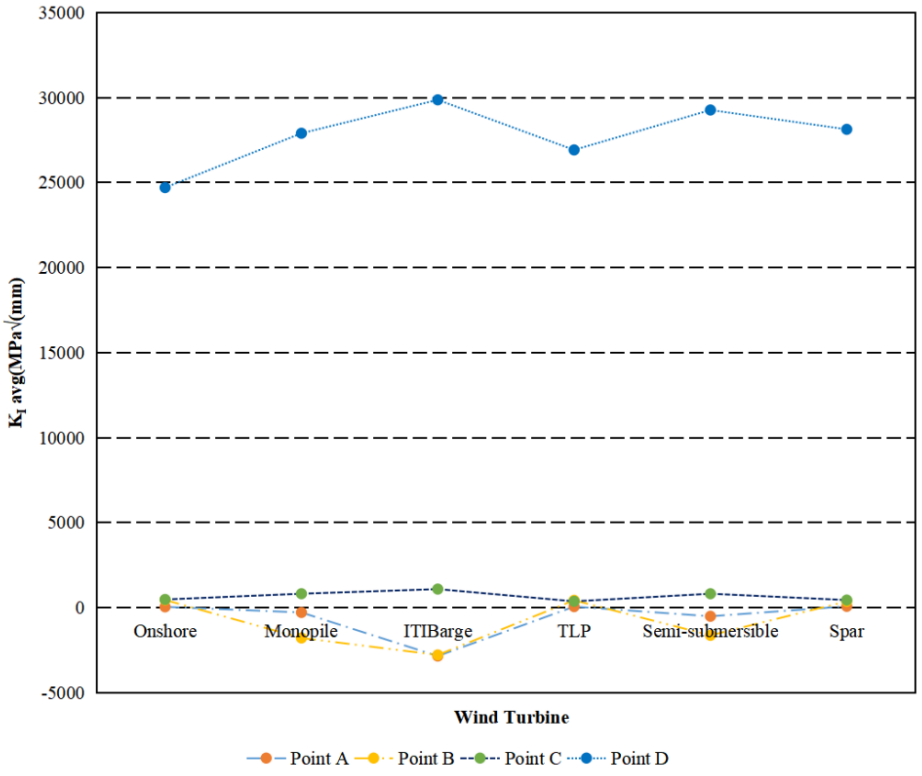

Figure 7.9 Yaw bearing K_I result with same initial defect at 10m/s

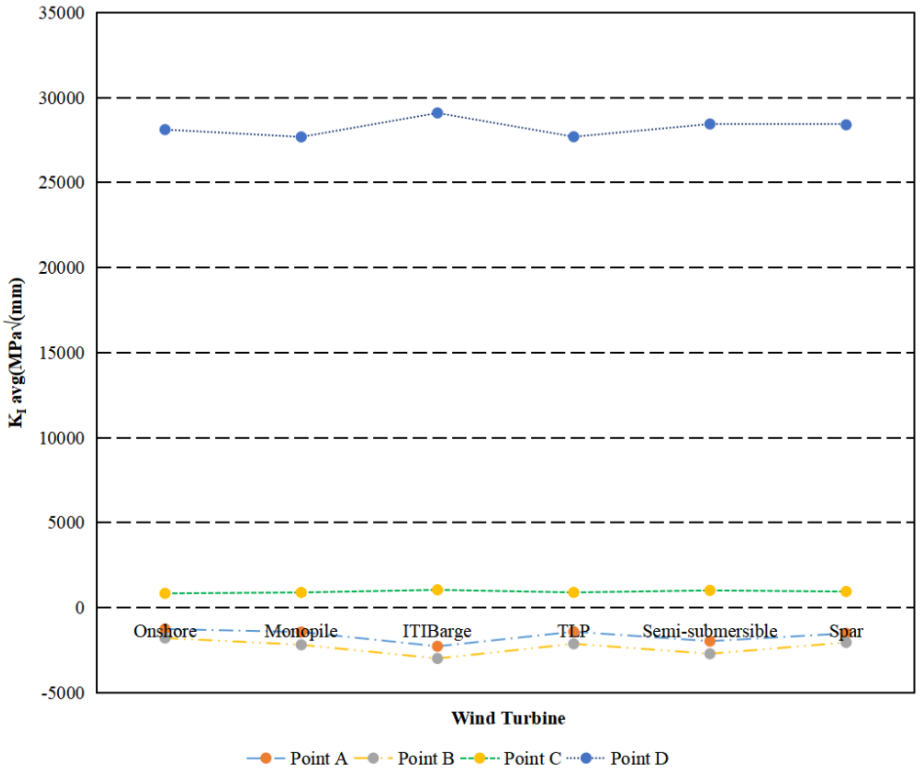

Figure 7.10 Yaw bearing K_I result with same initial defect at 12m/s

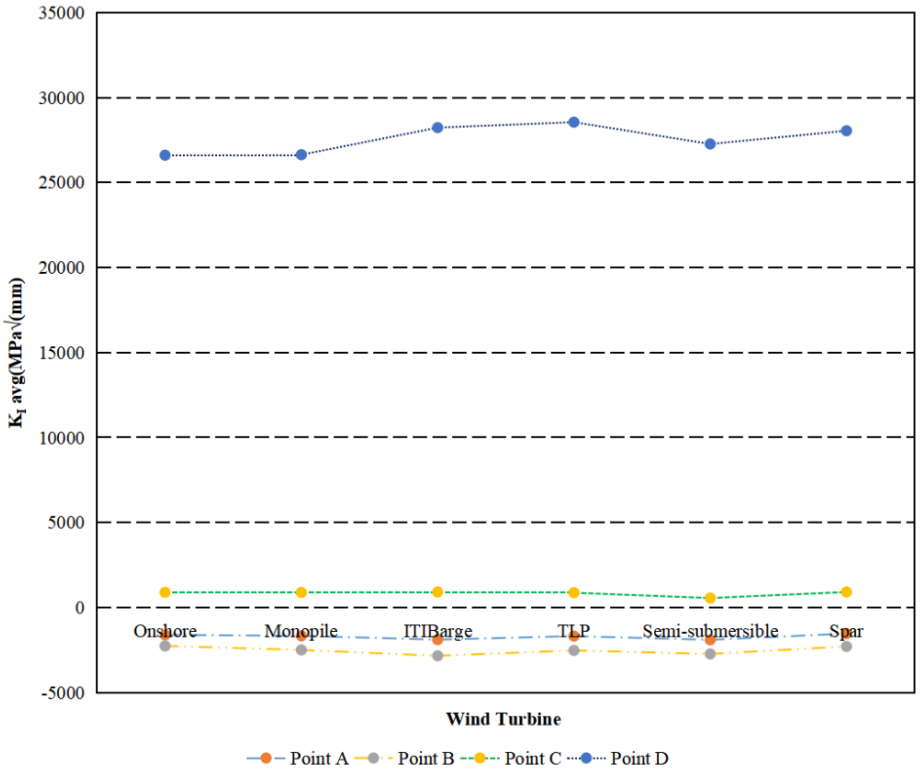

Figure 7.11 Yaw bearing K_I result with same initial defect at 14m/s

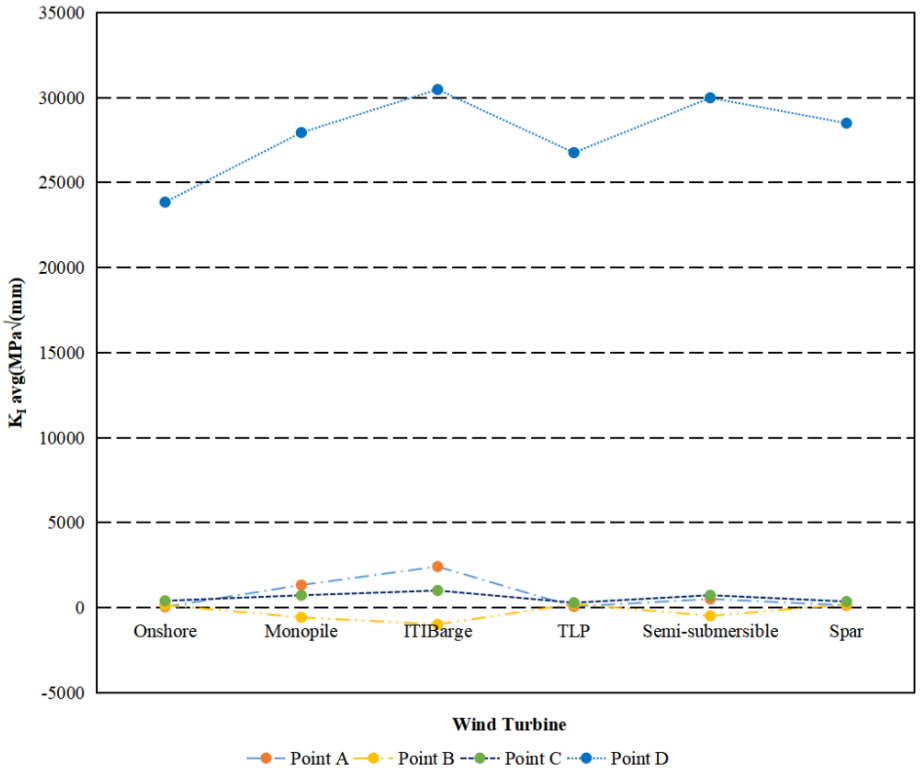

Figure 7.12 Yaw bearing K_{II} result with same initial defect at 10m/s

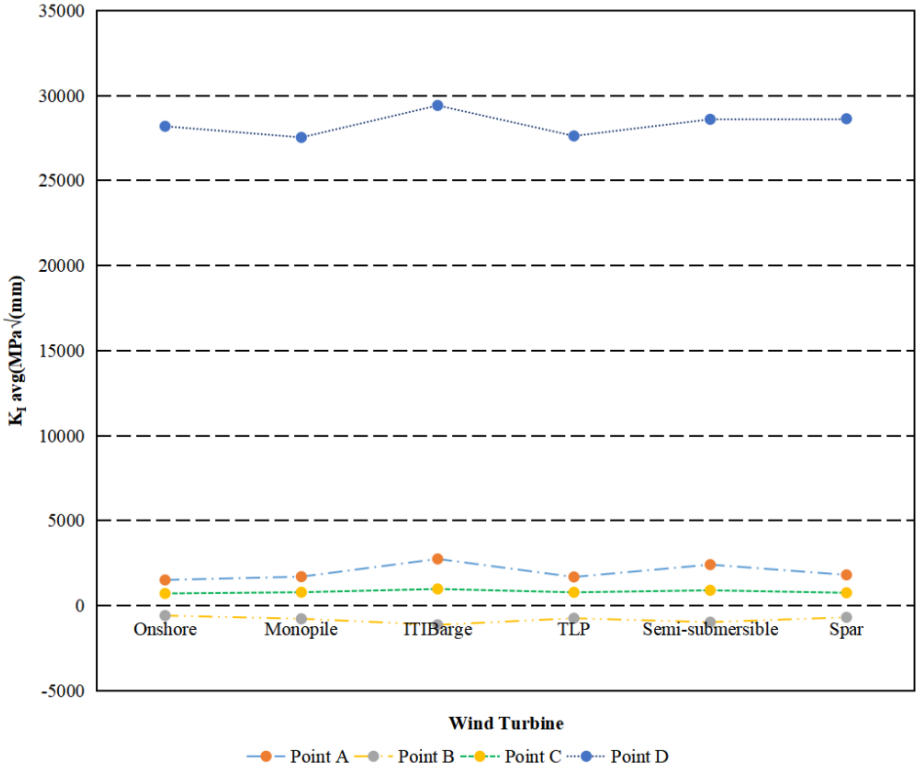

Figure 7.13 Yaw bearing K_{II} result with same initial defect at 12m/s

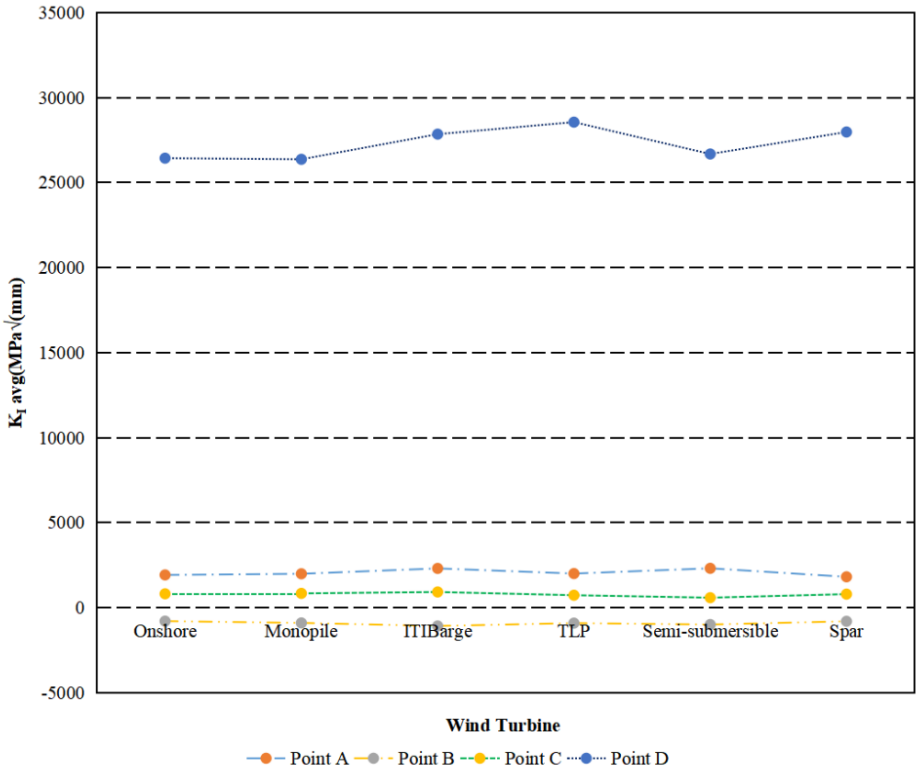

Figure 7.14 Yaw bearing K_{II} result with same initial defect at 14m/s

In addition to SIFs, the MTS directions of corresponding fracture modes at different locations in yaw bearings in wind turbines at different wind speeds are shown from Figure 7.15 to Figure 7.20. Figure 7.15, 7.16 and 7.17 show MTS direction of K_I with the same initial defect in yaw bearing at 10m/s, 12m/s and 14m/s respectively. Figure 7.18, 7.19 and 7.20 show MTS direction of K_{II} with the same initial defect in yaw bearing at 10m/s, 12m/s and 14m/s respectively. As same as the description in above section, the character Onshore in Figure 7.15 represents the condition that yaw bearing in onshore wind turbine operating at the wind speed of 10 m/s. The other characters in the remaining figures have similar meanings.

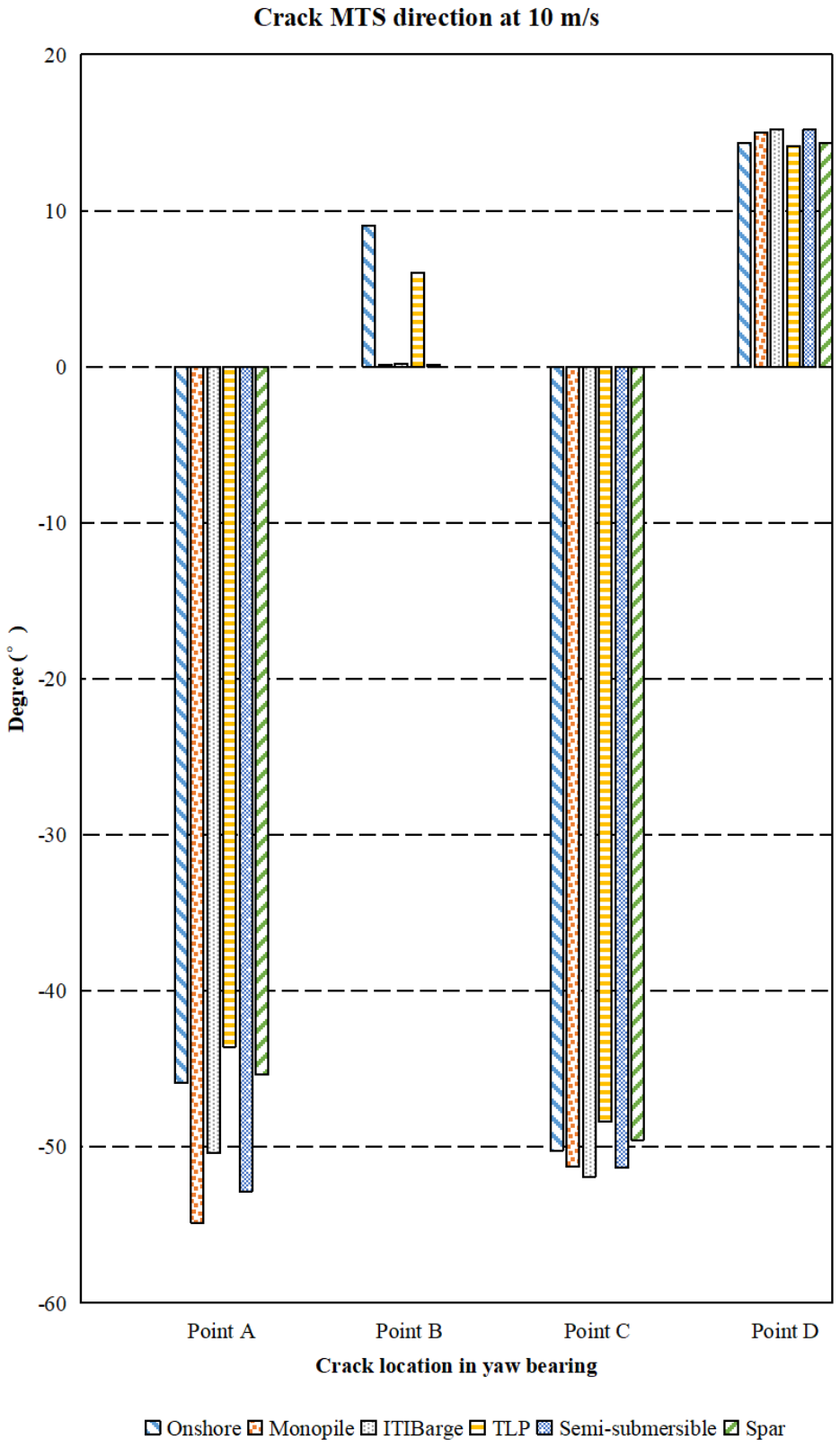

Figure 7.15 MTS direction of K_I with same initial defect in yaw bearing at 10m/s

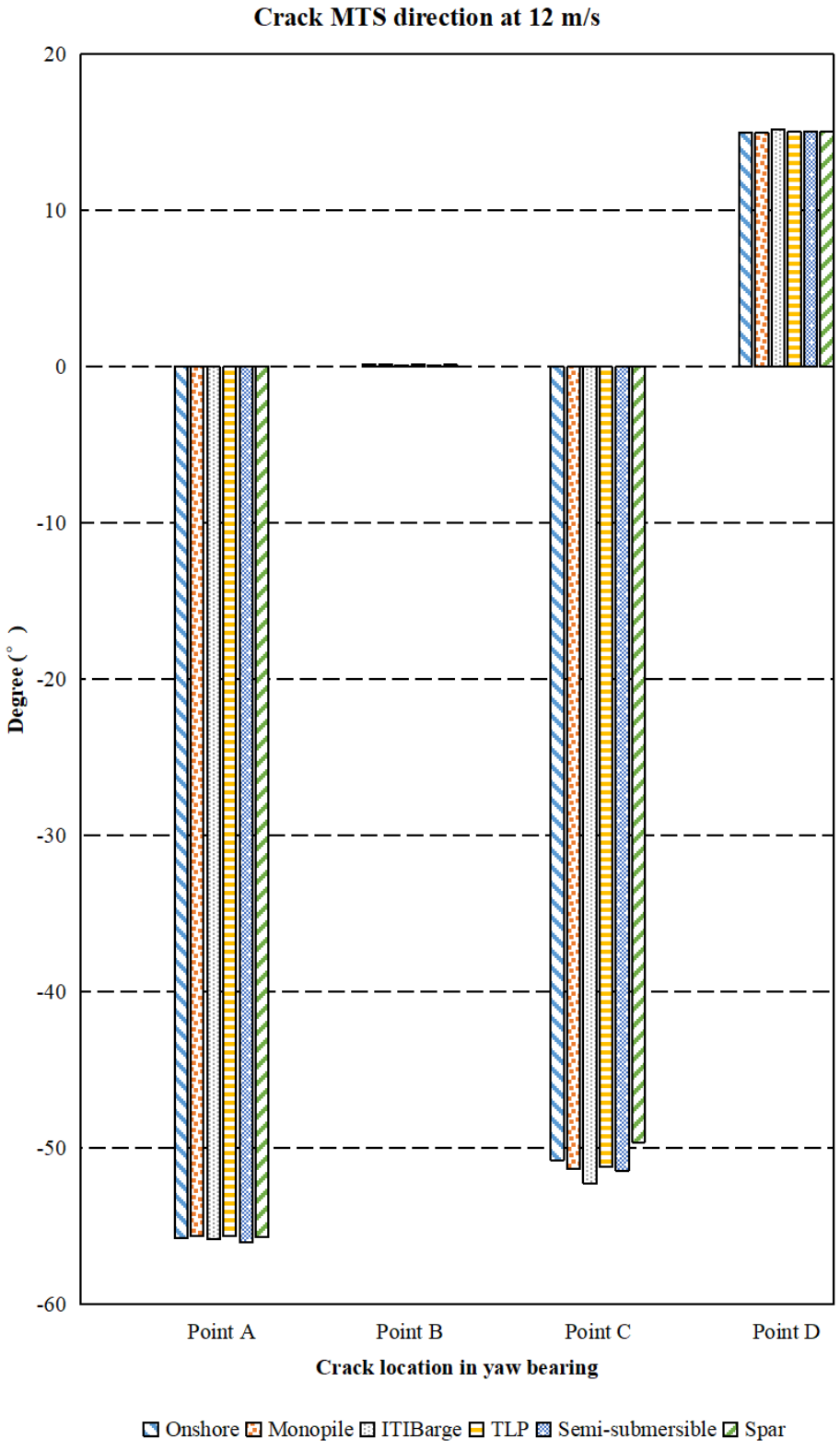

Figure 7.16 MTS direction of K_I with same initial defect in yaw bearing at 12m/s

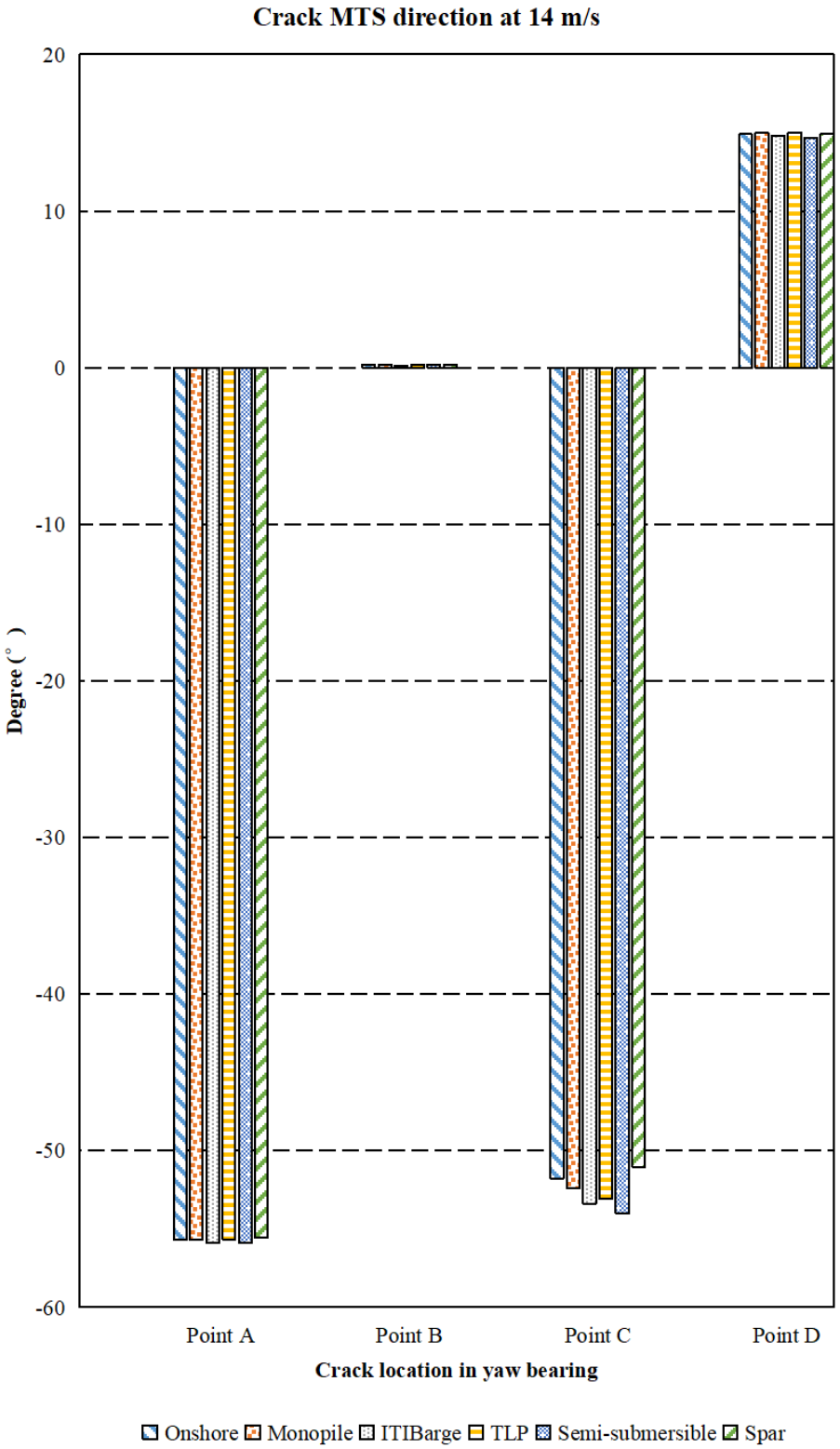

Figure 7.17 MTS direction of K_I with same initial defect in yaw bearing at 14m/s

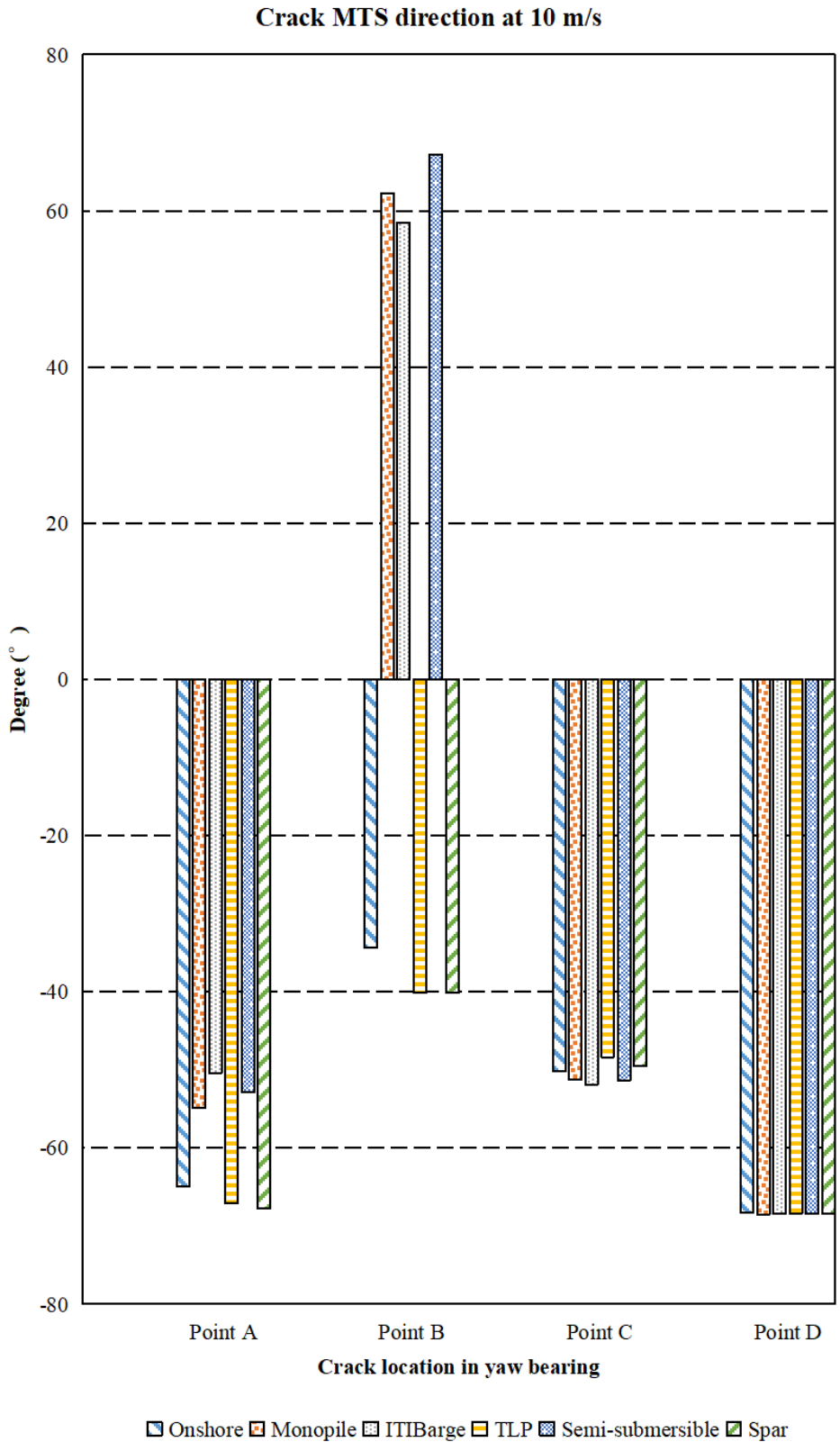

Figure 7.18 MTS direction of K_{II} with same initial defect in yaw bearing at 10m/s

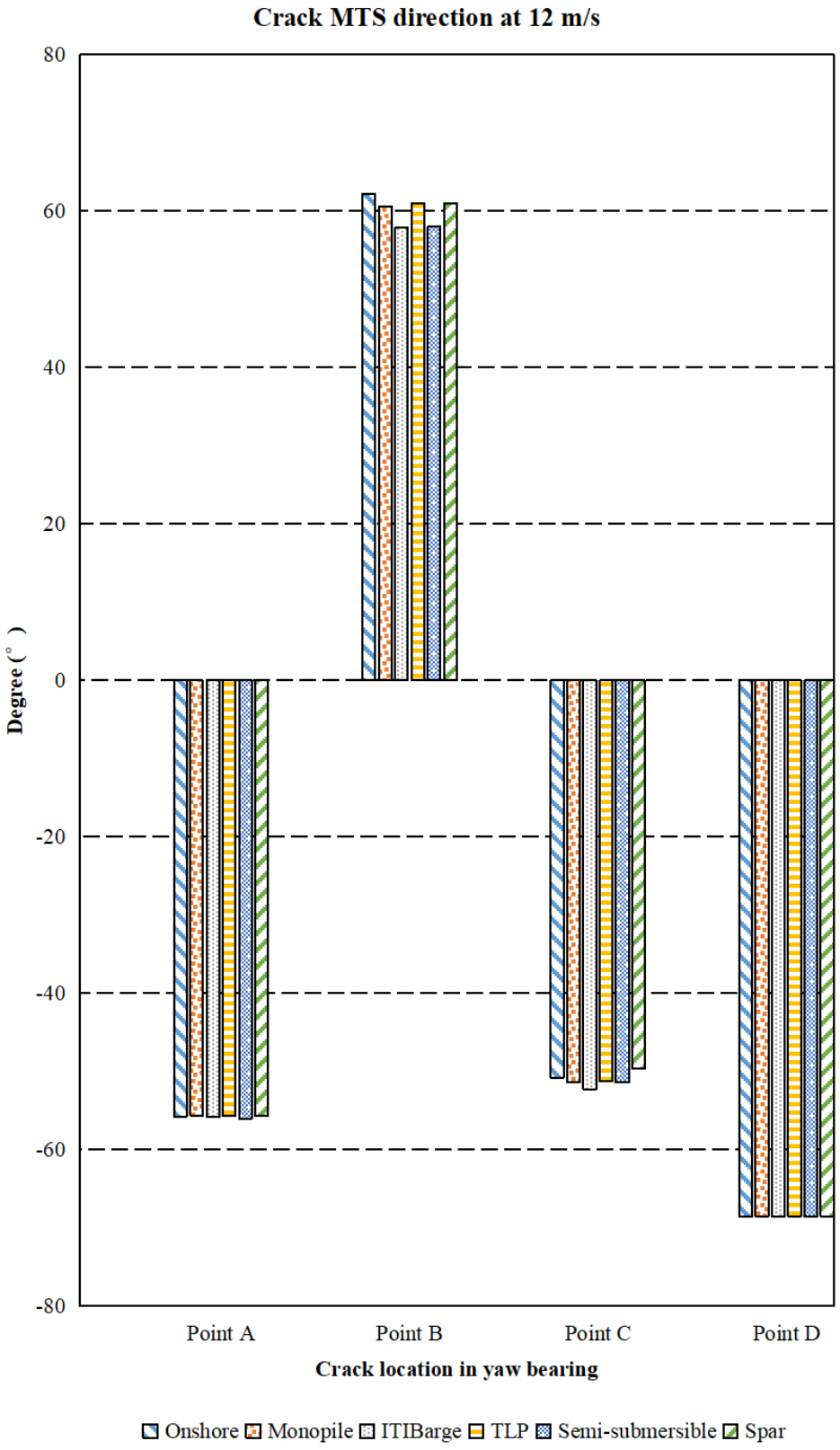

Figure 7.19 MTS direction of K_{II} with same initial defect in yaw bearing at 12m/s

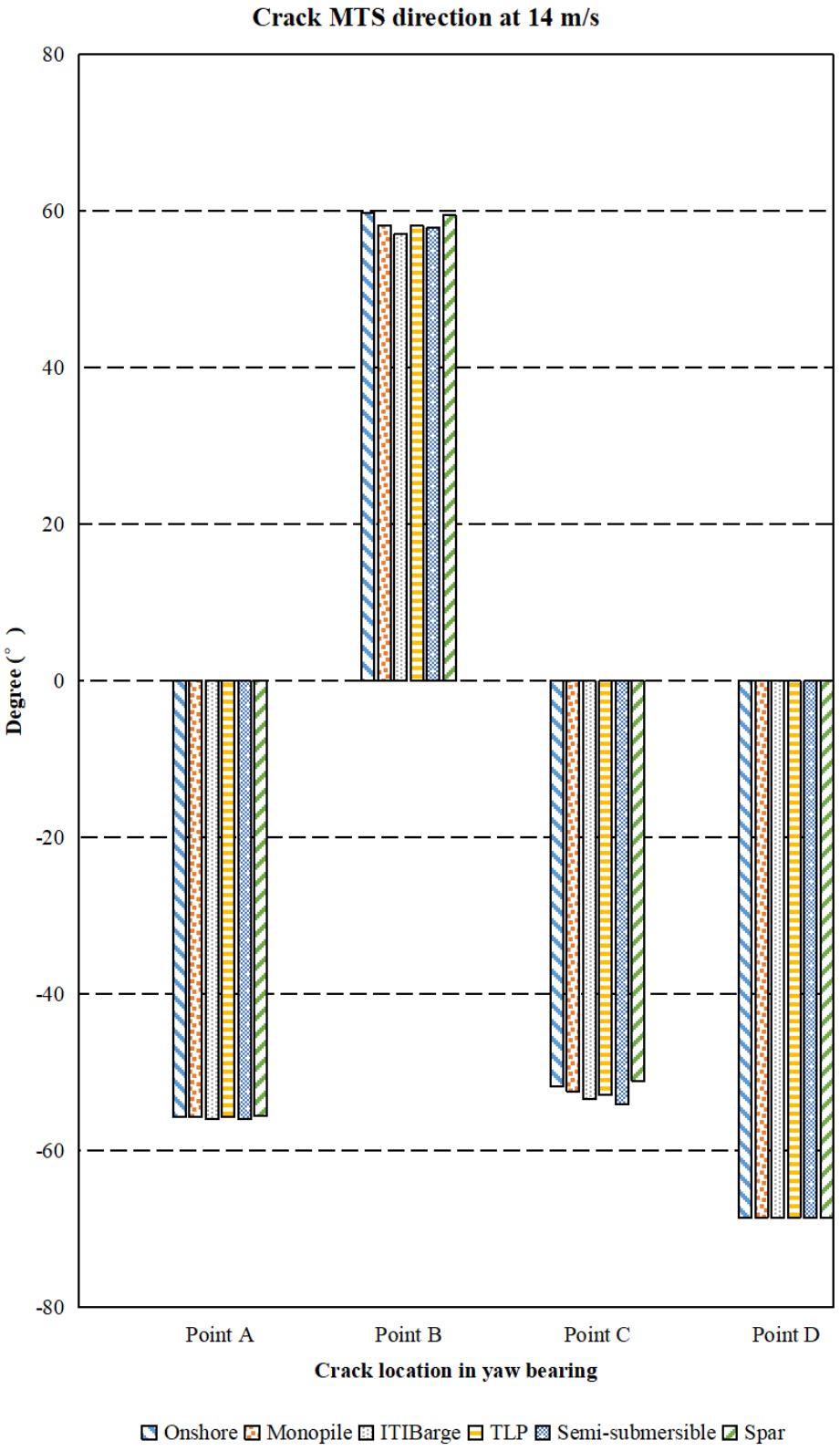

Figure 7.20 MTS direction of K_{II} with same initial defect in yaw bearing at 14m/s

7.4 Discussion

As the results from Figure 7.9 to Figure 7.14 show, the location of the initial crack in yaw bearings has a significant influence on their SIFs. This is described below in detail:

• For all wind turbines with different wind speeds, their maximum K_I and K_{II} values all occur at Point D and these values are obviously larger than the results at the other three points. This corresponds to the stress results in Chapter 6 that Point D is the area where maximum stress is located, as is shown in Section 6.3.

• In terms of the location Point D, the SIFs for the crack in the ITI Barge case are larger than in the other wind turbines. This matches the fatigue life of yaw bearing analysis which is shown in Chapter 6. In Section 6.4 it was found that the fatigue lives of yaw bearings on different wind turbines are different and for the case of the ITI Barge, it is the minimum.

• For the other three points, Point A, Point B and Point C, the absolute values of the results are similar. The results for ITI Barge are slightly larger than the other wind turbines.

• For the fixed wind turbines, onshore or monopile, their absolute values of results for Points A, B and C increase with wind speed. However, this trend is not seen for the other four FOWTs: ITI Barge, TLP, spar and semi-submersible. This suggests that the environment loads for fixed wind turbines are simpler than FOWTs and these variables affect the global loads less significantly. For fixed wind turbines, wave loads on the structures do not need to be taken into consideration. By contrast, FOWTs need to consider not only the factor of wind load, but also the factor of wave load.

Figure 7.15 to Figure 7.20 show that the location of the initial crack in the yaw bearing has some influence on the corresponding MTS directions, which represents the potential crack propagating angles. The results shown in the figures that MTS directions of cracks have commonalities, as well as characteristics. They are concluded separately below:

• For both fracture mode I and fracture mode II, the MTS directions of cracks in yaw bearings of different wind turbines are similar with each other at 12 m/s and 14 m/s. It can also be explained that under working conditions with a wind speed of 12m/s or 14m/s, the crack propagating angles are relatively stable, they show no significant difference among different wind turbines. In fracture mode I, the propagating angles of cracks at Point A are about -

55°which means 55 degrees below the initial crack plane inserted. The results at Point B are about 0° at Point B，-50°at Point C, 15°at Point D. In fracture mode II, the propagating angles of cracks are about -55 ° at Point A, 55° at Point B，-50°at Point C, -70°at Point D.

•However, under working conditions with a wind speed of 10 m/s, at some locations of cracks, the crack propagating directions vary from each other in wind turbines with different fixings. It is found that the difference between angles is obvious at Point B. In fracture mode I, the crack angles in some wind turbines are about 0, others are from 5° to 10°. In fracture mode II, the crack angles in some wind turbines are 60, others are from -35 to 40°. The crack propagating angles' difference at Point A is not obvious, they change from -45°to -55°in fracture mode I and -50° to -70°in fracture mode II. The crack propagating angles at Points C and D remain almost constant. At Point C, the angles are about -50° in fracture mode I and -50°in fracture mode II. At Point D, the angles are about -15° in fracture mode I and -70°in fracture mode II.

7.5 Summary

Following a fatigue life assessment of FOWTs, different parts in the yaw bearing are studied. The results in Chapter 6 showed that the fatigue lives of rings for different wind turbines are very different from each other. This chapter conducts further analysis on the crack in the ring. The yaw bearing model from Chapter 6 is used as global model and the submodel technique is adopted. XFEM is combined with the submodel technique for a high-efficiency calculation of SIF.

The choice of the initial crack in this chapter is based on the former stress result and some assumptions. The initial crack is supposed to originate from the subsurface of contact area and propagates to the contact surface. It is widely accepted that shear stress contributes to the origination of initial subsurface crack. Therefore, the length of the initial crack in this thesis is almost the same as the size of maximum shear stress area in the model. The results show that both fracture mode I and mode II exist in the yaw bearing model under complex loading. The SIFs of cracks at different locations of yaw bearings vary from each other and they show some similarities among different wind turbines. The corresponding MTS directions of cracks about the two fracture modes that existed in the yaw bearing are compared. The similarities and differences of crack propagating angles are discussed.

Point D is a focus as the maximum SIFs occurs here. Compared with the fixed wind turbines, the SIFs of the FOWTs are much larger which means that same crack in a FOWT propagates more easily. Complex working environmental conditions and supporting structures account for the difference. Thus, it is necessary to reassess current standards and guidelines for bearing design as they only consider the application of yaw bearings in fixed wind turbines and ignore the influence of the global response of offshore floating turbines on the fatigue life of yaw bearings. The comparative study in this chapter provides a foundation for the crack analysis of yaw bearing in different wind turbines and could be extended to other structure components in a wind turbine system.

Chapter 8 Conclusions

Wind turbines have been developed for decades for generating electricity. They are facing problems of limited land supply and complex working conditions. FOWTs are ideal devices to operate in deep water as offshore land is not as limited or expensive as onshore land. Therefore, various FOWTs have been proposed and trialed around the world. Compared with fixed turbines, FOWTs have more complex supporting structures and are subjected to harsh environmental conditions. As a result, the structural components in these wind turbines, which are designed and manufactured according to current standards and guidelines, are facing the potential of earlier failure. Based on these considerations, it is indispensable to carry out asset integrity management of these critical structural components in novel FOWTs.

In this thesis, a systematic methodology for assessing the integrity of yaw bearing in different wind turbines, especially in FOWTs, under different operating conditions is proposed. In this work, fatigue life assessments of yaw bearings are compared in 5MW wind turbines with six different support foundations. A time-domain method is applied to predict the aerodynamic and hydrodynamic loads on the yaw bearings using three representative wind velocity profiles. A Gumbel distribution, rain flow counting algorithm, linear cumulative damage law and S-N curve theory are used to generate damage equivalent loads. The fatigue life of the yaw bearing is then calculated separately using a finite element method and a code-based approach. Finally, a crack analysis in the yaw bearing is conducted based on a submodel technique and XFEM method.

The fatigue life results show the dynamics of the floating wind turbine are directly linked to the fatigue life of the yaw bearing and that the major components of the yaw bearing should be considered separately. The XFEM results show a crack propagates at different speeds at different locations of a yaw bearing and the corresponding propagation angle of different fracture modes show some similarities and differences between fixed wind turbines and FOWTs. The results verify the speculation that a yaw bearing, as an important structural component in wind turbines, is likely going to face earlier failure due to its complex and different operating conditions.

8.1 Contributions

The contribution of the research in this thesis is concluded below:

• A systematic methodology for assessing the integrity for yaw bearings in FOWTs as well as fixed wind turbines is proposed. This comprises turbulent wind fields calculation, combined dynamic loads calculation, DEL calculation, fatigue life calculation and crack propagation analysis.

• A novel full-scale finite element yaw bearing model is built with respect to its practical operating status. This yaw bearing model includes the inner ring, outer ring and all the rolling ball bearings.

• Based on the global yaw bearing model, a finite element fatigue life analysis is conducted. Comparing the fatigue lives of a wind turbine yaw bearing with different support foundations shows that the fatigue life of a yaw bearing is sensitive to its operating environment conditions and the global dynamic response of a wind turbine. For example, the yaw bearing for a wind turbine with a barge-type floater is subjected to more complex environmental loads. These loads cause higher motions of the wind turbine and yaw bearing compared to other floater designs. As a result, the yaw bearing undergoes larger time-series loading which reduces its fatigue life.

• The finite element fatigue life results are also compared with the results calculated from an analytical code-based method. The National Renewable Energy Laboratory yaw bearing design guidelines are found to be conservative compared to the finite element method for fixed wind turbines and less suitable for FOWTs. For example, for fixed wind turbines, the design guidelines only consider the fatigue life of the yaw bearing as a simple structure. They ignore the difference of inner ring, outering and rolling element. For FOWTs, they ignore the influence of support foundations.

• A deep analysis is conducted to study the fracture mechanics of a crack in a yaw bearing. XFEM and a submodel technique are combined to study a stationary crack and obtain its characteristics under different operating conditions. The novelty in this analysis is the combined application of two techniques to simulate a crack within a large bearing in an actual working environment.

• Both fracture mode I and fracture mode II exist in the crack propagating process in a yaw bearing. The SIF results show obvious differences in the cracks at different locations in the yaw bearing. Besides, the SIF results also show the influence of various supporting structure and operating conditions. For example, the SIF results for ITI Barge are slightly larger than the other wind turbines which matches the yaw bearing fatigue life analysis.

• Considering two fracture modes respectively, the crack propagating angles at four different locations in the yaw bearing are different. However, the difference of propagating angles of a crack at the same locations in the yaw bearing for different wind turbines is not obvious. Besides, the operating environment conditions of wind turbines have a limited effect on the difference of crack propagating angles.

8.2 Future Work

Although a systematic methodology has been developed for assessing the integrity of yaw bearings in FOWTs in this thesis, considering the length of thesis and time limit, the following research aspects are recommended for future work:

• This systematic methodology is applicable to other structural components in FOWTs to evaluate their asset integrity. For example, the pitch bearings in FOWTs. The corresponding results can be compared with current industrial standards or guidelines.

• The yaw bearing chosen in this research is a bearing with a single row of four-point contact balls. Other kinds of yaw bearings such as roller yaw bearing or a bearing with double row of eight-point contact balls could also be analyzed in the future. It is useful for designers to decide which kind of yaw bearing is better to be used.

• More working conditions of wind turbines can also be studied, such as parking and typhoon conditions. It is beneficial for assessing the yaw bearing in more complete working conditions.

• The crack analysis can be extended to research parameters such as crack length, crack depth, material characteristic, lubricating grease and so on.

• Experimental testing work of yaw bearing deserves to be performed to verify the findings of the thesis.

The above topics are proposed to improve the system of asset integrity management for FOWTs. These topics involve multidisciplinary knowledge and aim to study a structural component in wind turbines taking into account of external and internal factors. External factors include environmental conditions, structure dynamic, working status and so on. Internal factors include material properties, structure design, processing technology. With consideration of these influence factors, FOWT design could be optimized in terms of cost, safety, and reliability. This thesis intends to provide a basis for the development of FOWTs.

References

ABS AIM team (2021) *Asset integrity management technical solutions for operational challenges*.

Aditya A., W. & Farshid, S. (2017) "Rolling contact fatigue of case carburized steels," *International Journal of Fatigue*, 95pp. 264–281.

Agrawal, J.N. (2021) *Pipeline integrity management system*.

American National Standards Institute (1990a) *Load ratings and fatigue life for ball bearings*.

American National Standards Institute (1990b) *Load ratings and fatigue life for roller bearings*.

American Society of Mechanical Engineers (2005) *ASME B318S: Managing system integrity of gas pipelines*.

AssetInfinity company (2019) *What Are the 5 Key Stages of Asset Life Cycle Management (AssetInfinity)*. Available from: https://www.assetinfinity.com/blog/5-key-stages-of-asset-life-cycle-management (Accessed 30 September 2021).

Bansal, R.C., Bhatti, T.S. & Kothari, D.P. (2002) "On some of the design aspects of wind energy conversion systems." Energy Conversion and Management 43.

Barnsby, R., Duchowski, J., Harris, T., Ioannides, S., Loesche, T., Nixon, H. & Webster, M. (2003) *Life ratings for modern rolling bearings-A design guide for application of international standard ISO 281/2*. Vol. 14. New York: ASME.

Bertrand, L. (2007) "Implementing risk-based inspection on our FPSOs from a practical approach to the edge of R&D," in *Proceedings of the Offshore Technology Conference, OTC 07, pp. 409–424, Offshore Technology Conference*. Houston.

Bormetti, E., Donzella, G. & Mazzù, A. (2002) "Surface and subsurface cracks in rolling contact fatigue of hardened components," *Tribology Transactions*, 45(3), pp. 274–283.

Brown, M.W. & Miller, K.J. (1973) "A theory for fatigue failure under multiaxial stress-strain conditions," *Proceedings of the Institution of Mechanical Engineers*, 187(1), pp. 745–755.

Burton, T., Sharpe, D., Jenkins, N. & Bossanyi, E. (2008) *Wind Energy Handbook*. Wiley.

Carbon Trust (2021) *Floating wind joint industry project phase III summary report*.

Cordle, A. & Jonkman, J. (2011) *State of the art in floating wind turbine design tools*.

Dana Vanier, D.J. (2001) "Why industry needs asset management tools," *Journal of Computing in Civil Engineering*, pp. 35–43.

Dassault Systems (2017) *Abaqus analysis user's guide*. France: Dassault Systems.

David, A., Laino, J. & Hansen, A.C. (2002) *AeroDyn user's guide to the wind turbine aerodynamics computer software*.

David M, R. (2011) *The role of asset integrity and life extension in major accident prevention*. Aberdeen.

Deng, S., Qin, X. & Huang, S. (2015) “A study on the effect of subsurface crack propagation on rolling contact fatigue in a bearing ring,” *Journal of Mechanical Science and Technology*, 29(3), pp. 1029–1038.

Derks, A. (2008) *Development of a wind turbine drive train engineering model*.

Dinmohammadi, F. & Shafiee, M. (2013a) “A fuzzy-FMEA risk assessment approach for offshore wind turbines,” *International Journal of Prognostics and Health Management*, pp. 1–10.

Dinmohammadi, F. & Shafiee, M. (2013b) “An economical FEMEA-based risk assessment approach for wind turbine systems.,” in *Proceedings of the European Safety, Reliability and Risk Management(ESREL)*. Amsterdam.

Dolan, D.S.L. & Lehn, P.W. (2006) “Simulation model of wind turbine 3p torque oscillations due to wind shear and tower shadow,” *IEEE Transactions on Energy Conversion*, 21(3), pp. 717–724.

Erdogan, F. & Sih, G.C. (1963) “On the crack extension in plates under plane loading and transverse shear,” *Journal of Basic Engineering*, pp. 519–525.

François, D., Ali, M., Patrick, M. & Klaus, P. (2019) “Fracture mechanics assessment of large diameter wind turbine bearings,” *Journal of Multiscale Modelling*, 10(04), p. 1850010.

Freiburger, E., Praxair, P.E., Broadribb, M., Johnson, R.W. & Murphy, J.F. (2017) *New guidelines for asset (Mechanical) integrity management*.

Germanischer Lloyd. (2010) *Guideline for the certification of wind turbines*.

Global Wind Energy Council. (2021) *Global wind report 2021*.

Glodež, Srečko., Potočnik, Rok. & Flašker, Jože. (2012) “Computational model for calculation of static capacity and lifetime of large slewing bearing’s raceway,” *Mechanism and Machine Theory*, 47(1), pp. 16–30.

Gocodes company (2020) *Asset Life Cycle: Definition and Key Stages*. Available from: https://gocodes.com/asset-life-cycle/.

Göncza, Peter., Potočnik, Rok. & Glode, Srečko. (2010) “Fatigue behaviour of 42CrMo4 steel under contact loading,” *Procedia Engineering*, 2(1), pp. 1991–1999.

Guo, Y., Bergua, R., van Dam, J., Jove, J. & Campbell, J. (2015) “Improving wind turbine drivetrain designs to minimize the impacts of non-torque loads,” *Wind Energy*, 18(12), pp. 2199–2222.

Harris, T.A. & Kotzalas, M.N. (2007) *Rolling bearing analysis*. London: Taylor and Francis Group, CRC Press.

Harris, Tedric A & Kotzalas, M.N. (2007) *Rolling bearing analysis essential concepts of bearing technology*. Taylor and Francis Group, CRC Press.

Harris, T.A., Rumbarger, J.H. & Butterfield, C.P. (2009) *Wind turbine design guideline DG03: Yaw and pitch rolling bearing life. technical report: NREL/TP-500-42362*. (December).

He, Peiyu., Hong, Rongjing., Wang, Hua., Ji, Xu. & Lu, Cheng. (2018) “Calculation analysis of yaw bearings with a hardened raceway,” *International Journal of Mechanical Sciences*, 144(May), pp. 540–552.

He, Peiyu., Hong, Rongjing., Wang, Hua. & Lu, Cheng. (2018) “Fatigue life analysis of slewing bearings in wind turbines,” *International Journal of Fatigue*, 111(February), pp. 233–242.

Hearle, A.D. & Johnson, K.L. (1985) “Mode II stress intensity factors for a crack parallel to the surface of an elastic half-space subjected to a moving point load,” *Journal of the Mechanics and Physics of Solids*, 33(1), pp. 61–81.

Hu, W. (2018) *Advanced wind turbine technology*. Springer International Publishing.

Hu, W., Choi, K.K., Zhupanska, O. & Buchholz, J.H.J. (2016) “Integrating variable wind load, aerodynamic, and structural analyses towards accurate fatigue life prediction in composite wind turbine blades,” *Structural and Multidisciplinary Optimization*, 53(3), pp. 375–394.

International Electrotechnical Commission (2005) *IEC 61400-1: Wind turbines part 1: Design requirements*. 3.

International Electrotechnical Commission (2009) *IEC 61400-3: Wind turbines part 3: Design requirements for offshore wind turbines*.

International Organization for Standardization) (2014) *ISO 55000: Asset management overview, principles, and terminology*.

International Organization for Standardization (2008) “Rolling bearings - Dynamic load ratings and rating life.” British Standards Institution..

Ioannides, E. & Harris, T.A. (1985) “A new fatigue life model for rolling bearings,” *Journal of Tribology*, 107(3), pp. 367–377.

JAD analysis (2015) *Example type B report: Wind turbine blade pitch bearing analysis*.

James, Rhodri. & Ros, M.Costa. (2015) *Floating offshore wind: Market and technology review*.

Jonkman, B. & Jonkman, J. (2016) *FAST v8.16.00a-bjj*.

Jonkman, B.J. (2016) “TurbSim user’s guide v2.00.00.” National Renewable Energy Laboratory.

Jonkman, J., Butterfield, S., Musial, W. & Scott, G. (2009) “Definition of a 5-MW reference wind turbine for offshore system development.” National Renewable Energy Laboratory.

Jonkman, J.M. (2007) *Dynamics modelling and loads analysis of an offshore floating wind turbine*.

Jonkman, J.M. (2009) “Dynamics of offshore floating wind turbines - Model development and verification,” *Wind Energy*, 12(5), pp. 459–492.

Jonkman, J.M. & Buhl Jr, M.L. (2005) *FAST user’s guide*.

Jonkman, J.M., Robertson, A.N. & Hayman, G.J. (2014) *HydroDyn user’s guide and theory manual*.

Karimirad, M. (2014) *Offshore energy structures*. Springer International Publishing.

Karyotakis, A. & Bucknall, R. (2010) “Planned intervention as a maintenance and repair strategy for offshore wind turbines,” *Journal of Marine Engineering and Technology*, 9(1), pp. 27–35.

Kear, L.M. & Bryant, M.D. (1982) “A pitting model for rolling contact fatigue.,” *Journal of Lubrication Technology*, 105(April), pp. 198–205.

Kelley, N.D. & Jonkman, B.J. (2005) *Overview of the TurbSim stochastic inflow turbulence simulator*. (September).

Komvopoulos, K. (1996) “Subsurface crack mechanisms under indentation loading,” *Wear*, pp. 9–23.

Kong, C., Bang, J. & Sugiyama, Y. (2005) “Structural investigation of composite wind turbine blade considering various load cases and fatigue life,” in *Energy*. Elsevier Ltd. pp. 2101–2114.

Kong, C., Kim, T., Han, D. & Sugiyama, Y. (2006) “Investigation of fatigue life for a medium scale composite wind turbine blade,” *International Journal of Fatigue*, 28(10 SPEC. ISS.), pp. 1382–1388.

Kudish, I. (1986) “Study of the effect of subsurface defects in a elastic material on its fracture,” *Study, Calculation, and Design of Roller Bearings*, 2pp. 55–77.

Kudish, I.I. & Burris, K.W. (2000) “Modern state of experimentation and modelling in contact fatigue phenomenon: Part II—analysis of the existing statistical mathematical models of bearing and gear fatigue life. New statistical model of contact fatigue,” *Tribology Transactions*, 43(2), pp. 293–301.

Kudish, I.I. & Covitch, M.J. (2010) *Modelling and analytical methods in tribology*. CRC Press.

Kusumawardhani, M., Kumar, R. & Tore, M. (2016) “Asset integrity management: Offshore installations challenges,” *Journal of Quality in Maintenance Engineering*, 22(3), pp. 238–251.

Laura，Castro Santos & Vicente，Diaz-Casas (2016) *Floating offshore wind farms*. Switzerland: Spring Nature.

Lazakis, I. & Kougioumtzoglou, M.A. (2019) “Assessing offshore wind turbine reliability and availability,” *Proceedings of the Institution of Mechanical Engineers Part M: Journal of Engineering for the Maritime Environment*, 233(1), pp. 267–282.

Lee, K.Y., Tsao, S.H., Tzeng, C.W. & Lin, H.J. (2018) “Influence of the vertical wind and wind direction on the power output of a small vertical-axis wind turbine installed on the rooftop of a building,” *Applied Energy*, 209pp. 383–391.

Leimeister, M. & Kolios, A. (2018) “A review of reliability-based methods for risk analysis and their application in the offshore wind industry.” Renewable and Sustainable Energy Reviews 91 pp. 1065–1076.

Li, L., Hu, Z., Wang, J. & Ma, Y. (2015) *Development and validation of an Aero-Hydro simulation code for an offshore floating wind turbine*. 2 (1).

Li, Q., Murata, J., Endo, M., Maeda, T. & Kamada, Y. (2016) “Experimental and numerical investigation of the effect of turbulent inflow on a Horizontal Axis Wind Turbine (Part I: Power performance),” *Energy*, 113pp. 713–722.

Liu, C.R. & Choi, Y. (2008) “Rolling contact fatigue life model incorporating residual stress scatter,” *International Journal of Mechanical Sciences*, 50(12), pp. 1572–1577.

Liu, Y., Xiao, Q., Incecik, A., Peyrard, C. & Wan, D. (2017) “Establishing a fully coupled CFD analysis tool for floating offshore wind turbines,” *Renewable Energy*, 112pp. 280–301.

Lubitz, W.D. (2014) “Impact of ambient turbulence on performance of a small wind turbine,” *Renewable Energy*, 61pp. 69–73.

Lundberg, G. & Palmgren, A. (1947) “Dynamic capacity of rolling bearings,” *Acta Polytech Scand Mech Eng*, 1(52), p. 1947.

Manwell, James., McGowan, Jon. & Rogers, Anthony. (2009) *Wind energy explained: Theory, design, and application*. Second. A John Wiley and Sons Ltd.

Md, A.M. & Mohd, S.S. (2013) *Materials selection and design*. Springer.

Moriarty, P.J. & Hansen, A.C. (2005) *AeroDyn theory manual*.

Moriarty, P.J., Holley, W.E. & Butterfield, Sandy. (2004) “Extrapolation of extreme and fatigue loads using probabilistic methods.” National Renewable Energy Laboratory

Morrow, J. (1965) “Cyclic plastic strain energy and fatigue of metals,” *Internal Friction, Damping, and Cyclic Plasticity*, pp. 45–87.

National Renewable Energy Laboratory (2021a) *AeroDyn user’s guide and theory manual*.

National Renewable Energy Laboratory (2021b) *BeamDyn user’s guide and theory manual*.

National Renewable Energy Laboratory (2021c) *ElastoDyn user’s guide and theory manual*.

National Renewable Energy Laboratory (2021d) *HydroDyn user’s guide and theory manual*.

National Renewable Energy Laboratory (2021e) *ServoDyn user’s guide and theory manual*.

National Renewable Energy Laboratory (2021f) *SubDyn user’s guide and theory manual*.

Nicholson, J.C. (2011) *Design of wind turbine tower and foundation systems*.

Nielsen, J.S. & Sørensen, J.D. (2014) “Methods for risk-based planning of O&M of wind turbines,” *Energies*, 7(10), pp. 6645–6664.

Noda, M. & Flay, R.G.J. (1999) “A simulation model for wind turbine blade fatigue loads.” Journal of Wind Engineering and Industrial Aerodynamics 83.

O. M. Faltinsen (1990) *Sea loads on ships and offshore structures*. Cambridge University Press.

Ossai, C.I., Boswell, B. & Davies, I.J. (2014) “Sustainable asset integrity management: Strategic imperatives for economic renewable energy generation,” *Renewable Energy*, 67pp. 143–152.

Ozguc, O. (2020) “A new risk-based inspection methodology for offshore floating structures,” *Journal of Marine Engineering and Technology*, 19(1), pp. 40–55.

Quest Floating Wind Energy, L.L.C. (2021) *Global floating wind market and forecast report*.

Ramachandran, G.K. v, Robertson, A., Jonkman, J.M. & Masciola, M.D. (2013) *Investigation of response amplitude operators for floating offshore wind turbine*. Anchorage, Alaska: Proceedings of the 23rd International Ocean, Offshore and Polar Engineering Conference – ISOPE 2013.

Ratnayake, R.M.C. (2012) "Modelling of asset integrity management process: a case study for computing operational integrity preference weights," *Int. J. Computational Systems Engineering*, 1(1), pp. 3–12.

Renard, M.F. (2013) *Asset integrity management extends reach*.

Ringsberg, J.W. (2001) "Life prediction of rolling contact fatigue crack initiation," *International Journal of Fatigue*, 23pp. 575–586.

Robertson, A.N. & Jonkman, J.M. (2011) "Loads analysis of several offshore floating wind turbine concepts," in *Proceedings of the International Offshore and Polar Engineering Conference*. pp. 443–450.

Ronold, K.O. & Christensen, C.J. (2001) "Optimization of a design code for wind-turbine rotor blades in fatigue." Engineering Structures 23.

Ronold, K.O., Wedel-Heinen, J. & Christensen, C.J. (1999) "Reliability-based fatigue design of wind-turbine rotor blades." Engineering Structures 21.

Santus, C., Beghini, M., Bartilotta, I. & Facchini, M. (2012) "Surface and subsurface rolling contact fatigue characteristic depths and proposal of stress indexes," *International Journal of Fatigue*, 45pp. 71–81.

Schlicht, H., Schreiber, E. & Zwirlein, O. (1986) "Fatigue and failure mechanism of bearings," in *IMech E Conf*. IMech E Conf.

SGS company (2021) *Asset integrity management: Partnering to achieve your inspection, engineering, data management and safety goals*.

Shen, X., Zhu, X. & Du, Z. (2011) "Wind turbine aerodynamics and loads control in wind shear flow," *Energy*, 36(3), pp. 1424–1434.

Tang, Y., Jing, J., Zhang, Z. & Yang, Y. (2018) "A quantitative risk analysis method for the high hazard mechanical system in petroleum and petrochemical industry," *Energies*, 11(1).

Tang, Y., Yao, J., Wang, G., Zhang, Z., He, Y. & Jing, J. (2019) "Risk identification and quantitative evaluation method for asset integrity management of offshore platform equipment and facilities," *Mathematical Problems in Engineering*.

the Offshore Division of HSE's Hazardous Installations Directorate (2020) *Key programme 3 asset integrity programme*.

United Nations (2021) *COP26 Powering progress*. Available from: https://www.un.org/en/climatechange/day-5-powering-progress (Accessed 4 November 2021).

UpKeep company (2021) *What is an asset life cycle*. Available from: https://www.onupkeep.com/maintenance-glossary/asset-life-cycle.

Vera, F., Jens, S. & Brigitte, C. (2022) “Crack propagation modelling for service life prediction of large slewing bearings,” in Proceedings of the 2nd International Workshop on Plasticity, Damage and Fracture of Engineering Materials (IWPDF).

Vincent, Alain., Lormand, Gerard., Lamagnere, Pierre., Gosset, Laurence., Girodin, Daniel., Dudrangne, Gilles. & Fougeres., R. (1998) “From white etching areas formed around inclusions to crack nucleation in bearing steels under rolling contact fatigue,” in J. J. C. Hoo & W. B. Green (eds.) *Bearing Steels: Into the 21st Century*. American Society for Testing and Materials. pp. 109–123.

Xu, H. & Komvopoulos, K. (2013) “Fracture mechanics analysis of asperity cracking due to adhesive normal contact,” *International Journal of Fracture*, 181(2), pp. 273–283.

Zhang, Youwen. & Wang, Yingguang. (2015) “Comparison analysis about ultimate load and fatigue load of floating wind turbines,” *The Ocean Engineering*, 33(3), pp. 57-62,70.

Zulkifly, H. & Mohd, K.A.H. (2013) *Risk-based asset integrity management for offshore floating facilities in Malaysia*.